ISSN:2538-516X

Journal of Civil Engineering Researchers

Volume: 5; Number: 4; December 2023

J-Researchers

J-Researchers

JOURNAL OF CIVIL ENGINEERING RESEARCHERS

Volume 5, Number 4, December 2023

Contents

1. **Assessment of Composite Bars and FRP Panels for Seismic Bridge Decks** 1-15
Amir Mohammad Bakhtiari, Ali Harati

2. **Influence of Vegetation in The Flood Drainage Ditch** 16-21
Golnoosh Toosi

3. **A Method Based on Fracture Mechanics to Investigate the Deformation of Reinforced Concrete Columns** 22-30
Houman Mahmoodi Asl

4. **Incorporating Bacteria for Self-Healing Properties in Innovative Concrete Technology** 31-39
Soheil khalatbari

5. **Comprehensive Investigation of the Omega-Shaped Hybrid CFRP Sheet - Concrete Slab System: Experimental, Numerical and Analytical study** 40-55
Amir Mohammad Bakhtiari, Ali Harati

6. **The Effect of Polypropylene Fibers on the Behavior of Fiber Self-Compacting Concrete** 56-62
Morteza Jamshidi

J-Researchers

JOURNAL OF CIVIL ENGINEERING RESEARCHERS

Assessment of Composite Bars and FRP Panels for Seismic Bridge Decks

Amir Mohammad Bakhtiari,[a,*] Ali Harati[a]

[a]*Department of Civil Engineering, Arman Institution of Engineering and Technology, Tehran, Iran*

Journals-Researchers use only: Received date: 2023.06.21; revised date: 2023.08.10; accepted date: 2023.09.19

Abstract

Seismic Strengthening offers a cost-effective and sustainable solution for constructing bridges in seismic zones. In these rehabilitation interventions, Fiber Reinforced Polymer (FRP) composites are often used instead of steel members due to their lightweight nature, high strength, and excellent corrosion resistance. Researchers are now focusing on creating innovative FRP-concrete hybrid structures. This study specifically investigates the numerical modeling of the response of a hybrid FRP-concrete jacket bridge pier subjected to quasi-static tests. The Finite Element Method (FEM) results demonstrated a significant correlation with the experimental response, particularly in terms of the load-displacement curve failure mode. Once the model was validated, various alternative designs were numerically tested to evaluate the impact of each model on the load-bearing capacity. These designs included altering the height of the CFRP sheet, adjusting the height and congestion of the CFRP bar, and comparing the performance of the concrete jacket with and without the CFRP sheet. After reinforcing the CFRP sheets and incorporating Near-Surface-Mounted (NSM)-CFRP bars, the reinforcement system, along with the new concrete jacket, effectively transferred the integrity of the broken pier area and maintained a constant load-bearing capacity for the bridge pier. However, when the CFRP sheet was added to the aforementioned system, the load capacity of the bridge pier increased by more than 60%. Therefore, it can be concluded that seismic enhancement techniques utilizing CFRP sheets and mounted NSM-CFRP bars are successful in enhancing the strength and resilience of the concrete bridge pier. (DOI:**https//doi.org/10.52547/JCER.5.4.1**)

Keywords: Near-surface-mounted (NSM), Carbon Fiber Reinforced Polymer (CFRP), Numerical model, Seismic Strengthening

1. Introduction

An earthquake, a destructive natural phenomenon, has occurred in many regions around the world. There has been an increase in the frequency of earthquakes in recent times, leading to significant damage to bridges. Past experiences have taught us that the bridge piers are particularly vulnerable during earthquakes [1]. To enhance the seismic resistance of bridges, retrofitting methods have been developed, focusing on covering or coating the bridge piers with

* Corresponding author. Tel.: +989125148269; e-mail: bakhtiariamir96@gmail.com.

various materials such as steel pipes, thin concrete layers, carbon fiber reinforced polymer (CFRP), and other advanced composites [2]. Fiber-reinforced polymer (FRP) composites are an incredibly versatile technology that has proven to be highly efficient and advantageous. They possess a strong strength-to-weight ratio, do not corrode, require less labor, can be deployed quickly, and have lower long-term maintenance costs. FRP products find applications both for internal and external reinforcement of structures [3]. Different forms of FRP components like boards, laminates, rigid structures, bars, and tendons are crucial for the structural integrity of bridges. State-of-the-art articles provide detailed information on various aspects of FRP implementation, including reliability, statistical features, research methodology, and long-term performance. Recent studies have focused on the effectiveness of near-surface-mounted (NSM) FRP laminates to strengthen existing reinforced concrete (RC) beams [4], [5].

The NSM technique typically employs reinforcement that is produced via a pultrusion process, similar to the FRP rebars. These reinforcements may have a cross-section that is either round or square in shape. To achieve structural integrity, the reinforcement bars are carefully placed in grooves that are cut into the underside of the beam [6]. The adhesive utilized for bonding purposes is a high-viscosity epoxy or a cement paste [7]. By incorporating FRP rods into these grooves, the use of NSM reinforcement can substantially enhance the Flexi-security of RC beams, as well as improve their overall efficiency [8]. In particular, the NSM technique effectively shifts the failure zone from the column to the beam, thereby offering supplementary strength or ductility [9], [10]

The primary benefit of employing the NSM pre-stress strategy is its ability to enhance serviceability by effectively controlling flexural cracks, mitigating service load defects, and prolonging the initiation of steel reinforcement [8]. Extensive research has been conducted on the use of NSM FRP reinforcement to reinforce concrete beams, primarily focusing on concrete slabs [11], [12]. However, limited studies have been performed on the application of NSM FRP in bolstering columns. This is mainly due to the prevailing belief that NSM FRP laminates are ineffective in compression, as highlighted by Fib Bulletin 14 [13], which states that the compression elasticity modulus of FRP is lower than its stress module. This perception has hindered the widespread utilization of NSM FRP laminates for enhancing the strength of concrete columns [14], [15]. These findings are in line with the guidelines put forth by ACI 440.2R [16]

According to reports, it is not recommended to utilize FRP systems as a means to enhance compressive strength. The CAN/CSA S806 standards [17] have clarified that the reinforcement elements of FRP used in the compression zone of concrete are deemed to possess negligible compressive strength and rigidity with regard to construction purposes. ACI 440.2R does not endorse the utilization of FRPs for compression [16]

In view of the potential occurrence of premature defects [18], [19], such as the buckling of fibers on a small scale, unsupported or poorly preserved laminates buckling, and insufficient anchoring of substrates and FRP surfaces, alongside the unreliability of the compressive strength of laminates, it is crucial to address these issues [20], [21]. The micro buckling problem may arise from inadequate quality control of the FRP production, which might be attributed to the presence of ACI 440.2R vacuum in the resin [22]. However, adhering to quality control measures can effectively solve this problem.

As part of our study, we have examined the utilization of high-module externally bonded longitudinal FRPs on slender reinforced concrete (RC) columns. Our findings indicate that incorporating longitudinal FRP laminates enhances the load-carrying path of slender columns and optimizes their axial performance [23], [24]. This improvement is achieved by fortifying the stiffness of the columns through additional reinforcement provided by the longitudinal FRP laminates [25], [26].

In relation to the absence of compression laminates FRP and their effectiveness in terms of compressive behavior, it is crucial to thoroughly examine the compression behavior of NSM FRPs. Insufficient research has been conducted on the suitability of longitudinal compressive NSM FRP laminates in both bending and axially loaded cement bridge columns, particularly in terms of their strength, rigidity, and understanding of compression characteristics of FRPs. The potential risks associated with premature

cracking, corrosion, and buckling failure in NSM FRP reinforced concrete columns highlight the necessity for further studies. A model is utilized to determine the optimal design parameters for the specimens at a later stage. The primary objective of this research is to investigate the performance of the bridge column. It aims to design a hybrid solution that can maximize the benefits of CFRP while mitigating its drawbacks. The numerical analysis includes enhancements to the concrete and CFRP dimensions, the length and width of the CFRP layer, and modifications to the NSM bar dimensions. The bridge specimens are classified into eight distinct categories and simulated using a finite element method program. These specimens undergo monotonic loading tests in order to identify the most effective reinforcement schemes for new structures.

2. Experimental tests

The experimental investigation was carried out by Chen [27] has been used to validate numerical modeling. In this study, a scale model pier was designed, based on a 1/8 scale prototype pier [27]. The test setup and the retrofitting scheme are shown in Fig. 1(a). The height of the pier model was 2,500 mm and the cross section was 640×450 mm. In this case, the CFRP jacket was used on the pier faces in such a manner that one layer of the CFRP sheet is used in the longitudinal and transverse directions, the longitudinal layer is first wrapped and the transverse layer is then coated [27]. In addition, a new 20 cm high concrete jacket is constructed over the anchored reinforcement and forms an extended reinforced concrete frame to preserve the bottom-anchoring impact that the binding specimen is positioned at the end of the pier. The concrete used for the attachment had a compression power of 28 days of 30 MPa. Also, the steel used in both the longitudinal bars and the stirrups had an elasticity modulus of 210 GPa, the Poisson ratio was 0.3, the Yield tension of the stirrups was 335 MPa and the yield pressure of the longitudinal reinforcements was 335 MPa. The CFRP used for retrofitting had an elastic modulus of 243 GPa and a Poisson ratio of 0.3. The description of the specimen and the CFRP arrangement used is seen in Fig.1(b) [27].

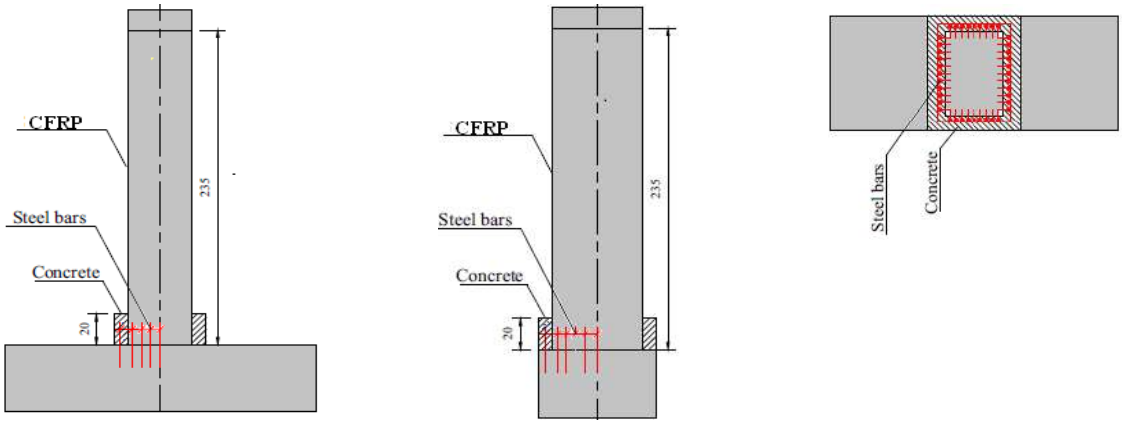

(a)

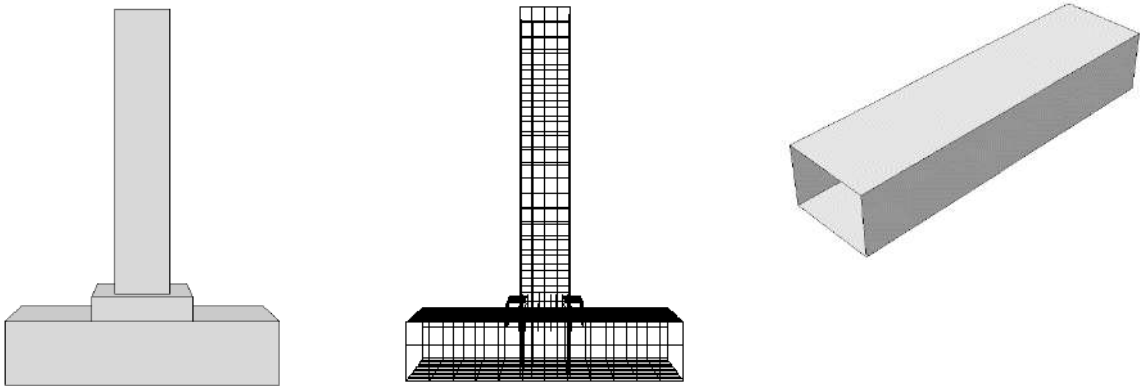

(b)

Fig. 1 View of the rebar and concrete arrangement [27].

3. Finite element method (Numerical models' description)

ABAQUS [28] General intent of the finite element program was used to model laboratory experiments to include a general technique that was commonly applicable to clinicians. The following subsections deal with geometry, components, mesh, boundary conditions, contacts, and estimation process descriptions of the model is applied. Models were divided into 3D sections, one for CFRP sheets, one for GFRP bars, one for concrete, and one for bars. With mesh and without mesh models, the experimental models developed in the laboratory and the corresponding measurements are shown in Fig. 3.

Fig. 3. displays the models (A to G) which were numerical models created by simulator software and the corresponding dimensions.

3.1. Materials in FEM

Concrete Damage Plasticity (CDP) was used in the composite pier simulation to describe the concrete behavior of FE modeling. The CDP model was built based on two concrete failure mechanisms: compressive crushing and tensile cracking [29],[30]. It combines isotropic, weakened elasticity with compressive plasticity and isotropic tensile. The two major failure mechanisms are called tensile cracking and compressive crushing of concrete [31],[32],[33]. After trying a lot of values, the following values selected as the most suitable ones; 0.15 for the Poisson's ratio of concrete, 30 degrees for the dilation angle Ψ of the reinforced concrete, and [34],[35] for nonlinear uniaxial behavior of concrete, the Kent and Park formulation was used [36]. According to this, compressive stress is calculated by equation (1):

$$\sigma_C = f'_{co}\left[2\left(\frac{\varepsilon_c}{\varepsilon'_c}\right) - \left(\frac{\varepsilon_c}{\varepsilon'_c}\right)^2\right] \quad (1)$$

Where ε_c is the compressive strain, f'_{co} and ε'_c are the compressive strength of unconfined cylindrical concrete specimen and the related strain respectively. The value of ε'_c is considered to be 0.002.

The compression damage parameter (dc), controls the unloading gradient of the stress-strain curve. In concrete and similar materials, such as masonry materials, the higher the plastic strain, the slope of the unloading curve will be reduced to a greater extent than the initial gradient (elasticity specimen). It is due to the damage caused by the loss induced in a brittle material. When damage starts, compressive stress is calculated based on the following equations (2) and (3) [31],[37],[38]:

$$\sigma_C = (1 - d_c)\, E_O\, (\varepsilon_C - \varepsilon_C{}^{\sim PL} \quad (2)$$

$$\varepsilon_C{}^{\sim PL} = \left(\varepsilon_C{}^{\sim in} - \frac{1}{(1 - d_c)}\frac{\sigma_c}{E_0}\right) \quad (3)$$

Where $\varepsilon_C{}^{\sim PL}$ is an inelastic strain, ε_C is the compressive strain, E_O is elasticity modulus, d_c is compressive damage, $\varepsilon_C{}^{\sim in}$ is strain related to damage.

Finally, equation 4 is used to calculate the compressive damage value dc [28]:

$$dc = 1 - \frac{\sigma_c}{f'_{co}} \quad (4)$$

For the simulation of the internal CFRP bar, two linear 3D truss elements (T3D2) were used to discrete the concrete volume, while three nodes triangular general-purpose shell finite membrane strains (S3R) were used with CFRP. Two node 3D truss elements were also used in the simulation of the internal CFRP bar [33],[36],[39]. Various grids according to each part's thickness (concrete, CFRP bar, and CFRP sheet) were applied. The convergence of digital solutions was controlled with mesh measurements of 100, 75, 50, and 25 mm in the concrete region and the mesh size of 50 mm was selected. It has been believed that the interaction between CFRP and the concrete is perfectly connected (tie). An integrated relationship of the CFRP bar with the concrete was modeled [40]. The Pier model was simply supported at the corresponding span and the load was indirectly modeled as an imposed displacement on the pier top. The reaction force associated with this imposed displacement was taken as the applied force. The procedure of analysis was done in implicit mode. Regarding quasi-static loading, the static general step was selected for analysis. For running 1 model, the Calculation time was approximately 23 hours with Intel® core i7 CPU.

3.2. Model fitting

In the key representative situations, experimental testing of CFRP bridge pier was selected to match the numerical model: with an attached carbon fiber plate. The default Kc = 0.667 values deliver the most reliable results of ultimate power and failure. The dilation angle (Ψ) ranged from 25 to 35 and the viscosity parameter for concrete harm measurements had a value of 0,001. Higher dilation angle values produce ductile response while lower dilation angle values give a fragile response. Compression (dc) measured damage parameter has a remarkable effect on the bending response of the hybrid structural elements. The use of a larger parameter for viscosity will reduce the measuring time considerably, but the results are worse. The conclusion shows that the value of the viscosity parameter must be carefully chosen and measured accordingly in realistic calculations using the CDP material model. The dilation, Kc, and viscosity values equal to 30, 1.16, and 0.667, respectively, are taken for the best fit. These values are consistent with Abaqus's guidance on the damaged plasticity of concrete and other research results [31]. According to CEB-FIB, the concrete stress-strain compression and the tensile post cracking behavior of the concrete were defined [39]. The results for the best fitting parameters are reported is shown in Fig 2. Between the experimental and numerical curves, a strong agreement can be seen. In particular, maximum loads were predicted with an average relative error of 3% (114.52kN predicted vs. 116.44kN experimental for the cases). The numerical model tends to slightly underestimate experimental load-bearing capacity. Regarding the stiffness, the model accurately predicts the force-displacement slope in most of the force increase range. As long as the CFRP-concrete contact was supposed to be completely bonded, when this condition is lost the model convergence is no longer possible and there is no predicted data for the post-critic response. Nevertheless, the loading branch is the most significant for designing procedures which was the initial aim of the research.

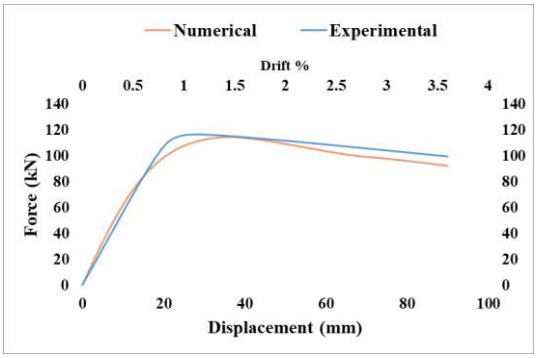

Fig. 2. The experimental and numerical load-deflection curves of the specimen bridge pier with CFRP

4. Geometric parameters study

To evaluate the performance of bridge pier configuration, various geometries were simulated with the parameters fixed in the previous fitting process. Simulated cases are summarized in Fig. 3.

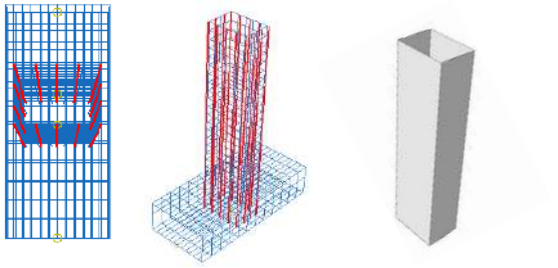

1) Case A. Concrete 2500 mm in height, section 640 × 450 mm. The pier sides were used in the CFRP jacket 2500 mm CFRP process, NSM CFRP bar so that, longitudinal direction in 5, transverse direction in 4, 20 mm width, 2500 mm height and 6 mm longitudinal diameter.

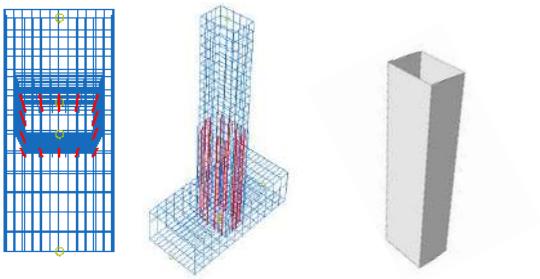

2) Case B. Concrete 2500 mm in height, section 640 × 450 mm. 2500 mm CFRP jacket, method NSM, CFRP bar were used in the pier faces Such that in the longitudinal direction in 5, in the transverse direction in 4 mm, in the depth of 20 mm, in the height of 1480 mm and the diameter of the longitudinal bar 6 mm.

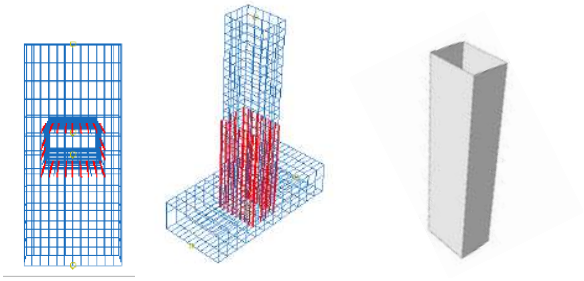

3) Case C. Concrete 2500 mm in height, section 640 × 450 mm. 2500 mm CFRP jacket, method NSM, CFRP bar is used in pier faces Such that the longitudinal direction is 9, the transverse direction in 4 mm, the depth of 20 mm, the height of 1480 mm and the diameter of the longitudinal bar in 6 mm.

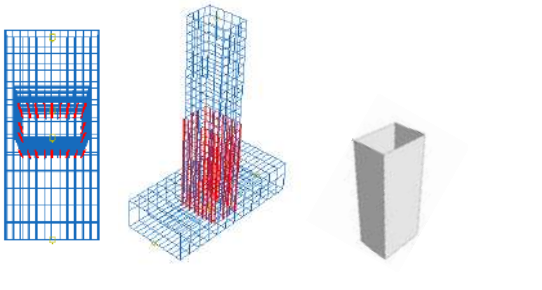

4) Case D. Concrete 2500 mm in height, section 640 × 450 mm. 1500 mm CFRP jacket, method NSM, CFRP bar were used in the pier faces In such a way, the longitudinal direction is 9, the transverse direction in 4 mm, the depth of 20 mm, the height of 1480 mm and the diameter of the longitudinal bar 6 mm.

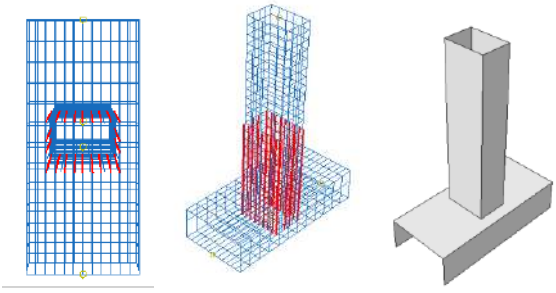

5) Case E. Concrete 2500 mm in height, section 640 × 450 mm. 1500 mm CFRP jacket and the base is also reinforced with a CFRP jacket, the NSM process, the CFRP bar has been used in the pier faces Such that the longitudinal direction is 9, the transverse direction in 4 mm, the depth of 20 mm, the height of 1480 mm and the diameter of the longitudinal bar is 6 mm.

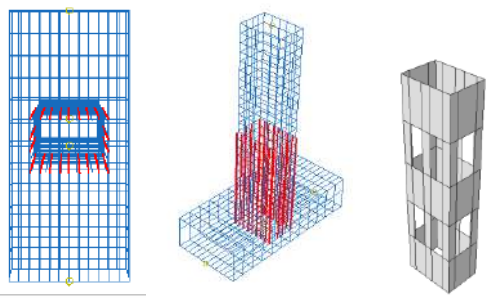

6) Case F. Concrete 2500 mm in height, section 640 × 450 mm. But the CFRP sheet was reduced by 30%, the NSM process, the CFRP bar is used in the pier faces So that the longitudinal direction is 9, the transverse direction in 4 mm, the depth of 20 mm, the height of 1480 mm, and the diameter of the longitudinal bar in 6 mm.

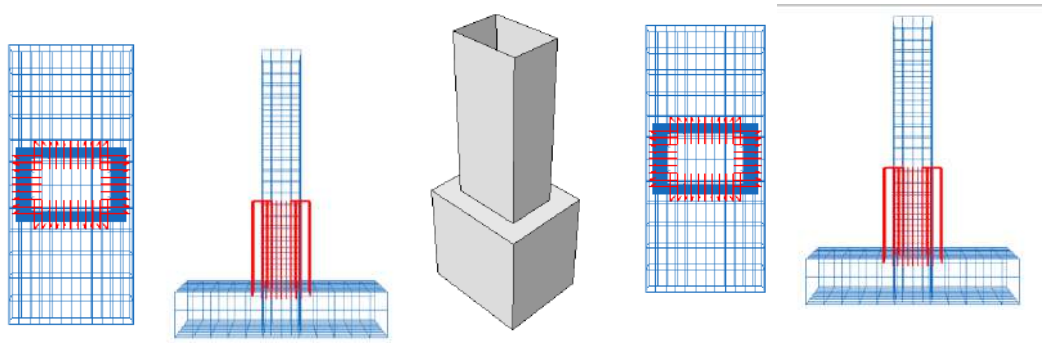

7) Case G. The model pier had a height of 2500 mm and its scale was 640 × 450 mm. CFRP jackets were used in the pier faces in such a way that one layer of CFRP sheet is used in the longitudinal and transverse directions, respectively. Besides, a new concrete jacket, 100 cm thick, is placed around the anchored reinforcement.

8) Case H. The height of the model pier was 2500 mm and the cross-section was 640 × 450 mm. There is no CFRP jacket in this specimen. Besides, a new concrete jacket, 100 cm thick, is placed over the anchored reinforcement. 20 mm deep, 1480 mm high, and 6 mm longitudinal bar diameter.

Fig. 3. Bridge pier, the cases under consideration.

5. Analysis of the force-displacement curves

In Fig. 4, force-displacement curves of cases A, B, C, D, E, F, G, and H are compared with those representing experimental tested cases. In Table 1, the values of ultimate strength (Fp), Deformation at the maximum capacity (du), and the area beneath the force-displacement curve (dissipated energy-Gd) are introduced. Results showed that increasing the concrete cross-section significantly increased the load-bearing capacity. Cases A and B, showed similar capacities, so increasing the height of the CFRP bar (NSM) is no effect if the CFRP-concrete jacket connection is assured. In case C, the intensity of the CFRP rebar (NSM) at the intersection between the column and the foundation causing a reduction in the system's dissipated energy in comparison with cases A, although the maximum load-bearing capacity was maintained. Comparing case D with cases A and B, the reduction in the height of the CFRP jacket was expected to reduce dissipated energy and maximum load-bearing capacity. Comparison of case E with case C shows that the retrofit of the foundation with the CFRP jacket does not affect increasing dissipated energy and maximum load-bearing capacity. Comparison of case F with case C shows that the use of the CFRP window arrangement has increased the increasing dissipated energy and maximum load-bearing capacity due to the reduced interaction between concrete and CFRP. Cases G and H had greater concrete area so showed greater initial stiffness although, the use of CFRP in Case G has increased increasing dissipated energy and maximum load-bearing capacity.

5.1. Analysis of the maximum plastic strain index

The ultimate plastic strain (Pe) criterion is an appropriate parameter in estimating the damage in concrete. This is a suitable criterion for investigating the number of cracks and the tensile and compression failures along with their alignment. Concrete damage is related to the CFRP-concrete debonding process. Tensile Damage Parameters (DAMAGET), compression damage (DAMAGEC), and stiffness Determination (SDEG) are other parameters that can be used to assess damage in concrete structures [32],[41]. Although these particular parameters are useful for evaluating the amount of damaged concrete, PE is more commonly used [31].

The model for the experimental case with mesh reached a maximum plastic strain value of about 0.454%, which indicated extensive tensile damage in concrete, and most of the cracks were formed at the intersection between the column and the foundation. The greatest cracks in this area were expected and obtained by the model as can be seen in Fig. 5 and Table 2.

The overall key plastic pressure is elevated as a function of the strength of the CFRP Rebar (NSM) and the wider concrete region showing the stress accumulation and a related rise in injury.

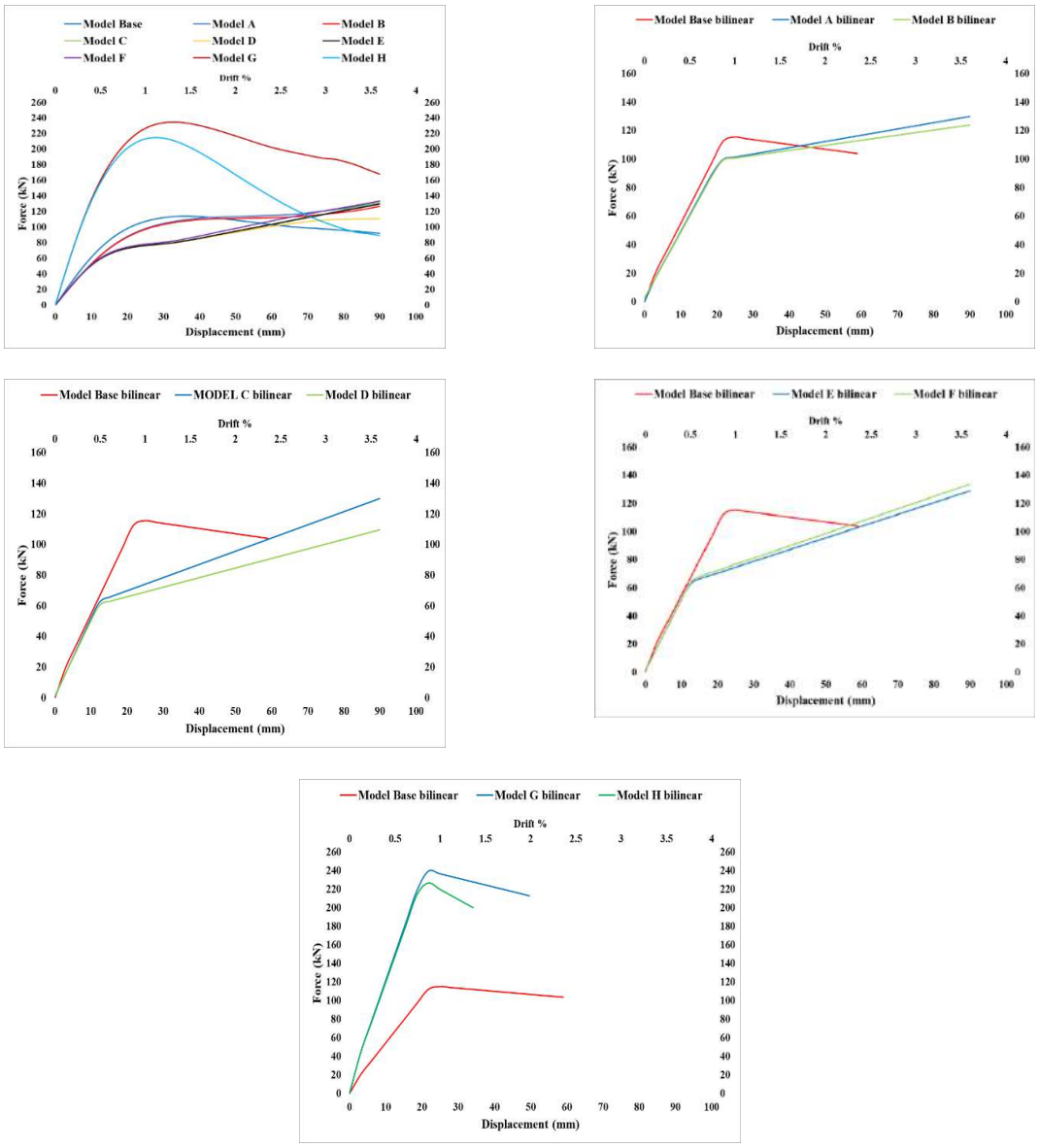

Fig. 4. Comparison of Force-Displacement curves for cases

Table 1.

Ductility ratio and the related factors in retrofitted and base cases

Cases	dy (mm)	du (mm)	$\mu = \frac{d_u}{d_y}$
Base	21.72 (0.87)	58.96 (2.36)	2.71
A	21.72 (0.87)	90 (3.6)	4.15
B	21.72 (0.87)	90 (3.6)	4.15
C	12.41 (0.50)	90 (3.6)	7.25
D	12.41 (0.50)	90 (3.6)	7.25
E	12.41 (0.50)	90 (3.6)	7.25
F	12.41 (0.50)	90 (3.6)	7.25
G	18.62 (0.75)	49.65 (1.98)	2.67
H	18.62 (0.75)	34.14 (1.37)	1.84

Table 2.

The maximum load-carrying capacity, the dissipated energy, and maximum principle plastic stain for all the cases

Cases	Maximum strength (kN)	Deformation at the maximum capacity (mm)	dissipated energy (kN.mm)	Maximum principal plastic strain (%)
Base	115.53	24.82	5375	0.454
A	130.15	90	9008	0.289
B	124.08	90	8780	0.267
C	130.17	90	7912	0.436
D	109.71	90	7025	0.424
E	128.95	90	7886	0.431
F	133.82	90	8115	0.464
G	239.62	21.72	9153	0.811
H	226.66	21.72	5405	0.690

In the case of A, the tensile damage to concrete (PE0.289 %) was seen to reduce as the height of the CFRP sheet increased. On the other hand, the case B with the decreased height of the CFRP bar (at the intersection between the column and the foundation region) showed that the tensile damage in concrete (PE0.267 %) was decreased when the height of the CFRP was reduced. When increasing the congestion bar between NSM (CFRP bar) in concrete (case C) there was less concrete at the intersection between the column and the foundation region of the case and the CFRP bar was concentrated there Increasing the possible tensile damage in concrete to PE=0.436% but reaching similar load-bearing capacity to the experimental case A. Increased concrete cross-section (case G and H) will significantly increase the system's shear capacity and eliminate the cracks at the crossroads between the column and the foundation area. In the case of G due to the use of FRP, PE achieved the highest value among the models: 0.811 trillion. This reality suggests that this case was the one that enabled the creation of more tensile damage in concrete, while higher loads were supposed to be resisted. A representative contour plot of the PE index is provided in Fig.5.

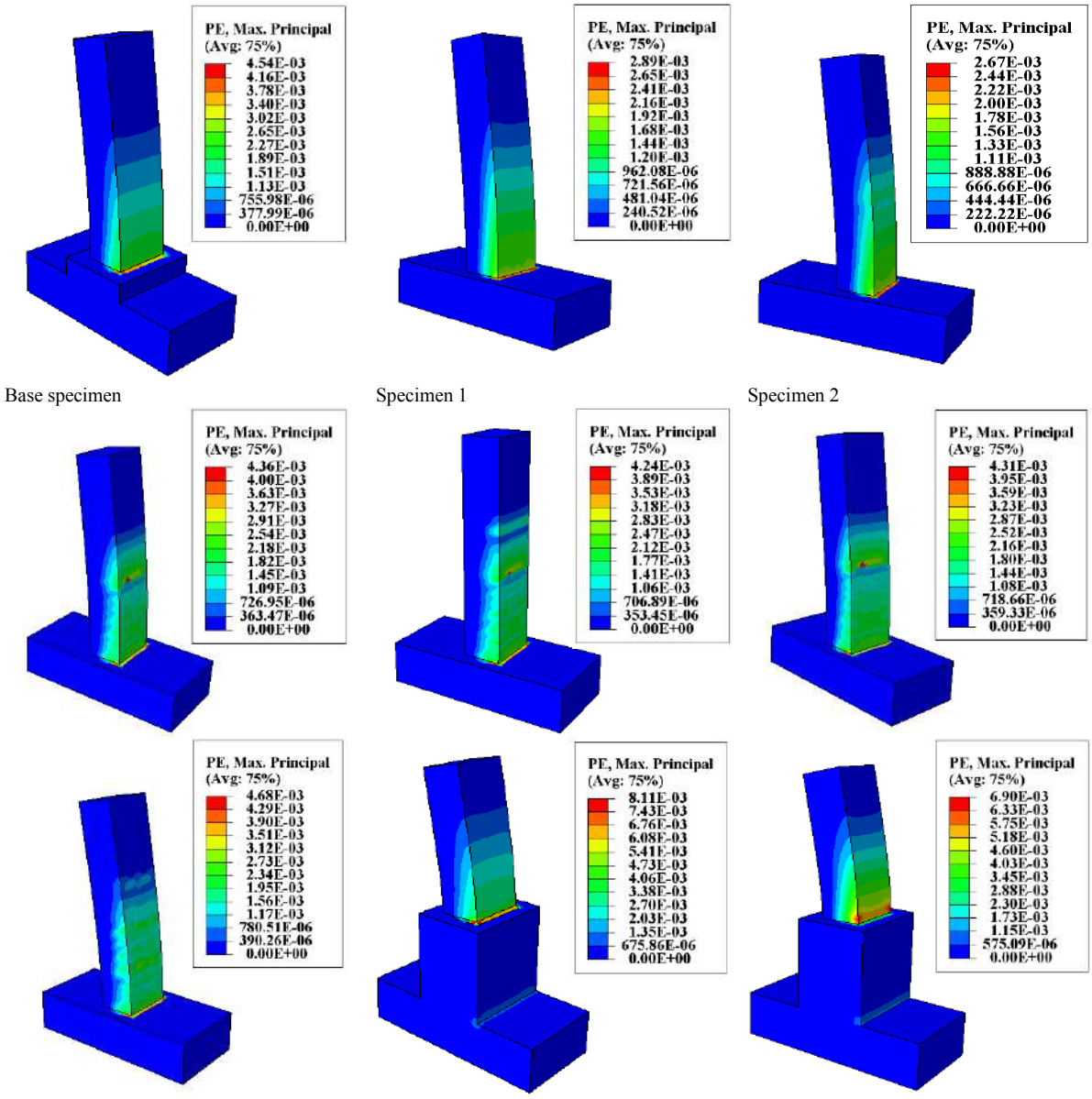

Fig. 5. Maximum principal plastic strain in the base and the proposed cases.

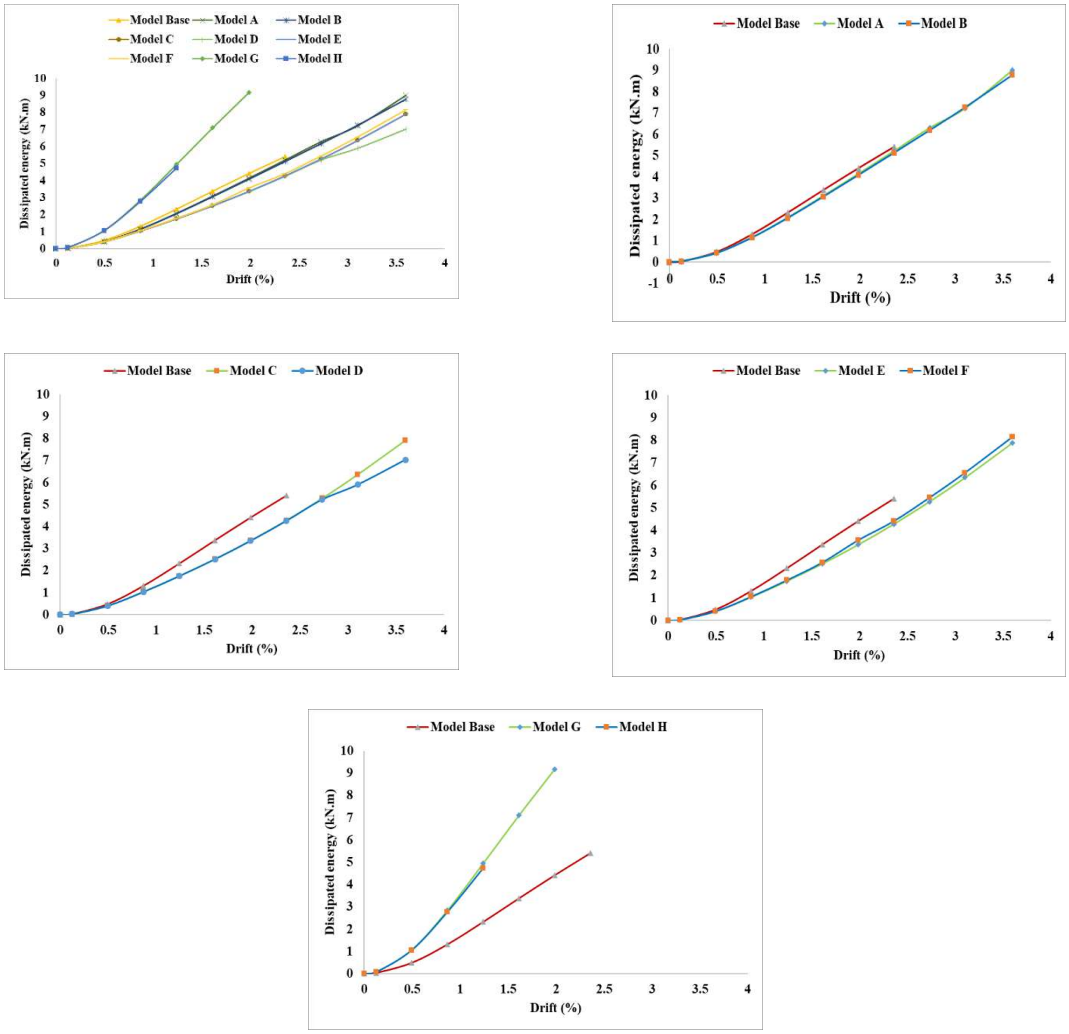

Fig. 6. Evolution of the dissipated energy during the monotonic loading in the base and the proposed specimens

5.2. Dissipated energy

The energy dissipation and inelastic deformation of the elongation load resistance system signify the ability of the structure to withstand the loading requirements of the seismic event. At each loading point, the sum of dissipated energy could be determined from the enclosed area as shown by the monotonous reaction of the lateral load vs. the lateral displacement. The addition of dissipated energy associated with the increase in lateral elongation would result in total dissipated energy at each point of inter-story elongation. The evolution of dissipated energy for all specimen states was shown in Fig. 6. Dissipated energy is analyzed in three areas of 1, 2, and 3, with area 1 being 0 to 1 drift and area 2 being 1 to 2.5 drifting, and area 2 being 3 being 2.5 to 3.5 drifting distances. Both specimens were related to the base specimen. Cases A, B, C, and D gave an energy dissipation potential of less than one base specimen in the respective specimen in areas 1 and 2 of the loading processes. Cases G and H have given an energy dissipation potential comparable to the base in all areas (1,2 and 3).

5.3. Analysis of secant stiffness

As a result of reversing and repetitive acts of monotonic loading, the stiffness of the Concrete Bridge Pier structure will deteriorate. Similarly, stiffness is often decreased along with an increase in load after plasticization effects have occurred. Secant stiffness related techniques use secant stiffness at the design reaction stage and the principle of equal viscous damping to describe the nonlinear behavior of structural structures [42]. Fig. 7. It also demonstrates how the secant or effective stiffness, K_{eff}, is defined as the strength ratio, VB, to the maximum possible displacement. In all modeled cases, the secant stiffness is assumed to be the slope of the straight line which connects the peak loads to the positive displacement of the load versus the displacement enveloping at each stage of deformation. To determine this stiffness loss, the secant stiffness is measured at various loading stages during the simulated monotonic load rise. Relationships are seen in Fig. 8. The simulated cases in the following plots have been compared with the mesh experimental plots. The simulation of the experimental case base revealed a poor qualitative response to stiffness. Although CFRP had a higher modulus than concrete, its area and height increase did not compensate for the reduction of the stiffness response from case D to case E. This difference is reduced as tensile damage in concrete progress being no appreciated for the highest loads. Declining the separation between the concrete of the CFRP sheet (case D and F compared with case A) reduced the stiffness of the system although differences tended to decrease as load increased and the tensile damage progress. Removing a significant part of the bottom CFRP (case E) was associated with the lowest stiffness all simulated test long. Cases G and H showed greater stiffness than the experimental case. Both had greater concrete area than the comparison case, being more effective.

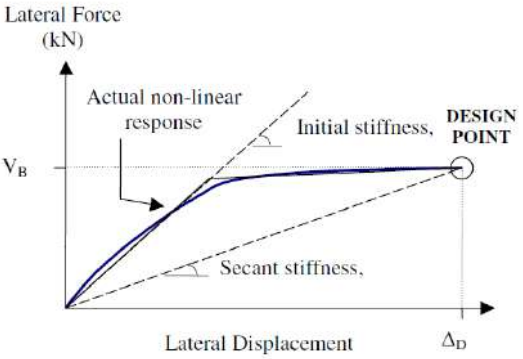

Fig. 7 Usage of initial-stiffness and secant stiffness concepts related to the complete non-linear response of the structure and its equation [42].

6. Conclusions

In this research, a comprehensive numerical analysis was performed to investigate the seismic strengthening of the concrete bridge pier, Hybrid systems, such as the carbon fiber-reinforced polymer (CFRP) sheet attached to the concrete, the Near-Surface-Mounted (NSM)-CFRP bar, and the Concrete jacket. Nine Concrete bridge pier systems with various geometries were simulated assuming concrete damaged plasticity (CDP). One of them was used to fit model parameters with experimental available results

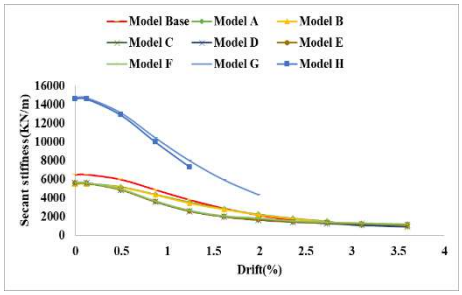

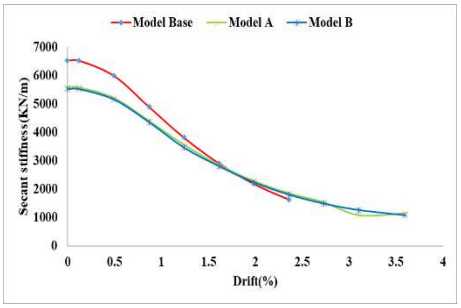

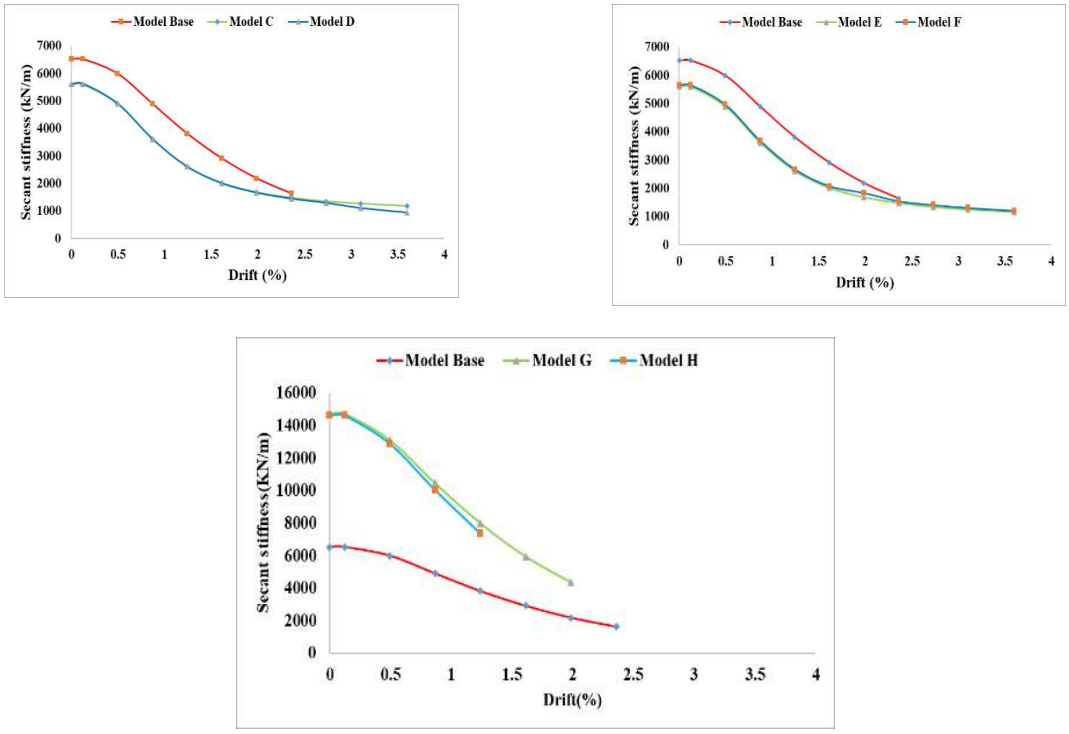

Fig. 8. Secant stiffness evolution

and the other seven to analyze possible alternative design options. From the pieces of evidence, it is possible to conclude:

1. The recommended model fitted full experimental force-displacement curves with a slight underestimation of the maximum load-bearing capacity of less than 3%.

2. Concrete damage plasticity dilation angle and viscosity are the most sensitive parameters to be adjusted in the model.

3. Increasing the width of concrete did not provide greater load-bearing capacity per unit width but a slightly stiffer response because of the higher proportion of concrete in the section.

4. Results showed that increasing the concrete cross-section significantly increased the load-bearing capacity. Cases A and B, showed similar capacities, so increasing the height of the CFRP bar (NSM) is no effect if the CFRP-concrete jacket connection is assured

5. The retrofitting techniques using a CFRP sheet and NSM-CFRP bar demonstrated that the strength and capability of the concrete bridge pier could be significantly improved, especially to strengthen the strength. The lateral carriage capability of the bridge pier increased by over 60% after reinforcement. Some problems remain, such as how the cost-efficient use of reinforcing materials in real structures to achieve a satisfactory outcome are needed for further study.

References

[1] O. Hassanshahi, T. A. Majid, T. L. Lau, A. Yousefi, and R. M. K. Tahara, “Seismic performance of the typical RC beam–column joint subjected to repeated earthquakes,” 2017, p. 120014. doi: 10.1063/1.5005755.

[2] C. L. Oh, K. K. Choong, T. Nishimura, J.-Y. Kim, and O. Hassanshahi, “Shape change analysis of tensegrity models,” Latin American Journal of Solids and Structures, vol. 16, no. 7, 2019, doi: 10.1590/1679-78255407.

[3] A. Mahboob, L. Gil, E. Bernat-Maso, and A. R. Eskenati, “Experimental and Numerical Study of Shear Interface Response of Hybrid Thin CFRP–Concrete Slabs,” Materials, vol. 14, no. 18, p. 5184, Sep. 2021, doi: 10.3390/ma14185184.

[4] A. Mahboob, L. Gil, E. Bernat-Maso, and A. R. Eskenati, “Flexible Fiber Fabric for FRP–Concrete Connection of Thin

Hybrid Slabs," Polymers (Basel), vol. 13, no. 17, p. 2862, Aug. 2021, doi: 10.3390/polym13172862.
[5] A. Salles, M. Salati, and L. Bragança, "Analyzing the Feasibility of Integrating Urban Sustainability Assessment Indicators with City Information Modelling (CIM)," Applied System Innovation, vol. 6, no. 2, p. 45, Mar. 2023, doi: 10.3390/asi6020045.
[6] G. M. Dalfré and J. A. O. Barros, "NSM technique to increase the load carrying capacity of continuous RC slabs," Eng Struct, vol. 56, pp. 137–153, Nov. 2013, doi: 10.1016/j.engstruct.2013.04.021.
[7] S. Abbasi, A. Mahboob, H. Bakhtiari Zamani, M. R. Bilesan, E. Repo, and A. Hakimi, "The Tribological Behavior of Nanocrystalline TiO2 Coating Produced by Plasma Electrolytic Oxidation," J Nanomater, vol. 2022, pp. 1–13, Jan. 2022, doi: 10.1155/2022/5675038.
[8] H. Lee, W. T. Jung, and W. Chung, "Field test of an old RC bridge before and after NSM strengthening," Compos Struct, vol. 202, pp. 793–801, Oct. 2018, doi: 10.1016/j.compstruct.2018.04.024.
[9] A. Mahboob, O. Hassanshahi, and A. S. Tabrizi, "Three-dimensional simulation of granular materials by discrete element method (DEM) by considering the fracture effect of particles," Journal of Civil Engineering Researchers, vol. 5, no. 2, pp. 14–28, 2023.
[10] A. R. Eskenati, A. Mahboob, A. Alirezaie, R. Askari, and S. M. S. Kolbadi, "INVESTIGATING THE EFFECT OF LONGITUDINAL GALLERY ON DYNAMICAL RESPONSE OF GRAVITY CONCRETE DAMS USING FEM," Journal of Southwest Jiaotong University, vol. 56, no. 4, pp. 804–811, Aug. 2021, doi: 10.35741/issn.0258-2724.56.4.69.
[11] A. R. Eskenati, A. Mahboob, E. Bernat-Maso, and L. Gil, "Experimental and Numerical Study of Adhesively and Bolted Connections of Pultruded GFRP I-Shape Profiles," Polymers (Basel), vol. 14, no. 5, p. 894, Feb. 2022, doi: 10.3390/polym14050894.
[12] M. Salati, L. Bragança, and R. Mateus, "Sustainability Assessment on an Urban Scale: Context, Challenges, and Most Relevant Indicators," Applied System Innovation, vol. 5, no. 2, p. 41, Apr. 2022, doi: 10.3390/asi5020041.
[13] J. A. Bogas and A. Gomes, "Analysis of the CFRP flexural strengthening reinforcement approaches proposed in Fib bulletin 14," Constr Build Mater, vol. 22, no. 10, pp. 2130–2140, Oct. 2008, doi: 10.1016/j.conbuildmat.2007.07.025.
[14] W. Y. Peen, C. K. Keong, and O. Hassanshahi, "Behaviour of hollow circular section with multiple perforations under compression, flexure and torsion," Latin American Journal of Solids and Structures, vol. 16, no. 2, 2019, doi: 10.1590/1679-78255387.
[15] M. Abedi et al., "A self-sensing and self-heating planar braided composite for smart civil infrastructures reinforcement," Constr Build Mater, vol. 387, p. 131617, Jul. 2023, doi: 10.1016/j.conbuildmat.2023.131617.
[16] P. Silva and R. Kanitkar, "ACI 440.2 R and The New Seismic Strengthening Guidelines Using FRP," Special Publication, vol. 327, pp. 20–21, 2018.
[17] M. M. Hassan and A. Deifalla, "Evaluating the new CAN/CSA-S806-12 torsion provisions for concrete beams with FRP reinforcements," Mater Struct, vol. 49, no. 7, pp. 2715–2729, Jul. 2016, doi: 10.1617/s11527-015-0680-9.
[18] S. MOTAMEDPOOYA and E. ASNAASHARI, "Organizational project management maturity from the construction practitioners point of view," 2016.
[19] A. R. Eskenati, A. Mahboob, E. Bernat-Maso, and L. Gil, "Characterizing the Structural Behavior of FRP Profiles—FRCM Hybrid Superficial Elements: Experimental and Numerical Studies," Polymers (Basel), vol. 14, no. 6, p. 1076, Mar. 2022, doi: 10.3390/polym14061076.
[20] A. Mahboob, A. R. Eskenati, and S. Moradalizadeh, "Numerical Investigation and Cost Analysis of FRP-Concrete Unidirectional Hybrid Slabs," International Journal of Applied Mechanics and Engineering, vol. 26, no. 4, pp. 156–166, Dec. 2021, doi: 10.2478/ijame-2021-0056.
[21] A. Yousefi, N. M. Bunnori, M. Khavarian, O. Hassanshahi, and T. A. Majid, "Experimental investigation on effect of multi-walled carbon nanotubes concentration on flexural properties and microstructure of cement mortar composite," 2017, p. 020032. doi: 10.1063/1.5005663.
[22] N. Uddin, S. Cauthen, L. Ramos, and U. K. Vaidya, "Vacuum assisted resin transfer molding (VARTM) for external strengthening of structures," in Developments in Fiber-Reinforced Polymer (FRP) Composites for Civil Engineering, Elsevier, 2013, pp. 77–114. doi: 10.1533/9780857098955.1.77.
[23] M. Abedi et al., "A sustainable cementitious composite reinforced with natural fibers: An experimental and numerical study," Constr Build Mater, vol. 378, p. 131093, May 2023, doi: 10.1016/j.conbuildmat.2023.131093.
[24] A. Mahboob, O. Hassanshahi, A. Hakimi, and M. Safi, "Evaluating the Performance of Hollow Core Slabs (HCS)-Concrete and Simplifying Their Implementation," Recent Prog Mater, vol. 05, no. 02, pp. 1–15, Apr. 2023, doi: 10.21926/rpm.2302016.
[25] M. Abedi, O. Hassanshahi, J. A. O. Barros, A. Gomes Correia, and R. Fangueiro, "Three-dimensional braided composites as innovative smart structural reinforcements," Compos Struct, vol. 297, p. 115912, Oct. 2022, doi: 10.1016/j.compstruct.2022.115912.
[26] M. Golabchi and E. Asnaashari, "Identification of Iran's road construction project risks in order to implement sustainable development (Pavement Technologies and Construction Activities)".
[27] X. Chen, M. Ding, X. Zhang, Z. Liu, and H. Ma, "Experimental investigation on seismic retrofit of gravity railway bridge pier with CFRP and steel materials," Constr Build Mater, 2018, doi: 10.1016/j.conbuildmat.2018.06.102.
[28] Simulia, "Abaqus User's Manual version 2019," Dassault Systèmes Simulia Corp.: Providence, RI, USA. 2019.
[29] J. Lubliner, J. Oliver, S. Oller, and E. Oñate, "A plastic-damage model for concrete," Int J Solids Struct, 1989, doi: 10.1016/0020-7683(89)90050-4.

[30] J. Lee and G. L. Fenves, "Plastic-Damage Model for Cyclic Loading of Concrete Structures," J Eng Mech, 1998, doi: 10.1061/(asce)0733-9399(1998)124:8(892).
[31] H. Behnam, J. S. Kuang, and B. Samali, "Parametric finite element analysis of RC wide beam-column connections," Comput Struct, 2018, doi: 10.1016/j.compstruc.2018.04.004.
[32] I. A. Sharaky, M. Baena, C. Barris, H. E. M. Sallam, and L. Torres, "Effect of axial stiffness of NSM FRP reinforcement and concrete cover confinement on flexural behaviour of strengthened RC beams: Experimental and numerical study," Eng Struct, 2018, doi: 10.1016/j.engstruct.2018.07.062.
[33] Y. sumer, "Defining parameters for concrete damage plasticity model," Challenge Journal of Structural Mechanics, 2015, doi: 10.20528/cjsmec.2015.07.023.
[34] Z. Wu, X. Wang, X. Zhao, and M. Noori, "State-of-the-art review of FRP composites for major construction with high performance and longevity," International Journal of Sustainable Materials and Structural Systems, 2014, doi: 10.1504/ijsmss.2014.062757.
[35] D. Zhang, Q. Zhao, F. Li, and Y. Huang, "Experimental and numerical study of the torsional response of a modular hybrid FRP-aluminum triangular deck-truss beam," Eng Struct, 2017, doi: 10.1016/j.engstruct.2016.12.007.
[36] D. Kent and R. Park, "FLEXURAL MEMBERS WITH CONFINED CONCRETE," Journal of the Structural Division, 1971.
[37] A. Demir, N. Caglar, H. Ozturk, and Y. Sumer, "Nonlinear finite element study on the improvement of shear capacity in reinforced concrete T-Section beams by an alternative diagonal shear reinforcement," Eng Struct, 2016, doi: 10.1016/j.engstruct.2016.04.029.
[38] A. Ganganagoudar, T. G. Mondal, and S. Suriya Prakash, "Analytical and finite element studies on behavior of FRP strengthened RC beams under torsion," Compos Struct, 2016, doi: 10.1016/j.compstruct.2016.07.014.
[39] I. Vilanova, L. Torres, M. Baena, and M. Llorens, "Numerical simulation of bond-slip interface and tension stiffening in GFRP RC tensile elements," Compos Struct, 2016, doi: 10.1016/j.compstruct.2016.06.048.
[40] M. H. Seleem, I. A. Sharaky, and H. E. M. Sallam, "Flexural behavior of steel beams strengthened by carbon fiber reinforced polymer plates - Three dimensional finite element simulation," Mater Des, 2010, doi: 10.1016/j.matdes.2009.09.010.
[41] V. V. Degtyarev, "Concentrated load distribution in corrugated steel decks: A parametric finite element study," Eng Struct, 2020, doi: 10.1016/j.engstruct.2019.110158.
[42] T. J. Sullivan, G. M. Calvi, and M. J. N. Priestley, "Initial Stiffness Versus Secant Stiffness in Displacement Based Design," 13th World Conference on Earthquake Engineering, 2004.

Journal of Civil Engineering Researchers

J-Researchers

JOURNAL OF CIVIL ENGINEERING RESEARCHERS

Influence of Vegetation in The Flood Drainage Ditch

Golnoosh Toosi[a,*]

[a]*Department of Industrial Engineering, K. N. Toosi University of Technology, Tehran, Iran*

Journals-Researchers use only: Received date: 2023.06.21; revised date: 2023.08.10; accepted date: 2023.09.26

Abstract

Flood drainage ditches serve as critical infrastructure, directing and managing floodwaters to prevent indiscriminate flow, reduce flooding risks, and curb erosion. Vegetation plays a crucial role in enhancing the effectiveness of these ditches. It acts as a natural barrier, mitigating floodwater speed and impact while stabilizing soil and preventing erosion. Furthermore, vegetation aids in water quality improvement by filtering pollutants and nutrients, making it safer for humans, animals, and plants. It also reduces peak flows and attenuates floodwaters, thereby minimizing urban flooding risks. Additionally, the presence of vegetation in floodplains provides extra storage capacity for excess water, supporting floodplain management and biodiversity conservation. The study emphasizes the importance of carefully considering vegetation type, characteristics, and management practices to optimize flood drainage ditch performance. Selection of suitable plant species and morphological optimization significantly enhances drainage capacity and infiltration rates. Proper maintenance and management practices are vital to ensure unimpeded water flow and prevent obstruction. (DOI:**https//doi.org/10.52547/JCER.5.4.16**)

Keywords: Vegetation; Flood drainage ditches; Soil stabilization; Erosion.

1. Introduction

Flood drainage ditches are essential in reducing the impact of floods. These ditches help to control the water flow by directing it to a safe location where it can be absorbed into the ground or diverted away from property and communities. Without flood drainage ditches, water would flow indiscriminately, leading to severe flooding and erosion. They play a crucial role in preventing floods by providing a way for water to move away from areas where it can cause damage [1, 2].

Vegetation is equally important in the prevention of floods. Vegetation acts as a natural buffer against floods by reducing the speed and impact of floodwaters. Trees, grasses, and other vegetation hold the soil in place, preventing erosion and reducing the amount of sediment that can be carried away by floodwaters. Vegetation also increases the absorption of water, reducing the amount of water that reaches streams and rivers, and thus reducing the risk of flooding [3-5].

When vegetation is planted near a flood drainage ditch, it not only provides an additional barrier to the flow of water but also helps to filter the water.

* Corresponding author. Tel.: +989109130035; e-mail: golnoosh2c@gmail.com.

Vegetation helps to remove pollutants from the water, preventing them from entering rivers and streams. As a result, flood drainage ditches and vegetation work together to provide multiple benefits for the environment and communities [7, 8].

Figure 1. Vegetation in The Flood Drainage Ditch after and before flood [6]

Flood drainage ditches and vegetation are also essential for the preservation of wildlife habitats. The ditches provide a source of water for many animals, while vegetation provides food and shelter. This makes it possible for wildlife to thrive in areas prone to flooding, improving the overall health and diversity of the ecosystem [9].

Finally, flood drainage ditches and vegetation have economic benefits. By reducing the risk of flooding, they protect property and infrastructure, reducing the need for costly repairs and insurance claims. Additionally, they can increase the value of nearby properties by improving the quality of life in the area. These benefits make the installation of flood drainage ditches and vegetation a worthwhile investment for both individuals and communities [10, 11].

2. The Role of Vegetation in Enhancing Flood Water Quality in Drainage Ditches

The presence of vegetation helps to filter the floodwater by removing pollutants and other harmful substances from the water. This enhances the quality of the water, making it safer for people, animals, and plants. Vegetation also helps to slow down the flow of water, reducing the likelihood of erosion and sedimentation, which can lead to further water quality issues [12].

Vegetation acts as a natural filter, removing nutrients and other pollutants from the floodwater. The roots of the plants absorb and retain nutrients, preventing them from entering streams and rivers, where they can cause harmful algal blooms and other water quality issues. The plants also absorb heavy metals, pesticides, and other chemicals, preventing them from entering the water supply and harming aquatic life [13, 14].

The presence of vegetation in drainage ditches helps to stabilize the soil, reducing erosion and sedimentation. When soil erodes, it can carry pollutants, nutrients, and other harmful substances into waterways, leading to water quality issues. Vegetation helps to prevent this by holding the soil in place with their roots. As a result, the floodwater that passes through the drainage ditches is cleaner and less likely to cause damage to the surrounding environment [15, 16]. Vegetation also provides habitat and food for wildlife. By enhancing the water quality in drainage ditches, vegetation creates a healthy ecosystem that supports a diverse range of wildlife, including fish, birds, insects, and mammals. This, in turn, helps to maintain the overall health and balance of the ecosystem [17].

3. Vegetation Effects on Hydraulic Performance of Flood Drainage Ditches

Vegetation has a significant impact on the hydraulic performance of flood drainage ditches. The presence of vegetation can affect the flow of water

through the ditches, the amount of sediment that is carried away, and the overall capacity of the ditches to manage floodwaters. Understanding these effects is essential for designing effective drainage systems that can minimize the risk of flooding and erosion [18].

The presence of vegetation along a river causes an increase in roughness, leading to a reduction in the average speed of water flow, diminished flow energy, and alterations in the velocity profile across the river's cross-section. During floods, many natural canals and rivers become covered with vegetation. The roughness of a canal is significantly influenced by plants, thereby exerting a substantial impact on flow resistance during floods. The resistance to flow caused by the roughness of plants is dependent on flow conditions and the type of vegetation present. Therefore, when modeling the current velocity in a canal, it is essential to consider the effects of velocity, flow depth, and the specific vegetation type along the canal. A total of 48 models were simulated to examine the impact of roughness in the canal. The results revealed that when the velocity is increased, the influence of vegetation on reducing the velocity of the riverbed is negligible. However, when the current speed is lower, the effect of vegetation on decreasing the riverbed velocity is significantly notable [19, 20].

[21] research examines how foliage and reconfiguration of riparian plants impact water flow and mixing in partially vegetated channels. The study investigates velocity patterns, turbulent structures, and momentum transport at the vegetation-water interface. Findings show that foliage increases velocity differences, enhances shear layer mixing, and complex plant reconfiguration improves lateral momentum transport.

Vegetation also plays a critical role in stabilizing the soil in flood drainage ditches. The roots of the plants help to hold the soil in place, preventing erosion and sedimentation. This is particularly important in areas with high water flows, where soil erosion can cause significant damage to surrounding property and infrastructure. In addition, vegetation can help to trap sediment, preventing it from being carried away and reducing the overall capacity of the drainage system [22].

The type of vegetation present in flood drainage ditches can also affect their hydraulic performance. Trees, for example, can have a significant impact on the capacity of the drainage system, as their roots can grow into the ditch and reduce its overall capacity. On the other hand, grasses and other smaller plants can be beneficial in improving the hydraulic performance of the drainage system, as they can help to filter the water and reduce the amount of sediment that is carried away [23].

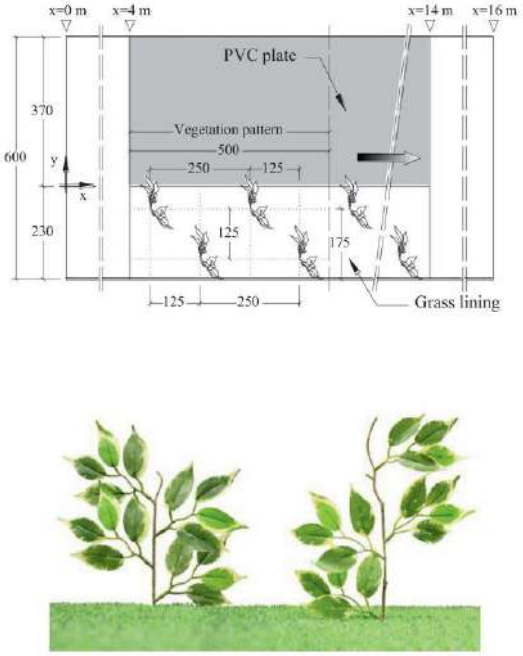

Figure 2. Top view of the experimental flume with the repetitive vegetation pattern and flume coordinate system [21]

Different categories of aquatic vegetation: submerged, emerged, and suspended investigated by [24]. Suspended vegetation, which floats without rooting, can have negative effects by blocking sunlight and clogging waterways, but also positive aspects like biogas production. While ecological impacts of suspended vegetation have been studied, hydrodynamic properties of its flow are less explored. Previous research on open-channel flow with submerged vegetation focused on phenomena like shearing vortices. [25]'s study examined turbulent flow through suspended vegetation, developing an analytical model for vertical velocity and Reynolds stress distribution.

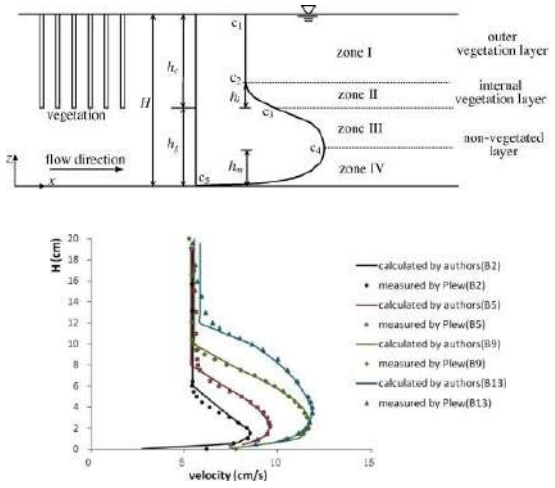

Figure 3. a) experiment flume [24] b) [24] vs [25] results

4. The Effectiveness of Vegetation in Flood Control and Management

4.1. Vegetation as a Natural Barrier

Vegetation, including trees, shrubs, and grasses, acts as a natural barrier against flooding. Their roots help to stabilize soil, reducing erosion and maintaining the integrity of riverbanks. By holding the soil together, vegetation minimizes sedimentation in rivers and streams, thus preventing the accumulation of debris that can obstruct water flow [26-28].

4.2. Absorption and Retention of Water

Vegetation plays a vital role in absorbing and retaining excess water during heavy rainfall. The leaves and branches of plants intercept rainfall, reducing the speed at which water reaches the ground. This process, known as interception, helps to delay and slow down the runoff, allowing more time for infiltration into the soil. Vegetation also enhances soil permeability, promoting water absorption and reducing surface runoff [29].

4.3. Reduction of Peak Flows

The presence of vegetation along riverbanks and in floodplains can significantly reduce the peak flows during flood events. Vegetation acts as a buffer, absorbing and storing water, thereby attenuating the intensity of floodwaters. By slowing down the flow rate, vegetation reduces the pressure on river channels and flood control infrastructure, reducing the risk of breaches and overflow [30].

4.4. Improved Floodplain Management

Vegetation in floodplains plays a crucial role in flood management strategies. Floodplain vegetation acts as a natural floodwater storage area, allowing excess water to spread out horizontally. This process, known as floodplain attenuation, reduces the volume and velocity of floodwaters downstream, minimizing the risk of flooding in urban areas. Additionally, floodplain vegetation provides habitat for diverse plant and animal species, contributing to biodiversity conservation [31, 32].

4.5. Long-Term Benefits and Sustainability

The effectiveness of vegetation in flood control and management extends beyond immediate flood events. By promoting sustainable land management practices, including reforestation and the preservation of wetlands, vegetation contributes to long-term flood risk reduction. Vegetation also improves water quality by filtering pollutants and nutrients, enhancing overall ecosystem health [33].

5. The Influence of Vegetation Type and Characteristics on Flood Drainage Ditch Performance

5.1. Vegetation Type

The type of vegetation present in flood drainage ditches can have a profound impact on their performance. Different plant species exhibit varying characteristics, such as root structure, density, and water absorption capacity. Grasses, for example, with their fibrous root systems, can effectively stabilize the soil, preventing erosion and maintaining the structural integrity of the ditch. Additionally, grasses can enhance infiltration rates, allowing water to penetrate the soil more readily [34-36].

5.2. Root Characteristics

The root characteristics of vegetation within flood drainage ditches significantly influence their drainage capacity. Plants with deep and extensive root systems, such as certain tree species, can help to enhance water infiltration and improve soil permeability. These roots create pathways for water to move vertically and horizontally, reducing the potential for waterlogging and enhancing drainage efficiency [37].

5.3. Vegetation Density

The density of vegetation in flood drainage ditches is another crucial factor by affecting Manning coefficient. A dense cover of vegetation can effectively slow down the flow of water, allowing more time for infiltration and reducing the velocity of runoff. This reduced flow velocity minimizes erosion and sedimentation, preventing the accumulation of debris that may impede drainage. However, excessive vegetation density should be avoided, as it may impede the flow of water and increase the risk of blockages [38, 39].

5.4. Plant Growth Patterns

The growth patterns of vegetation within flood drainage ditches also impact their performance. Plants that exhibit rapid growth and regrowth rates can help maintain the effectiveness of the ditch over time. Such vegetation can quickly recover from flood events, ensuring continuous drainage capacity and reducing the need for frequent maintenance interventions [40, 41].

6. Future Directions for Research and Implementation of Vegetation in Flood Drainage Ditches

Future research and implementation of vegetation in flood drainage ditches should focus on key areas. This includes selecting plant species suitable for the conditions of flood drainage ditches and understanding the relationships between vegetation morphology and drainage performance. Research should investigate root depth, density, leaf characteristics, and growth rates. Additionally, the impact of climate change on vegetation performance in flood drainage ditches must be examined. Optimization of maintenance practices, such as vegetation trimming and control of density, is necessary for unimpeded water flow and ecological benefits. Integration of modeling approaches, like hydrological and vegetation growth models, can enhance understanding of vegetation-drainage interactions. Collaboration between researchers, engineers, policymakers, and communities is essential for successful implementation and resilient flood management strategies.

7. Conclusion

In conclusion, the combination of flood drainage ditches and vegetation offers a highly effective approach to flood control and management. Flood drainage ditches serve as essential infrastructure for directing and managing floodwaters, preventing indiscriminate water flow, and reducing the risk of flooding and erosion. Vegetation, on the other hand, plays a crucial role in enhancing the effectiveness of flood drainage ditches.

Vegetation acts as a natural barrier against floods, reducing the speed and impact of floodwaters while stabilizing soil and preventing erosion. It improves water quality by filtering pollutants and nutrients, making it safer for humans, animals, and plants. Moreover, vegetation helps to reduce peak flows and attenuate floodwaters, minimizing the risk of flooding in urban areas. The presence of vegetation in floodplains provides additional storage capacity for excess water, enhancing floodplain management and supporting biodiversity conservation.

Furthermore, the influence of vegetation type, characteristics, and management practices on flood drainage ditch performance should be carefully considered. Selecting suitable plant species and optimizing vegetation morphology can significantly enhance drainage capacity and infiltration rates. Proper maintenance and management practices are essential for ensuring unimpeded water flow while preventing obstruction.

Future research should focus on species adaptation to changing climatic conditions, modeling and simulation of vegetation-drainage interactions, and promoting interdisciplinary collaboration to bridge the gap between research and practical implementation. By addressing these future directions, the effectiveness of vegetation in flood control and management can be further improved, leading to resilient flood management strategies, enhanced water quality, ecological benefits, and economic advantages.

Overall, the integration of flood drainage ditches and vegetation provides multiple benefits, including flood risk reduction, improved water quality, wildlife habitat preservation, and economic advantages. Embracing and implementing this approach will contribute to more sustainable and effective flood management practices, ensuring the safety and well-being of communities and the environment.

References

[1] M. M. Santos, A. V. Ferreira, and J. C. Lanzinha, "The Possibilities of Capturing Rainwater and Reducing the Impact of Floods: A Proposal for the City of Beira, Mozambique," Sustainability, vol. 15, no. 3, p. 2276, 2023.

[2] R. Vaduva and R. M. Rusu, "LAND USE PLANNING TO REDUCE THE IMPACT OF FLOODING IN URBAN AREAS," International Multidisciplinary Scientific GeoConference: SGEM, vol. 3, p. 761, 2012.

[3] W. H. Patrick Jr, D. S. Mikkelsen, and B. Wells, "Plant nutrient behavior in flooded soil," Fertilizer technology and use, pp. 197-228, 1985.

[4] R. A. Machado, A. G. Oliveira, and R. C. Lois-González, "Urban ecological infrastructure: The importance of vegetation cover in the control of floods and landslides in Salvador/Bahia, Brazil," Land use policy, vol. 89, p. 104180, 2019.

[5] G. Boedeltje, J. P. Bakker, A. Ten Brinke, J. M. Van Groenendael, and M. Soesbergen, "Dispersal phenology of hydrochorous plants in relation to discharge, seed release time and buoyancy of seeds: the flood pulse concept supported," Journal of Ecology, vol. 92, no. 5, pp. 786-796, 2004.

[6] H. Grežo et al., "Flood risk assessment for the long-term strategic planning considering the placement of industrial parks in Slovakia," Sustainability, vol. 12, no. 10, p. 4144, 2020.

[7] J. Cooper, J. Gilliam, R. Daniels, and W. Robarge, "Riparian areas as filters for agricultural sediment," Soil science society of America journal, vol. 51, no. 2, pp. 416-420, 1987.

[8] Z. Rosolova, A. Baylis, S. Rose, and A. Parrott, "Energy crops on floodplains–flood risk or benefit," in Geophysical Research Abstracts, 2010, vol. 12, p. 6681.

[9] I. Herzon and J. Helenius, "Agricultural drainage ditches, their biological importance and functioning," Biological conservation, vol. 141, no. 5, pp. 1171-1183, 2008.

[10] P. Li et al., "The Formation and Development of a Dam System in a Small Watershed in the Loess Plateau," Check Dam Construction for Sustainable Watershed Management and Planning, pp. 1-21, 2022.

[11] N. Z. Huang, J. M. Zhong, and S. Deng, "Vision of curriculum and teaching from ecological sustainability," in MATEC Web of Conferences, 2016, vol. 63: EDP Sciences, p. 05005.

[12] S. Mielke and J. Rockney, "Aquatic Vegetation Density Mapping-BioBase 2015 Report," Prior Lake–Spring Lake Watershed District: Prior Lake, MN, USA, 2016.

[13] E. Denman, P. May, and G. Moore, "The potential role of urban forests in removing nutrients from stormwater," Journal of environmental quality, vol. 45, no. 1, pp. 207-214, 2016.

[14] R. Hubbard, G. Gascho, and G. Newton, "Use of floating vegetation to remove nutrients from swine lagoon wastewater," Transactions of the ASAE, vol. 47, no. 6, p. 1963, 2004.

[15] T. Elahi, M. Islam, and M. Islam, "Effect of vegetation and nailing for prevention of landslides in Rangamati," in Proceedings, international conference on disaster risk mitigation (ICDRM 2019), Dhaka, Bangladesh, 2019, pp. 193-197.

[16] M. Hann and R. Morgan, "Evaluating erosion control measures for biorestoration between the time of soil reinstatement and vegetation establishment," Earth Surface Processes and Landforms: The Journal of the British Geomorphological Research Group, vol. 31, no. 5, pp. 589-597, 2006.

[17] B. W. Sweeney and J. D. Newbold, "Streamside forest buffer width needed to protect stream water quality, habitat, and organisms: a literature review," JAWRA Journal of the American Water Resources Association, vol. 50, no. 3, pp. 560-584, 2014.

[18] S. H. Keefe, J. S. Daniels, R. L. Runkel, R. D. Wass, E. A. Stiles, and L. B. Barber, "Influence of hummocks and emergent vegetation on hydraulic performance in a surface flow wastewater treatment wetland," Water Resources Research, vol. 46, no. 11, 2010.

[19] M. Feizbahr, N. Tonekaboni, G.-J. Jiang, and H.-X. Chen, "Optimized vegetation density to dissipate energy of flood flow in open canals," Mathematical Problems in Engineering, vol. 2021, pp. 1-18, 2021.

[20] M. Feizbahr, C. Kok Keong, F. Rostami, and M. Shahrokhi, "Wave energy dissipation using perforated and non perforated piles," International Journal of Engineering, vol. 31, no. 2, pp. 212-219, 2018.

[21] G. Caroppi, K. Västilä, J. Järvelä, P. M. Rowiński, and M. Giugni, "Turbulence at water-vegetation interface in open channel flow: Experiments with natural-like plants," Advances in Water Resources, vol. 127, pp. 180-191, 2019.

[22] K. Kobiela-Mendrek, A. Salachna, D. Chmura, H. Klama, and J. Broda, "The Influence of Geotextiles Stabilizing the Soil on Vegetation of Post-Excavation Slopes and Drainage Ditches,"

Journal of Ecological Engineering, vol. 20, no. 1, pp. 125-131, 2019.
[23] J. M. Pijanowski et al., "An Expert Approach to an Assessment of the Needs of Land Consolidation within the Scope of Improving Water Resource Management," Sustainability, vol. 14, no. 24, p. 16651, 2022.
[24] W. Huai, Y. Hu, Y. Zeng, and J. Han, "Velocity distribution for open channel flows with suspended vegetation," Advances in Water Resources, vol. 49, pp. 56-61, 2012.
[25] D. R. Plew, "Depth-averaged drag coefficient for modeling flow through suspended canopies," Journal of Hydraulic engineering, vol. 137, no. 2, pp. 234-247, 2011.
[26] R. Thornton, "HOW DO WE REDUCE VEHICLE RELATED DEATHS: EXPLORING AUSTRALIAN FLOOD FATALITIES," 2015.
[27] T.-Y. Yang and I.-C. Chan, "Drag Force Modeling of Surface Wave Dissipation by a Vegetation Field," Water, vol. 12, no. 9, p. 2513, 2020.
[28] M. Safaei and A. Mahan, "Impact of mechanical and biological watershed treatments on surface runoff," Open Journal of Geology, vol. 8, no. 09, p. 896, 2018.
[29] Q. Chen et al., "A new method for mapping aquatic vegetation especially underwater vegetation in Lake Ulansuhai using GF-1 satellite data," Remote Sensing, vol. 10, no. 8, p. 1279, 2018.
[30] H. Woo, J. S. Kim, K. H. Cho, and H. J. Cho, "Vegetation recruitment on the 'white'sandbars on the N akdong R iver at the historical village of H ahoe, K orea," Water and Environment Journal, vol. 28, no. 4, pp. 577-591, 2014.
[31] B. Hooper, "Floodplain Management and Farmer Decision Behaviour," ed: Centre for Water Policy Research, University of New England, Armidale, New …, 1993.
[32] S. E. Toogood, C. B. Joyce, and S. Waite, "Response of floodplain grassland plant communities to altered water regimes," Plant Ecology, vol. 197, pp. 285-298, 2008.
[33] O. Vigiak, O. Ribolzi, A. Pierret, C. Valentin, O. Sengtaheuanghoung, and A. Noble, "Filtering of water pollutants by riparian vegetation: bamboo versus native grasses and rice in a Lao catchment," UNASYLVA-FAO-, vol. 229, p. 11, 2008.
[34] J. A. P. Manage, "The impact of mechanical harvesting regimes on the species composition of Dutch ditch vegetation: a quantitative approach," Copy, vol. 31, p. 148, 1993.
[35] M. J. Rousta, S. M. Soleimanpour, M. Enayati, and M. Pakparvar, "Effect of Vegetation Type and Soil Chemical Properties on the Organic Carbon Content in the Soil of Flood Spreading Fields of Kowsar Station," Ecology of Iranian Forest, vol. 10, no. 19, pp. 171-182, 2022.
[36] A. Nicosia and V. Ferro, "Flow resistance due to shrubs and woody vegetation," Flow Measurement and Instrumentation, p. 102308, 2023.
[37] H. I. Mohamed, A.-E. M. Abd-Elaal, A. A. Mahmoud, and A. A. Mahmoud, "Flow characteristics of open channels with floating vegetation," JES. Journal of Engineering Sciences, vol. 48, no. 2, pp. 186-196, 2020.
[38] W. G. Xu, H. Y. Zhang, Z. Y. Wang, and W. P. Huang, "A study of manning coefficient related with vegetation density along the vegetated channel," in Applied Mechanics and Materials, 2012, vol. 212: Trans Tech Publ, pp. 744-747.
[39] Y. Li et al., "Flow characteristics in different densities of submerged flexible vegetation from an open-channel flume study of artificial plants," Geomorphology, vol. 204, pp. 314-324, 2014.
[40] D. J. Kerr, H. T. Shen, and S. F. Daly, "Evolution and hydraulic resistance of anchor ice on gravel bed," Cold Regions Science and Technology, vol. 35, no. 2, pp. 101-114, 2002.
[41] A. Errico, G. F. C. Lama, S. Francalanci, G. B. Chirico, L. Solari, and F. Preti, "Flow dynamics and turbulence patterns in a drainage channel colonized by common reed (Phragmites australis) under different scenarios of vegetation management," Ecological Engineering, vol. 133, pp. 39-52, 2019

J-Researchers

JOURNAL OF CIVIL ENGINEERING RESEARCHERS

A Method Based on Fracture Mechanics to Investigate the Deformation of Reinforced Concrete Columns

Houman Mahmoodi Asl[a,*]

[a]*Master graduate, Department of Civil Engineering, Ayatollah Amoli Branch, Islamic Azad University, Amol, Iran*

Journals-Researchers use only: Received date: 2023.03.17; revised date: 2023.08.18; accepted date: 2023.09.17

Abstract

In the use of non-linear structural performance models, including models that consider the critical over-performance at the failure stage, is very important when performing seismic calculations of reinforced concrete buildings and structures.The use of such models is especially important if the structures have primary damage caused by fire or corrosion, as well as mechanical damage caused by force factors. The purpose of this study is to develop an analytical model of the deformation of eccentrically compressed reinforced concrete columns by considering the failure stage, which includes processes such as peeling of the protective layer, reduction of the stability of the compressed reinforcement and softening of the encased concrete after reaching the design strength. , the existing models that describe the residual behavior of reinforced concrete structures under low cycle loading have been investigated. The models are analyzed considering monotonic curves, which are cyclic deformation boundaries.The model proposed in the research is constructed by analyzing the stages of the stress-strain state of a reinforced concrete column. At each stage, formulas are found for determining moment and curvature by solving equations of equilibrium of internal forces. Calculations based on the obtained model for a particular reinforced concrete column are carried out, monotonous diagrams are obtained, and a conclusion about the significant influence of the level of axial load on the character of deformation is made. On the basis of the obtained model, the construction of hysteresis diagrams under low-cycle loading is expected in the future. (DOI:**https//doi.org/10.52547/JCER.5.4.22**)

Keywords: reinforced concrete column, deformation diagram, stages of destruction, hysteresis, seismic, low-cycle loads

1. Note

When performing calculations of reinforced concrete buildings and structures, it is quite important to apply non-linear methods of analysis which allow to ensure economical and reliable structures and to reveal reserves of bearing capacity of the system.

A widespread type of structural system used in seismic areas is the reinforced concrete frame, the feature of which is the perception of the horizontal component of seismic load due to the rigid joint between beams and columns.

* Corresponding author. Tel.: +989125148269; e-mail: shenavar676@gmail.com.

In the nonlinear stage of frames, local areas of elastoplastic deformations occur in the vicinity of the girder support nodes. In accordance with this, in the design diagrams of frames, the nonlinear properties are concentrated in separate areas, which are called plastic joints, while the columns and spanning sections of the beams work elastically [1]. The appearance of plastic joints in columns is considered unacceptable in normal cases.

However, columns designed for elastic operation may suffer some damage during operation, e.g. caused by fire [2], reinforcement corrosion [3], mechanical damage, earthquake, etc.

In such a case, due to the reduced mechanical characteristics, the behavior of the column in the elastic-plastic domain will have to be taken into account when carrying out verification calculations or justifying the reinforcement.

Description of nonlinear behavior of columns and beams in the plastic hinge region is usually carried out with the help of hysteresis diagrams (Figure 1), which take into account degradation of strength and stiffness at low-cycle vibrations, loss of dissipative energy, change of stiffness at opening and closing of cracks (pinching effect) [4]. Hysteresis diagrams are usually plotted in the axes "bending moment-curvature" or "horizontal force horizontal displacement".

The basic element of a hysteresis diagram is the monotonic loading curve, commonly referred to as skeleton curves. The monotonic curve limits the range of possible deformation under low-cycle loading (Figure 1).

The monotonic curves should, wherever possible, take into account the greatest ductility of reinforced concrete structures and include areas of hardening and softening to establish the true nature of the redistribution of forces in the system.

Many hysteresis models of varying degrees of accuracy have been developed by individual researchers.

Let's consider these models in terms of monotonic curves used.

In [5] a bilinear elastic-plastic diagram is proposed which has a linear-elastic first section with an equivalent stiffness Ke, after reaching the bearing capacity the stiffness becomes zero – a yield point occurs. The determination of the value of carrying capacity and equivalent stiffness for a particular structure is a rather complex task, for reinforced concrete columns the method proposed in [6] can be used. Despite its simplicity, the bilinear diagram [5] is quite popular for seismic calculations as it has clear computational advantages.

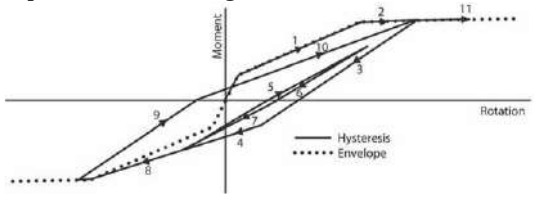

Figure 1. Hysteresis diagram based on the model of Takeda et al. [7]

In the bending of reinforced concrete columns and beams, the redistribution of stresses will cause the individual cross-sectional areas to engage gradually due to the non-linear behaviour of the reinforcement and the concrete. In this way, the bearing capacity of the elements will be realized and the possibility of absorbing a larger moment will be realized. In the deformation diagram, this can be accounted for by introducing a nonzero stiffness after the limit force is reached. This approach is implemented in the bilinear diagram proposed in [8]. The stiffness is usually determined by approximating real curvilinear diagrams obtained from experiments or numerical analysis. The bilinear diagram with strengthening combines computational simplicity and a more accurate account of strengthening effects, which justifies the choice of this model as the basis by other authors [9; 10].

A characteristic feature of reinforced concrete structures is the formation of normal and inclined cracks, which reduce the initial stiffness. In order to account for cracking, a three-line diagram of deformation has been proposed in [7] with a successive decrease in stiffness after the cracking force is reached and then when the yield strength in the reinforcement is reached. This approach makes it possible not only to take into account crack opening at the initial stages of deformation of the element, but also to provide a basis for describing the process of reopening and closing of cracks in subsequent cycles.

In addition to piecewise linear diagrams, some researchers use curvilinear diagrams in their models [11].

This allows a more accurate approximation of the real deformation diagram of the element and takes into account the consistent reduction of stiffness. In practice, this approach is less popular, which is justified by the complexity of the calculations and analysis of the results. It should also be noted that curvilinear diagrams have a rather narrow field of application, since the dependencies describing eccentrically compressed and bendable elements will be different.

Columns and beams adjacent to the frame nodes where the highest bending moments occur, according to the standards of most countries, must be reinforced by densely placed, closed cross clamps, which in addition to providing the strength of the sloping sections act as indirect reinforcement. The indirect reinforcement increases the load-bearing capacity of the elements and the plastic deformation capacity, which contributes to the redistribution of forces in the system and a fuller use of the load-bearing capacity reserves. In addition, after the limit forces are reached, when the stresses in the clamps reach the yield strength, there is no sudden failure of the element, but a gradual reduction in the bearing capacity with increasing plastic deformations follows [12]. Strengthening can take place when such phenomena as loss of stability of compressed reinforcement, geometric nonlinearity, chipping of concrete cover layer are taken into account.

The described processes can be taken into account in models which include a branch of unstrengthening [13].

The model allows to take into account the true nature of force redistribution in the framework more accurately and is particularly relevant when carrying out the analysis of bearing capacity reserves for elements with initial damage [14].

The unstrengthening branch allows taking into account an important aspect of low-cycle operation of reinforced concrete elements, such as within-cycle degradation of strength. This is especially important in loading programs with sharply varying amplitudes, which can lead to sudden collapse of the structure.

The hysteresis diagrams were further developed in [15], which takes into account the presence of residual strength after unstrengthening, which is observed in tests of reinforced concrete structures under low-cycle loading.

The presence of residual strength makes it possible to take into account the incomplete disconnection of an element from operation and an increase in the resilience of the structural system as a whole when performing calculations based on the criterion of no collapse.

It should be noted that the description of the reference points of hysteresis diagrams can be made in different ways. The most common approach is the approximation of experimental diagrams or by using empirical dependencies, e.g. in [15]. This method can also be applied in combination with diagrams derived from numerical calculations [14]. This somewhat limits the scope of application of the model and does not allow direct consideration of processes related to concrete rebound, loss of reinforcement stability, etc.

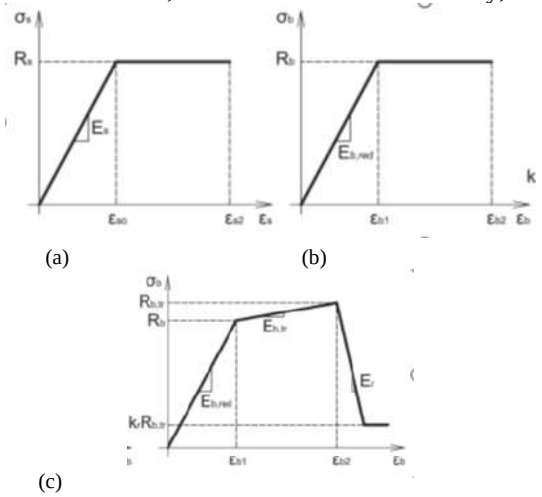

Figure 2. Deformation diagrams of materials:
a – reinforcement; b – unconfined concrete; c – confined concrete

Another approach would be to plot the diagrams based on taking into account the dissipation energy on the oscillation cycle. In this case, the dissipation energy can have either a constant value [16] or it can decrease with time based on the experimental dependence [17]. This approach allows a more accurate account of the energy dissipated by the structure at each cycle, however, it has the same drawbacks as the first one.

A more accurate way of setting the monotonic curve is the method based on the analysis of the stages of the stress-strain state (STS) of a reinforced concrete element. The procedure of the method is based on the identification of reference points in the diagram where

the change in stiffness is observed. In this case, forces and displacements can be found both analytically and numerically. For bendable reinforced concrete elements such a diagram has been obtained in [18], which, however, does not take into account the branch of softening after reaching the limit force.

In this paper, the method based on the stages of the stress-strain diagram for the monotonic deformation of reinforced concrete columns is used to construct a monotonic deformation diagram.

This approach is a generalization of the method of ultimate forces, which is accepted in domestic and foreign design standards, taking into account the specific features of work of reinforced concrete element at the stage of failure: the value of axial load, the presence of indirect reinforcement in the form of clamps, concrete spalling of protective layer, loss of stability of compressed reinforcement, the presence of residual carrying capacity.

2. Methods and materials

As noted above, the basis for constructing a monotonic diagram will be to consider the actual deformation pattern of the reinforced concrete column and to identify the characteristic stages at which the stiffness will change and the transition to a new stage of the stress-strain state will be observed.

The monotonic diagram will be plotted in the axis "bending moment M – curvature ρ". For a given column, the longitudinal force N is assumed to be constant during all loading phases. Such a diagram can serve as a basis for the transition to the horizontal force-displacement relation, in which case not only the bending stiffness but also the shear stiffness must be considered, and the displacements caused by the slip of the reinforcement must also be taken into account [18].

The diagram is based on a number of general assumptions inherent to the limit force method: – flat section hypothesis – the cross-sections are flat before deformation and remain so afterwards; – the following state diagrams are adopted for the materials: bilinear for compressed concrete (Figure 2, a) and reinforcement (Figure 2, b); three-linear for concrete bounded by transverse collars (Figure 2, c) [19]; – geometric non-linearity caused by the longitudinal bending of the reinforced concrete column is taken into account by means of an appropriate coefficient η;

– the work of the tensile concrete is taken into account only at stage 1 – before the formation of cracks; – stresses in concrete and reinforcement are found by composing and solving equations of equilibrium.

Assumptions made at specific stages will be described in the course of the presentation.

A general view of the deformation diagram of a reinforced concrete column is shown in (Figure 3).

The diagram has 6 characteristic stages of deformation. Consider each stage separately and determine corresponding values of ultimate bending moment and curvature.

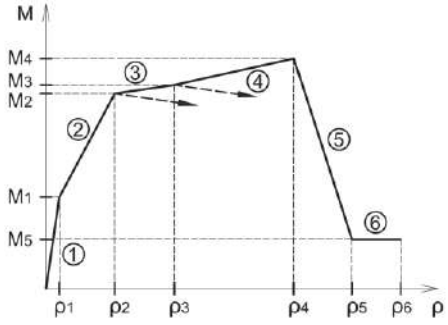

Figure 3. General view of reinforced concrete column deformation model

At the 1st stage (before cracking) the reinforcement and concrete in the tensile zone will be deformed together.

The stress profile in the tensile concrete is non-linear trapezoidal and the highest stresses reach the design tensile strength of concrete Rbt (Figure 4, a).

Compressed concrete works elastically, stress diagrams have a triangular shape. The ultimate bending moment at stage 1 is given by the equation:

$$M_1 = R_{bt} W_{pl} + N e_x \qquad (1)$$

where W_{pl}– elastic-plastic moment of resistance of the section;

$$W_{pl} = 1.3 W_{red} \qquad (2)$$

e_x– distance from the core point furthest from the tensile face to the force application point N;

$$e_x = \frac{W_{red}}{A_{red}} \qquad (3)$$

The curvature corresponding to the moment M1 is determined by the equation

$$p_1 = \frac{M_1}{D_1} \quad (4)$$

where D – bending stiffness of reinforced concrete section at stage 1;

$$D_{1=}E_{b.red}I_{red} \quad (5)$$

In formulae (1)–(5) the geometric characteristics of the reduced section (area A_{red}, moment of inertia I_{red}, resistance torque W_{red}) are determined taking into account the entire cross-section of concrete and reinforcement.

Stage 2 is characterized by the operation after the formation of cracks in the tensile zone. The ultimate force in this stage can be achieved in two cases: the stresses in the reinforcement reach the yield stress R_s (stage 2.1) or the stresses in the concrete throughout the compressed zone have reached their design resistance R_b (stage 2.2). As we know which case the ratio of the relative height of the compressed zone ξ to its boundary value determines ξ_R: $\xi \leq \xi_R$ – case of large eccentricities (stage 2.1); $\xi > \xi_R$ – the case of small eccentricities (stage 2.2). Note here, however, that in the first case, unlike in the second, the element does not enter the fracture stage.

Consider stage 2.1 in more detail (Figure 4, c). As noted, the stresses in the reinforcement at this stage reach the design resistance R_s. Stresses in the compressed concrete and in the compressed reinforcement do not exceed the corresponding design resistance R_b and Rsc. The compressive stresses in the concrete are assumed to be triangular.

The values of the stresses in the concrete and the compressed reinforcement are then determined from the consideration of the deformations in the flat section (flat section hypothesis). If at stage 2.1 the deformations in the tensile reinforcement reach a value of $\varepsilon_s = \varepsilon_{so}$, then the required stresses are found from the expressions

$$\sigma_b = E_{b.red}\frac{\varepsilon_{so}x}{h_o - x} \leq R_b \quad (6)$$

$$\sigma_{sc} = E_s\frac{\varepsilon_{so}(x-a')}{h_o - x} \leq R_{sc} \quad (7)$$

The symbols used in formulae (6) and (7) are given in Figure 4, c.

Note that if the stresses in formula (6) exceed the design resistance, then the stress diagram should be corrected by taking it in trapezoidal form, whereby the boundary between the triangular and rectangular parts of the diagram will be the fiber where the condition is fulfilled $\varepsilon_b = \varepsilon_{b1}$. Composing the equilibrium conditions for the internal forces and the moments of these forces with respect to the center of gravity of the stretched reinforcement, we find the height of the concrete compressed zone and the ultimate bending moment

$$X = \frac{N + R_s A_s - \sigma_{sc} A_s'}{0.5\sigma_b b} \quad (8)$$

$$Ne_{2.1} = \sigma_{sc}A_s'(h_o - a') + \frac{1}{2}\sigma_b x b\left(h_o - \frac{x}{3}\right) \quad (9)$$

where A_s and $A_{s'}$ – the areas of tensile and compressed reinforcement respectively.

The limiting bending moment with respect to the center of gravity will be found by taking into account the effects of longitudinal bending

$$M_i = \frac{Ne_i - N\dfrac{h_o - a'}{2}}{\eta} \quad (10)$$

where *i* – index denoting the stress train stage number; η – coefficient longitudinal bending

$$\eta_i = \frac{1}{1 - \dfrac{N}{N_{cri}}} \quad (11)$$

Where N_{cre}– critical force at *i* stage;

$$N_{cri} = \frac{\pi^2 D_i}{l_0^2} \quad (12)$$

where *lo* – design element length.

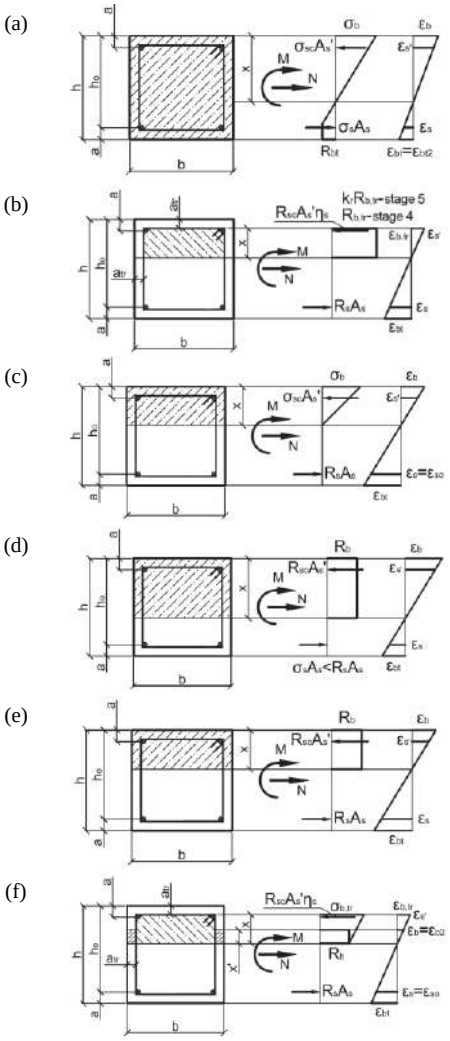

Figure 4. Stages of the stress-strain state of a reinforced concrete column: a – stage 1; b – stages 4 and 5; c – stage 2.1; d – stage 2.2; e – stage 3.1; f – stage 3.2

Stiffness in this and subsequent stages Di we find with the variable height of the compression zone x_m and tensile concrete work between cracks, which is taken into account by the coefficient ψs. The relevant formulas are described in sufficient detail in the regulatory literature (SP63.13330.2018. Concrete and reinforced concrete structures) and, due to their cumbersome nature, are not given in the text of this article.

Stage 2.2 will in turn correspond to the failure stage of the reinforced concrete section for the case of small eccentricities. The stresses in the compressed concrete are distributed according to a rectangular law and are equal to the design resistance *Rb*, in the compressed reinforcement, the stresses also reach the design resistance *Rsc*, and in the stretched one less than the value *Rs* (Figure 4, d). Composing and transforming the equilibrium equations we find

$$x = \frac{N + R_s A_s \frac{1+\xi_R}{1-\xi_R} - R_{sc} A_s{}'}{R_b b + \frac{2R_s A_s}{h_o(1-\xi_R)}} \qquad (13)$$

$$N_{e2.2} = R_s A_s'(h_o - a') + R_b x b(h_o - 0.5x) \qquad (14)$$

The limiting bending moment and curvature will be obtained from formulae (4) and (10).

Stage 3 will also be considered in two variants. In stage 3.1, for elements operating with large eccentricities, a subsequent increase in bending moment due to the yield strength of the tensile reinforcement will result in an increase in compressive stresses in the concrete to the value of R_b and stresses in the compressed reinforcement up to R_{sc} (Figure 4, e). The reinforced concrete section will enter the fracture stage. From the equilibrium conditions we have

$$x = \frac{N + R_s A_s - R_{sc} A_s{}'}{R_b b} \qquad (15)$$

$$N_{e3.1} = N_{e2.2} \qquad (16)$$

In turn, if the element failed at low eccentricities, a transition to stage 3.2 will follow (Figure 4, f). The deformation in this stage will take place until the yield point is reached in the stretched reinforcement. The compressed zone of the concrete will be divided into two parts: a protective layer and a concrete core bounded by transverse collars. If the bending moment increases, the concrete protective layer for the fibers will splinter off, where the relative deformations of the unconfined concrete reach the limit values $\varepsilon_b = \varepsilon_{b2}$. Then only the height of the compressed concrete protection layer will be taken into account in the calculation x'.

At this stage the indirect reinforcement is activated, as a result of which the stresses in the concrete core will increase. The compressive stress profile is

assumed to be trapezoidal with a minimum value at the neutral fibre equal to R_b and maximum value $\sigma_{b.tr}$.

Applying the plane section hypothesis, determine the values of x' and $\sigma_{b.tr}$ considering that the relative deformations in the reinforcement reach the limit values $\varepsilon_s = \varepsilon_{so}$

$$x' = \frac{\varepsilon_{b2}(h_o - x - a_{tr})}{\varepsilon_{so}} \quad (17)$$

$$\sigma_{b.tr} = E_{b.tr}\frac{\varepsilon_{so}x}{h_o - x - a_{tr}} \quad (18)$$

Composing and solving the equilibrium equations we obtain

$$x = \frac{N + R_sA_s - R_{sc}A'_s\eta_s - 2R_bx'a_{tr}}{0.5b(R_b + \sigma_{b3})} \quad (19)$$

$$\begin{aligned} N_{e3.2} = {} & R_{sc}A'_s\eta_s(h_o - a') \\ & + 2R_bx'a_{tr}(h_o - x - a_{tr} + 0.5x') \\ & + R_bxb(h_o - a_{tr} - 0.5x) \\ & + \frac{1}{2}(\sigma_{b.tr} - R_b)xb\left(h_o - a_{tr} \right. \\ & \left. - \frac{x}{3}\right) \end{aligned} \quad (20)$$

where η_s = 0–1 – a coefficient which takes into account the reduced contribution to the load-bearing capacity of the part of reinforcement bars which have lost stability due to ineffective retention by transverse reinforcement in the free-bending section of the clamp.

It is important to note that in stage 3.2 it is possible to increase the bending moment limit as well as to decrease it. This depends on the fraction of the resistance that the cross-section loses when the concrete protection layer rebounds and part of the compressed reinforcement becomes unstable. In Figure 3 the possible directions of unstrengthening are shown by the dotted arrow lines.

At stage 4, the load-bearing capacity of the section will be exhausted. As the bending moment increases, the stresses in the concrete core will reach their design resistance $R_{b,tr}$, which will be accompanied by the transverse clamps flowing (Figure 4, b).

The strength of confined concrete $R_{b,tr}$ depends on the strength of unconfined concrete R_b and the effective lateral pressure R_e which results from the resistance of the clamps to the transverse deformations of concrete.

According to [12] the strength of confined concrete can be determined as

$$R_{b.tr} = R_b + 4.1R_e \quad (21)$$

The effective lateral pressure Re in the case of a square cross-section is

$$R_e = k_e\rho_sR_{sw} \quad (22)$$

where R_{sw}–yield strength of transverse reinforcement; k_e–retention factor, which takes into account the uneven compression of concrete in cross-sections other than circular; ρ_s–transverse reinforcement coefficient by volume.

In view of the considerable deformations in the cross-section and the consequent low height of the compressed zone x', the component related to the resistance of the unconfined concrete at this stage will be neglected.

Composing and solving the equilibrium equations we obtain

$$x = \frac{N + R_sA_s - R_{sc}A'_s\eta_s}{R_{b.tr}b} \quad (23)$$

$$\begin{aligned} N_{e4} = {} & R_{sc}A'_s\eta_s(h_o - a') \\ & + R_{b.tr}xb(h_{o-}a_{tr} - 0.5x) \end{aligned} \quad (24)$$

At stage 5, the load-bearing capacity of the reinforced concrete cross-section will be reduced, which is reflected in the diagram by the presence of a softening branch. Stresses in the concrete core will decrease to the value of $k_{rRb,tr}$, where k_r – is the residual strength factor of the confined concrete (Figure 4, b). Otherwise, the design dependencies will be similar to the corresponding ones in stage 4.

The curvature in stage 6 will increase with a constant value of bending moment until the longitudinal or transverse reinforcement reaches the limit of relative strain ε_{s2}, which will be accompanied by a rupture of the reinforcement and complete exhaustion of the load-bearing capacity.

It is worth noting that the latter criterion must be monitored at all stress-strain stages.

3. Results and discussion

The dependencies obtained will be considered on the example of a reinforced concrete column of a frame structure. We will carry out the calculation in two variants – with the coefficient of longitudinal force ν=0,3 and ν= 0,6.

$$v = \frac{N}{R_b A_b} \qquad (25)$$

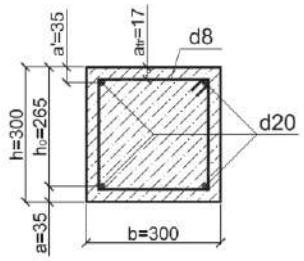

(a)

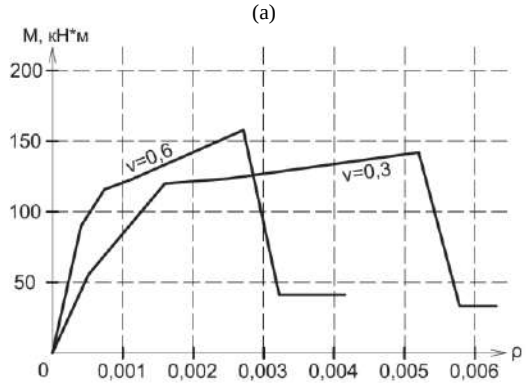

(b)

Figure 5. (a) Cross-section of a reinforced concrete column; (b) "moment – curvature" diagrams based on the results of calculations based on the proposed model

The cross-section of the column is square 300×300 mm, the geometric dimensions are given in Figure 5, a.

Longitudinal reinforcement of 4 bars Φ25A400, $A_s = A_s' = 982\ mm^2$. Cross reinforcement from Φ8A400 with pitch s_w = 100 mm, ρ_s = 0,005.

The design length of the column is assumed to be l_o=3m. Consider all reinforcement effectively secured against loss of stability η_s=1. The residual strength coefficient is assumed to be k_r = 0,25 [20]. Concrete class B20.

The calculation results are shown in Figure 5, b. It can be seen from the graphs that the ultimate bearing capacity for the column with a higher longitudinal force coefficient ν higher, although this column shows less load-bearing capacity prior to the failure of the protective layer than with $v = 0,3$.

It should be noted that due to the inclusion of the compressed zone of concrete in the work, the more loaded column has greater stiffness in all stress-strain stages. While the less loaded column shows a greater capacity for plastic deformation, especially at the stage after the inclusion of indirect reinforcement.

The residual load-bearing capacity for the column at $v= 0,6$ is slightly higher. Failure in both cases is due to clamp rupture when the relative strain limits are reached.

4. Conclusion

The analytical model for the construction of monotone diagram "moment – curvature" for reinforced concrete columns at different level of axial load, taking into account indirect reinforcement by transverse collars, loss of stability of compressed reinforcement, residual strength of concrete is obtained. The model takes into account all stages of the static deformation of eccentrically compressed reinforced concrete elements, including the noncritical phases of operation. The model can also be used for the calculation of frame beams.

The authors consider that the main purpose of constructing such a monotonic diagram is to use it as a basis for a hysteresis diagram that describes the behavior of reinforced concrete elements under low-cycle seismic loads. It is worth considering that bringing reinforced concrete elements to supercritical stages when there is destruction of the concrete protective layer and loss of stability of compressed rods, is not always justified in terms of efficiency of repair and further operation of structure. But when designing buildings based on the concept of non-destruction, the proposed model will allow to reveal reserves of bearing capacity of the system.

The developed model is suitable for solving by hand calculation, however in case of more complex deformation, e.g. oblique eccentric compression, section damage due to fire or corrosion, sections other

than rectangular shape it is possible to apply for solving equilibrium equations at each stage a non-linear deformation model.

Acknowledgments

Author would like to appreciate the faculty members of Faculty of Civil Engineering in Amol Islamic Azad University of Iran who kindly examined the research and suggested useful comments and modifications.

References

[1] Tamrazyan A.G., Chernik V.I. Consideration of the effects of fire in the design of reinforced concrete buildings in earthquake-prone areas. Proceedings XIV Russian National Conference on Earthquake Engineering and Seismic Zoning (with International Participation). Sochi, Moscow; 2021. p. 114–117. (In Russ.) https://doi.org/10.37153/2687-0045-2021-14-114-117

[2] Tamrazyan A.G., Avetisyan L.A. Behavior of compressed reinforced concrete columns under thermodynamic influences taking into account increased concrete deformability. IOP Conference Series: Materials Science and Engineering. 2018;365:052034. https://doi.org/10.1088/1757-899X/365/5/052034

[3] Tamrazyan A., Popov D. Reduce of bearing strength of the bent reinforce-concrete elements on a sloping section with the corrosive damage of transversal armature. MATEC Web of Conferences. 2017;117:00162. https://doi.org/10.1051/matecconf/201711700162

[4] Sengupta P., Li B. Hysteresis modeling of reinforced concrete structures: state of the art. ACI Structural Journal. 2017;114(1):25–38. https://doi.org/10.14359/51689422

[5] Veletsos A.S., Newmark N.M., Chelapati C.V. Deformation spectra for elastic and elastoplastic systems subjected to ground shock and earthquake motions. Proceedings of 3rd World Conference on Earthquake Engineering. 1965;V(II):663–682.

[6] Chernik V.I. Effective stiffness of reinforced concrete columns after a fire. Science Prospects. 2022;(5):82–86. (In Russ.)

[7] Takeda T., Sozen M.A., Nielson N.N. Reinforced concrete response to simulated earthquakes. Journal of the Structural Division, ASCE. 1970;96:2557–2573.

[8] Clough R.W., Johnston S.B. Effect of stiffness degradation on earthquake ductility requirements. Proceedings of 2nd Japan National Conference on Earthquake Engineering. Tokyo; 1966. p. 227–232.

[9] Imbeault F.A., Nielsen N.N. Effect of degrading stiffness on the response of multistory frames subjected to earthquakes. Proceedings of 5th World Conference on Earthquake Engineering, Rome, 26–29 June 1973. Rome; 1973. p. 1756–1765.

[10] Saidi M., Sozen M.A. Simple and complex models for nonlinear seismic response of reinforced concrete structures. A report to the National Science Foundation, University of Illinois at Urbana-Champaign. Champaign; 1979.

[11] Ozcebe G., Saatcioglu M. Hysteresis shear models for reinforced concrete members. Journal of Engineering Mechanics. 1989;115(1):132–148.

[12] Mander J.B., Priestley J.N., Park R. Theoretical stress-strain model for confined concrete. Engineering Structures. 1989;116:1804–1825.

[13] Dowell R.K., Seible F., Wilson E.L. Pivot hysteresis model for reinforced concrete members. ACI Structural Journal, ASCE. 1998;95(5):607–617.

[14] Tamrazyan A., Chernik V. Equivalent viscous damping ratio for a RC column under seismic load after a fire. IOP Conference Series: Materials Science and Engineering. 2021;1030:012095. https://doi.org/10.1088/1757-899X/1030/1/012095

[15] Ibarra L.F., Medina R.A., Krawinkler H. Hysteretic models that incorporate strength and stiffness deterioration. Earthquake Engineering& Structural Dynamics. 2005;34(12):1489–1511. https://doi.org/10.1002/eqe.495

[16] Bondarenko V.M., Yagupov B.A. About connection between force load level and energy losses at deformation of

[17] reinforced concrete structures. Structural Mechanics of Engineering Constructions and Buildings. 2016;(3):44–50. (In Russ.) Sucuoglu H., Erberik A. Energy-based hysteresis and damage models for deteriorating systems. Earthquake Engineering & Structural Dynamics. 2004;33(1):69–88. https://doi.org/10.1002/eqe.338

[18] Moehle J. Seismic design of reinforced concrete buildings. McGraw-Hill; 2014.

[19] Tamrazyan A.G., Manaenkov I.K. To calculation of bendable reinforced concrete elements with indirect reinforcement of compressed zone. Industrial and Civil Engineering. 2016;(7):41–44. (In Russ.)

[20] Chernik V.I., Samarina S.E. Numerical model of a compressed concrete element strengthened by FRP jackets. Building and Reconstruction. 2020;(1):40–53. (In Russ.) https://doi.org/10.33979/2073-7416-2020-87-1-40-53

J-Researchers

JOURNAL OF CIVIL ENGINEERING RESEARCHERS

Incorporating Bacteria for Self-Healing Properties in Innovative Concrete Technology

Soheil khalatbari, [a,*]

[a]*Department of Civil Engineering, Ramsar Branch, Islamic Azad University, Ramsar, Iran*

Journals-Researchers use only: Received date: 2023.04.21; revised date: 2023.06.10; accepted date: 2023.06.19

Abstract

Nanotechnology is poised to offer a viable solution for achieving high performance in future construction projects. Among the innovative technologies being explored, smart concrete has garnered significant attention and undergone extensive research in reputable scientific centers worldwide in recent years. A notable advancement within this field is the development of self-healing concrete. Concrete structures are undeniably susceptible to cracking, primarily due to natural processes. These cracks serve as pathways for harmful substances to infiltrate and corrode the reinforcement bars, ultimately leading to the degradation of the concrete. Traditional approaches to address this issue involve the use of repair materials, particularly various polymers. However, these materials not only complicate the repair process but also have adverse environmental consequences. In light of these challenges, scientists have discovered an alternative method that involves incorporating bacteria into concrete production to create self-healing properties. This method not only reduces maintenance and repair costs but also minimizes environmental impact, thereby enhancing the durability and performance of the concrete while extending its service life. By harnessing the power of bacteria, self-healing concrete represents a significant breakthrough in sustainable construction practices. (DOI:**https//doi.org/10.52547/JCER.5.4.31**)

Keywords: Concrete; Self-healing; Bacteria; Smart concrete; Civil engineering

1. Introduction

Currently, one of the most prominent and widely discussed topics in scientific communities worldwide is nanotechnology. Among the various innovative technologies within this field, smart concrete has garnered significant attention and has been extensively studied in reputable scientific institutions globally [1]. One specific area of focus is self-healing concrete. Concrete plays a vital role in civil engineering projects and is extensively utilized in infrastructure development. However, it is an undeniable reality that concrete structures are susceptible to cracking. Natural processes such as ground settlement, earthquakes, moisture fluctuations, and temperature variations contribute to the formation of cracks in concrete, allowing harmful substances to penetrate and corrode

* Corresponding author. Tel.: +989112002034; e-mail: soheilkhtow@gmail.com.

the reinforcement bars, ultimately leading to the deterioration of the concrete structure [2, 3]. To address this issue, it becomes imperative to enhance the quality of concrete. Nevertheless, completely preventing cracking is only achievable to a certain extent and often involves substantial costs. Therefore, scientists have turned to researching the use of bacteria in concrete production for self-healing concrete technology, which significantly increases the durability and service life of concrete [4]. The creation of microcracks in concrete is an undeniable reality, and traditional methods combat this issue by using repair materials, particularly various polymers, which not only incur high costs but also have negative environmental impacts. The alternative method that scientists have discovered involves using bacteria in concrete production to create self-healing concrete. This method not only reduces maintenance and repair costs but also has minimal environmental impact, contributing to the durability and performance of concrete and extending its service life [5, 6].

2. Concrete repair using traditional methods

Concrete repair using traditional methods begins from the time of the first concrete casting, but this term is mostly used for surface repair after cracking, spalling, and overall concrete deterioration. To initiate the repair process, a proper and comprehensive assessment of the cause and impact of concrete deterioration must be conducted. Based on the results of this assessment, the appropriate materials and repair method can be determined. The repaired surface of the concrete should replace the damaged concrete and restore the required structural performance, similar to its initial state, while also protecting the underlying layer [7, 8]. All potential stresses in the consumable materials of the repaired section, as well as stresses at the interface between the repaired section and the underlying concrete layer, need to be examined and analyzed. Stresses in the repaired section occur due to relative volume changes between the repair area and the underlying concrete layer, as well as various types of loading. Stresses in the repaired section should be within the capacity of existing materials and new materials; otherwise, failure may occur [9]. In areas where some materials are affected by different stresses, they are redistributed around the repaired section multiple times. To prevent additional negative effects on the repaired section during reloading, complete load transfer should be achieved from adjacent members through shoring and jacking during repair operations. Repair materials should be fully utilized and applied until reaching a predetermined strength capable of bearing loads before reloading is performed on the targeted member to avoid any damage to the repaired section [10].

3. Repair materials

To select the appropriate repair materials, a proper understanding of the behavior of these materials in different operating and non-operating conditions, as well as in various environmental conditions, is necessary. One of the major challenges for successful performance of repair materials is their behavior relative to the underlying layer or existing concrete. Relative dimensional changes can create internal stresses in the repair materials and the underlying layer, which can lead to tensile cracking or failure. To minimize these stresses, repair materials should be chosen that have relative dimensional changes compatible with the existing structure.

Another challenge in selecting repair materials is their suitability for structural applications. The ultimate goal of selecting repair materials is to restore the stress tolerance level in the repaired section to its pre-damaged state [11, 12]. To fully achieve this goal, the following factors should be considered: firstly, during the repair process, loading should be removed from the targeted area; secondly, there should be a compatible interaction between the repaired section and the underlying or adjacent section, which is often quite challenging; thirdly, suitable materials should be found that can completely fill cracks or voids without undergoing excessive shrinkage during the repair process; and finally, they should exhibit behavior similar to the original concrete in terms of initial deformations [13-15].

In most cases, cementitious materials such as mortar and well-graded aggregate materials are used for deep repairs. The durability of these repair materials can be enhanced by adding special pozzolans

such as microsilica, polymers like latex, or permeability-reducing additives. When using repair materials containing Portland cements, attention should be paid to shrinkage and concrete processing phenomena. It is important to use materials with minimal shrinkage whenever possible [16, 17].

4. Methods and Practical Tips for Repairing Concrete

In each of the methods for implementing repair materials, the selected repair materials should be able to be applied onto the prepared underlying layer according to the technical specifications. The repair materials should have proper and sufficient adhesion and bonding with the existing layer, fill the voids, and completely cover the reinforcement. The adhesion of repair materials to the underlying layer largely depends on the mechanical interlock with the prepared concrete surface. Sufficient force should be applied to the repair materials to establish complete contact with the prepared surface in order for this to occur [18, 19]. Additionally, the repair materials should have sufficient flowability to penetrate into the voids of the underlying layer and interact with the prepared surface. The method of applying load to the repair materials depends on the desired level of adhesion and varies depending on the implementation technique. In methods that involve troweling, for example, pressure applied during troweling can cause the repair materials to enter into voids and irregularities on the prepared surface [20-22].

5. Protection of repaired concrete

Concrete structures are exposed to various conditions that may have undesirable effects on their performance. These unfavorable conditions can sometimes occur even after repair, resulting in the failure of the repair operation and damage to the repaired structure. Protective measures are implemented to control and prevent the causes of failure and improper utilization of the structure. These measures include: 1. Improving operating and environmental conditions, 2. Enhancing the physical properties of concrete, 3. Installing a barrier between environmental conditions and concrete, 4. Modifying electrochemical behavior when steel corrosion occurs within reinforced concrete.

Protective methods for concrete are usually selected in a way that allows for longer intervals between repair and maintenance cycles. Protecting concrete against aggressive operating and environmental conditions and damaging agents is achieved through the use of coatings, membranes, coverings, and sealants [23, 24]. However, protecting concrete in terms of improper utilization of the structure involves modifying and changing conditions that disrupt the operation of the structure. There are various techniques and methods for protecting concrete. Protective systems can be installed during construction or at any time during the lifespan of the structure. Good design for new buildings ensures the fulfillment of expected protective requirements. Protecting existing structures is usually more challenging and provides us with fewer choices compared to new buildings. The goal of protective strategies is to prevent corrosion of reinforcing steel in concrete, which can lead to cracking, delamination, and spalling of the concrete layer. One important cause of steel corrosion is the ingress of chloride ions. Protecting steel against corrosion involves directly combating the corrosive effects of chlorides [25-27]. The application of an epoxy coating by fusion bonding onto the reinforcement is the most common method for coating rebars. Additionally, additives in concrete mixtures, such as calcium nitrite, can prevent chloride-induced damage. Another method for protection against chlorides is low permeability concrete. One effective approach to reduce chloride ion penetration in concrete is the use of surface coatings and penetrating sealers. Penetrating sealers include silanes and siloxanes, while surface coatings include epoxies, urethanes, chlorinated rubber, and methacrylates [28, 29]. Carbonation is another condition in concrete that allows for the occurrence of corrosion in the presence of moisture and oxygen. Carbonation of concrete occurs when it comes into contact with acidic gases, and the best way to combat it is by using low permeability concrete. The attack of aggressive chemicals on the surface of concrete can be controlled by adding chemical-resistant materials to the concrete mixture or by using surface coatings, membranes, or other surface protection systems [20, 30, 31].

6. Self-healing concrete

One of the smart concretes that has gained attention in recent years is self-healing concrete. Imagine concrete materials that, when cracked, can self-initiate repair and reconstruction without human intervention, solely through water and carbon dioxide. The creation of microcracks in concrete is an undeniable reality, and traditional methods for dealing with it involve the use of concrete repair materials, especially various polymers, which not only incur high costs but also have adverse environmental effects. The alternative approach that scientists have discovered is the use of bacteria in concrete and the production of self-healing concrete, which not only reduces the costs of concrete repair and maintenance but also contributes to the durability and performance of concrete, increasing its service life [32-34]. Under flexural conditions, self-healing concrete only experiences small flexural cracks, whereas non-reinforced conventional (ordinary) concretes would exhibit significant failure and collapse with the same amount of flexural deformation [35].

We can demonstrate this concept using a straightforward illustration. When a human hand sustains a minor scratch, as long as the size and depth of the scratch are small, the body has the ability to naturally heal it without difficulty. However, if the injury is significantly extensive and deep, external surgical procedures such as sutures are required. The performance of self-healing concretes follows a similar pattern in that continuous healing and maintenance of small cracks prevent their propagation and the formation of deep fissures, even under repeated loading of the concrete specimen. The initial report on this matter was made public in April 2009 by a team of researchers from the University of Michigan. Professor Victor Li, the original creator, conducted a series of experiments on self-healing concrete, and we will now delve into the findings of his study.If the applied force increases the length by up to 3%, this sample repairs the resulting cracks or, in other words, withstands this level of strain. Steel in this state undergoes minimal deformation, while ordinary concrete collapses dramatically. Furthermore, in Europe, specifically in the Netherlands, a group of researchers also delved into this subject [35-37]. Henk Jonkers from Delft University of Technology in the Netherlands invented a bio-concrete that can self-heal using bacteria. This concrete is composed like other regular concretes but has an additional primary material that facilitates its self-repair. This material remains untouched during the mixing process and only becomes active if cracks occur in the concrete and water penetrates. He initiated this project in 2006 when a concrete specialist asked him if it was possible to use bacteria in concrete to create self-healing properties. It took Henk Jonkers several years to solve this issue, but there were still some challenges that needed to be overcome. He needed a type of bacteria that could survive in the harsh environment of concrete [38, 39]. Concrete is a hard and very dry material. It is highly alkaline, and the repairing bacteria had to remain inactive for years until activated by water. He used Bacillus bacteria for this purpose because these bacteria can survive in alkaline conditions and produce spores that can remain alive for decades without food or oxygen [40].

The next challenge was activating the bacteria in the concrete. Additionally, these bacteria had to produce repairing materials for the concrete, which turned out to be limestone. The bacteria needed to be fed to produce limestone. They could have used sugar, but sugar weakened the concrete. Ultimately, they used calcium lactate, and they encapsulated the bacteria with calcium lactate inside plastic capsules. These capsules were added to moist concrete. When the concrete cracked, water penetrated it and caused the capsules to open. The bacteria then grew, multiplied, and fed on the calcium lactate. In this process, calcium combined with carbonate ions to form calcium carbonate or limestone, which filled the crack [41].

7. Scientific investigation of the use of bacteria in concrete

In order to achieve high-quality concrete, various materials such as fly ash, blast furnace slag, silica fume, metakaolin, and similar substances have traditionally been used as additives. However, a recent advancement in technology known as bacterial mineral precipitation has emerged. This innovative approach involves the use of specific microorganisms within the concrete that engage in metabolic activities

to initiate precipitation. The result is an enhancement in the long-term durability and stability of concrete properties. This process can occur either inside or outside microbial cells, or even at a distance from them within the concrete matrix. The effectiveness of these bacteria often relies on their ability to alter the chemistry of the solution present in their environment, thereby creating supersaturation and facilitating mineral deposition [42].

The use of this biomineralization technology in concrete has created a new potential for innovations in producing a new type of concrete known as bacterial concrete. Bacterial concrete is designed and constructed based on the ability of bacteria to precipitate calcite. The carbonate precipitation, known as Microbially Induced Calcium Carbonate Precipitation (MICP), has proven its high capability in filling cracks and fine fissures in granites, stones, and sands as a microbial sealant. The calcite precipitation technology using bacteria is an attractive and valuable process. The major appeal of this technology stems from its environmentally friendly nature and natural occurrence. This technology can be used to improve the compressive strength and hardness of cracked concrete specimens or concrete structures under tensile stress [43, 44].

Bacteria can continuously produce an impermeable layer of extraordinary calcite on the surface of concrete. The formed precipitation has a coarse crystalline structure that easily adheres to the surface of the concrete in the form of shells. In addition to their continuous production and growth capability, these exceptional layers are highly impermeable to water. They resist the penetration of harmful agents such as chlorides, sulfates, and carbon dioxide into the concrete, thereby reducing the detrimental effects of these factors on the concrete [45, 46].

Due to the inherent ability of bacteria to continuously precipitate calcite, this type of concrete can be considered as a smart biomaterial for concrete repair. The acidity or pH is an important factor in the activity or inactivity of bacteria in the concrete environment. The fundamental mechanism of bacterial crack healing is based on bacteria acting as catalysts, converting the initial materials into a suitable filler. The newly produced materials, such as calcium carbonate-based minerals that precipitate, should act as a type of bio-cement and effectively seal the created cracks. Therefore, both bacteria and initiator materials should be present for effective self-healing capability in concrete. The presence of these added materials should not alter the desired properties of the concrete [47, 48]. Bacteria that can tolerate the concrete environment are naturally occurring and belong to a specific group of alkali-resistant spore-forming bacteria. An interesting characteristic of these bacteria is their production of thick-walled spherical cells similar to plant seeds. These spores can exist as dormant cells within the concrete and withstand environmental stresses. In dry environments, these bacteria can remain alive for over 50 years. Unfortunately, when these bacteria are directly added to concrete, their lifespan is limited to one or two months [49]. The reduction in spore lifespan from several decades in a dry environment to several months in concrete may be due to continuous hydration of cement. It is important to note that adding organic-mineral initiator materials to concrete should not result in a reduction in concrete properties. Previous studies have shown that these materials, such as yeast extract and calcium acetate, significantly reduce compressive strength in concrete. The only exception is calcium lactate, which increases strength by up to 10% compared to the initial sample [8, 50, 51].

8. Types of bacteria used in concrete

The types of bacteria that have been investigated for their application in bacterial concrete include: Bacillus pasteurii, Bacillus sphaericus, Escherichia coli, and Bacillus subtilis. These bacteria have been used in the production of bacterial concrete and have contributed to improving its properties, mainly through the process of calcium carbonate precipitation induced by bacterial activity. As mentioned earlier, this process is referred to as bacterial-induced mineral precipitation. Calcium carbonate precipitation is carried out by many bacteria and is a common process among them, which has led to its scientific investigation by many researchers [52-54]. The mechanisms of action of bacteria in the formation of calcareous precipitates have been proposed to be diverse. Based on research conducted in this field, it has been accepted that the activity of bacteria can be

influenced by various chemical and physical parameters of the environment. It can also be dependent on metabolic activity and surface structure of the bacterial cells. In general, suitable metabolic pathways for increasing the alkaline pH of the environment can lead to the precipitation of calcium carbonate in the presence of calcium ions. In some studies conducted to investigate the increase in bacterial lifespan in concrete environments and the influence of factors, it has been found that protecting bacterial spores by immobilizing them within porous clay particles before adding them to the concrete mixture increases their lifespan. Based on research conducted, it has been shown that bacterial-induced calcium carbonate precipitates are much more adhesive compared to lime-induced calcium carbonate precipitates and have better compatibility with concrete [55, 56]

Overall, four key factors have been identified to influence the chemical process of calcium carbonate precipitation: 1. Calcium concentration, 2. Dissolved mineral carbon concentration, 3. pH, and 4. Availability of sites for initial precipitation. It is assumed as a fundamental principle that microorganisms have the necessary ability to function in an alkaline environment while performing various physiological activities. In addition to aging the environment, bacteria can induce calcium carbonate precipitation by creating sites for initial deposition or increasing local calcium concentration [57, 58].

9. Performance of self-healing concrete

In simpler terms, self-healing concrete works by reacting a small amount of dry cementitious material present in the cracks with carbon dioxide and water, forming a thin white layer of calcium carbonate. This layer acts as a barrier and prevents the cracks from expanding, essentially repairing them. Calcium carbonate is a very durable compound that is abundantly found in strong structures like shells, turtle shells, and snails in nature. It may take 4 to 5 cycles of wetting and drying for the concrete to fully heal the cracks. Nowadays, builders reinforce concrete with steel bars to minimize crack formation, but these cracks are still not small enough to be self-repaired [53, 59]. As a result, salts that penetrate the concrete through cracks for de-icing purposes can cause corrosion in the reinforcement bars and weaken the overall strength of reinforced concrete. Self-healing concrete does not require reinforcement and strengthening to keep cracks small, making it resistant to corrosion. By reversing the deterioration process of concrete and reducing costs and environmental impacts, using this self-healing concrete in new construction projects can extend the lifespan of buildings and optimize its use [60, 61].

10.Use of bacteria for self-healing concrete

When William McDonough and other pioneers of sustainable architecture first expressed their ideas about the concept of living buildings, it is safe to say that they did not have structures made of real-life organisms and bacteria in mind. However, it was Henk Jonkers from Delft University in the Netherlands who first introduced this idea [62]. What Henk and his colleagues possibly expanded upon was a hybrid of self-healing bacterial concrete, which could potentially set the course towards sustainable architecture that McDonough had envisioned. While this may seem unprecedented, scientists have been using bacteria for building repair for several years now. Bacterial mineral products have been used in various practical applications such as sand hardening and repairing cement cracks. However, there are two main forms of this method: the reaction of these bacteria to certain substances and the production of ammonia, which is a toxic material. Since the bacteria need to be manually applied, a worker or a team of workers must inspect and repair every small crack in each concrete slab for several weeks [63, 64]. But Jonkers' solution was to search for bacteria with different characteristics that could survive in concrete for a long time and easily thrive. Since the bacteria need to be mixed into the concrete from the beginning, they can quickly repair any small cracks before they are exposed to water and resulting deterioration. Researchers found suitable options: a group of highly resilient spores belonging to the Bacillus group that have been able to survive for a long time in alkaline lakes in Russia and Egypt. Jonkers and his colleagues prevented their premature activation by placing these spores and their food source in small ceramic capsules within the wet concrete mixture. The spores remain dormant until the formation of a crack that allows hidden movement into the concrete, and it is at this

point that they become active and start working. When they start feeding, they avidly absorb water and nutrients and produce a significant amount of crystalline limestone, quickly filling up pores and holes [59, 65].

10. Self-healing concrete and the environment

More than seven percent of global CO2 emissions are attributed to cement, which is a major component of concrete, and new materials need to be developed to reduce greenhouse gas emissions. Self-healing concrete can increase the lifespan of buildings by 50% and reduce the need for annual repairs. It can also prevent corrosion of steel reinforcements, making self-healing concrete an environmentally-friendly solution [66, 67].

11. Conclusion

By employing self-healing concrete instead of traditional methods of concrete repair, the exorbitant costs of maintenance and repair of concrete structures can be reduced. Additionally, using less cement and avoiding the use of polymer materials in repair materials can significantly contribute to environmental preservation. In the case of self-healing concrete, the healing process begins immediately after the occurrence of a crack, preventing harmful substances from penetrating into the concrete and causing damage. However, in the case of ordinary concrete, cracks first appear, allowing harmful substances to enter and damage the concrete. This requires time and expense to search for cracks and damages, find suitable repair materials, and then dedicate further efforts to maintaining the repaired section.

References

[1] Amran M, Onaizi AM, Fediuk R, Vatin NI, Muhammad Rashid RS, Abdelgader H, et al. Self-healing concrete as a prospective construction material: a review. Materials. 2022;15(9):3214.

[2] Hossain MR, Sultana R, Patwary MM, Khunga N, Sharma P, Shaker SJ. Self-healing concrete for sustainable buildings. A review. Environmental Chemistry Letters. 2022:1-9.

[3] Tang Y, Xu J. Application of microbial precipitation in self-healing concrete: A review on the protection strategies for bacteria. Construction and Building Materials. 2021;306:124950.

[4] Bagga M, Hamley-Bennett C, Alex A, Freeman BL, Justo-Reinoso I, Mihai IC, et al. Advancements in bacteria based self-healing concrete and the promise of modelling. Construction and Building Materials. 2022;358:129412.

[5] Nodehi M, Ozbakkaloglu T, Gholampour A. A systematic review of bacteria-based self-healing concrete: Biomineralization, mechanical, and durability properties. Journal of Building Engineering. 2022;49:104038.

[6] Yang D, Xu G, Duan Y, Dong S. Self-healing cement composites based on bleaching earth immobilized bacteria. Journal of Cleaner Production. 2022;358:132045.

[7] Siddika A, Al Mamun MA, Alyousef R, Amran YM. Strengthening of reinforced concrete beams by using fiber-reinforced polymer composites: A review. Journal of Building Engineering. 2019;25:100798.

[8] Ivanov V, Chu J. Applications of microorganisms to geotechnical engineering for bioclogging and biocementation of soil in situ. Reviews in Environmental Science and Bio/Technology. 2008;7:139-53.

[9] Ventolà L, Vendrell M, Giraldez P, Merino L. Traditional organic additives improve lime mortars: New old materials for restoration and building natural stone fabrics. Construction and Building Materials. 2011;25(8):3313-8.

[10] Arıoglu N, Acun S. A research about a method for restoration of traditional lime mortars and plasters: A staging system approach. Building and Environment. 2006;41(9):1223-30.

[11] Ghaffary A, Moustafa MA. Synthesis of repair materials and methods for reinforced concrete and prestressed bridge girders. Materials. 2020;13(18):4079.

[12] Kumar DP, Amit S, Chand MSR. Influence of various nano-size materials on fresh and hardened state of fast setting high early strength concrete [FSHESC]: A state-of-the-art review. Construction and Building Materials. 2021;277:122299.

[13] da Rocha Gomes S, Ferrara L, Sánchez L, Moreno MS. A comprehensive review of cementitious grouts: Composition, properties, requirements and advanced performance. Construction and Building Materials. 2023;375:130991.

[14] Negahban E, Bagheri A, Sanjayan J. One-Year study of restrained shrinkage and creep behaviours of geopolymer concrete. Construction and Building Materials. 2023;376:131057.

[15] Medjigbodo S, Bendimerad AZ, Rozière E, Loukili A. How do recycled concrete aggregates modify the shrinkage and self-healing properties? Cement and Concrete Composites. 2018;86:72-86.

[16] Van Tittelboom K, De Belie N, De Muynck W, Verstraete W. Use of bacteria to repair cracks in concrete. Cement and concrete research. 2010;40(1):157-66.

[17] Fowler DW. Polymers in concrete: a vision for the 21st century. Cement and concrete composites. 1999;21(5-6):449-52.

[18] Firdharini C, Wismogroho AS, Widayatno WB, Barliansyah A, Jayadi J, editors. Preliminary and experimental study of

mortar development for cracked concrete repair with injection method. AIP Conference Proceedings; 2022: AIP Publishing.
[19] Yu S, Sun Z, Qian W, Yu J, Yang J. A meshless method for modeling the microscopic drying shrinkage cracking processes of concrete and its applications. Engineering Fracture Mechanics. 2023;277:109014.
[20] Choi S-G, Wang K, Wen Z, Chu J. Mortar crack repair using microbial induced calcite precipitation method. Cement and Concrete Composites. 2017;83:209-21.
[21] Jongvivatsakul P, Janprasit K, Nuaklong P, Pungrasmi W, Likitlersuang S. Investigation of the crack healing performance in mortar using microbially induced calcium carbonate precipitation (MICP) method. Construction and Building Materials. 2019;212:737-44.
[22] Mondal S, Ghosh AD. Review on microbial induced calcite precipitation mechanisms leading to bacterial selection for microbial concrete. Construction and Building Materials. 2019;225:67-75.
[23] Bertolini L, Elsener B, Pedeferri P, Redaelli E, Polder RB. Corrosion of steel in concrete: prevention, diagnosis, repair: John Wiley & Sons; 2013.
[24] Tabatabai H, Pritzl MD, Ghorbanpoor A. Evaluation of select methods of corrosion prevention, corrosion control, and repair in reinforced concrete bridges. Wisconsin Highway Research Program; 2009.
[25] Broomfield JP. Corrosion of steel in concrete: understanding, investigation and repair: Crc Press; 2023.
[26] Uludag D. The Effect of Chloride-Induced Corrosion Patterns on the Crack Width of Reinforced Concrete. 2023.
[27] Qu F, Li W, Dong W, Tam VW, Yu T. Durability deterioration of concrete under marine environment from material to structure: A critical review. Journal of Building Engineering. 2021;35:102074.
[28] Jappie L. Literature review of the use of common protective coatings for concrete structures with experiences in the South African context. 2019.
[29] Di Mundo R, Labianca C, Carbone G, Notarnicola M. Recent advances in hydrophobic and icephobic surface treatments of concrete. Coatings. 2020;10(5):449.
[30] Nodehi M. Epoxy, polyester and vinyl ester based polymer concrete: a review. Innovative Infrastructure Solutions. 2022;7(1):64.
[31] Zhang Z, Zhang H, Liu T, Lv W. Study on the micro-mechanism and structure of unsaturated polyester resin modified concrete for bridge deck pavement. Construction and Building Materials. 2021;289:123174.
[32] Makul N. Advanced smart concrete-A review of current progress, benefits and challenges. Journal of Cleaner Production. 2020;274:122899.
[33] Uddin MN, Tafsirojjaman T, Shanmugasundaram N, Praveenkumar S, Li L-z. Smart self-healing bacterial concrete for sustainable goal. Innovative Infrastructure Solutions. 2023;8(1):46.
[34] Zheng T, Su Y, Zhang X, Zhou H, Qian C. Effect and mechanism of encapsulation-based spores on self-healing concrete at different curing ages. ACS Applied Materials & Interfaces. 2020;12(47):52415-32.
[35] Zdanowicz K. Chemical prestressing of thin concrete elements with carbon textile reinforcement. 2021.
[36] 36. Shah AA, Ribakov Y. Recent trends in steel fibered high-strength concrete. Materials & Design. 2011;32(8-9):4122-51.
[37] Şoşdean C. Experimental and numerical investigations of the influence of cracks on mass diffusion in mortar and concrete: Timişoara: Editura Politehnica; 2015.
[38] Kaur P, Singh V, Arora A. Microbial concrete—a sustainable solution for concrete construction. Applied Biochemistry and Biotechnology. 2022;194(3):1401-16.
[39] Jonkers H. Self-healing concrete. Ingenia. 2011;46:39-43.
[40] De Belie N, Gruyaert E, Al-Tabbaa A, Antonaci P, Baera C, Bajare D, et al. A review of self-healing concrete for damage management of structures. Advanced materials interfaces. 2018;5(17):1800074.
[41] Ajer AKS, Olsen DH. Enterprise architecture implementation is a bumpy ride: a case study in the Norwegian public sector. Electronic Journal of e-Government. 2019;17(2):pp79‑94-pp79‑94.
[42] Durga CSS, Ruben N, Chand MSR, Indira M, Venkatesh C. Comprehensive microbiological studies on screening bacteria for self-healing concrete. Materialia. 2021;15:101051.
[43] Chuo SC, Mohamed SF, Mohd Setapar SH, Ahmad A, Jawaid M, Wani WA, et al. Insights into the current trends in the utilization of bacteria for microbially induced calcium carbonate precipitation. Materials. 2020;13(21):4993.
[44] Maste J. Bacterial concrete-A remedy for micro cracks. 2016.
[45] Stanaszek-Tomal E. Bacterial concrete as a sustainable building material? Sustainability. 2020;12(2):696.
[46] Prasad CVSR, Lakshmi TV. Emerging Way to Enhance the Durability of Concrete Structures through Bacterial addition: Bacterial concrete. Indian Concrete Journal. 2017:58-61.
[47] Siddique R, Chahal NK. Effect of ureolytic bacteria on concrete properties. Construction and building materials. 2011;25(10):3791-801.
[48] Wang J, Mignon A, Snoeck D, Wiktor V, Van Vliergerghe S, Boon N, et al. Application of modified-alginate encapsulated carbonate producing bacteria in concrete: A promising strategy for crack self-healing. Frontiers in microbiology. 2015;6:1088.
[49] Dinesh S, Shanmugapriyan R, Sheen SN. A review on bacteria-based self-healing concrete. Imperial Journal of Interdisciplinary Research. 2017;3(1):2454-1362.
[50] Osinubi K, Eberemu A, Ijimdiya T, Yakubu S, Gadzama E, Sani J, et al. Review of the use of microorganisms in geotechnical engineering applications. SN Applied Sciences. 2020;2:1-19.
[51] El Mountassir G, Minto JM, van Paassen LA, Salifu E, Lunn RJ. Applications of microbial processes in geotechnical engineering. Advances in applied microbiology. 2018;104:39-91.
[52] Mondal S, Das P, Chakraborty AK. Application of bacteria in concrete. Materials Today: Proceedings. 2017;4(9):9833-6.
[53] Vijay K, Murmu M, Deo SV. Bacteria based self healing concrete–A review. Construction and building materials. 2017;152:1008-14.

[54] De Belie N, Wang J, Bundur ZB, Paine K. Bacteria-based concrete. Eco-efficient repair and rehabilitation of concrete infrastructures: Elsevier; 2018. p. 531-67.
[55] Pappupreethi K, Ammakunnoth R, Magudeaswaran P. Bacterial concrete: A review. Int J Civ Eng Technol. 2017;8(2):588-94.
[56] Vekariya MS, Pitroda J. Bacterial concrete: new era for construction industry. Int J Eng Trends Technol. 2013;4(9):4128-37.
[57] Jakubovskis R, Ivaškė A, Malaiškienė J, Urbonavičius J. Impact of Portland cement type on bacterial viability in biological concrete. Cement and Concrete Composites. 2022;127:104413.
[58] Shadhar MH, Mohammed MM, Abdullah MH, Shather A, Alalwan HA. Self-healing of concrete using bacteria: Investigation of the impact of the process's conditions. Innovative Infrastructure Solutions. 2023;8(4):115.
[59] Wiktor V, Jonkers H. Bacteria-based concrete: from concept to market. Smart Materials and Structures. 2016;25(8):084006.
[60] Krishnapriya S, Babu DV. Isolation and identification of bacteria to improve the strength of concrete. Microbiological research. 2015;174:48-55.
[61] Karimi N, Mostofinejad D. Bacillus subtilis bacteria used in fiber reinforced concrete and their effects on concrete penetrability. Construction and Building Materials. 2020;230:117051.
[62] McDonough W, Braungart M. Towards a sustaining architecture for the 21st century: the promise of cradle-to-cradle design. Industry and environment. 2003;26(2):13-6.
[63] Naik TR. Sustainability of concrete construction. Practice periodical on structural design and construction. 2008;13(2):98-103.
[64] Naik TR, editor Sustainability of cement and concrete industries. Proceedings of the International Conference on Achieving Sustainability in Construction; 2005: Citeseer.
[65] Jonkers HM, Thijssen A, Muyzer G, Copuroglu O, Schlangen E. Application of bacteria as self-healing agent for the development of sustainable concrete. Ecological engineering. 2010;36(2):230-5.
[66] Williams SL, Kirisits MJ, Ferron RD. Influence of concrete-related environmental stressors on biomineralizing bacteria used in self-healing concrete. Construction and Building Materials. 2017;139:611-8.
[67] Talaiekhozani A, Abd Majid MZ. A review of self-healing concrete research development. Journal of Environmental Treatment Techniques. 2014;2(1):1-11.

Journal of Civil Engineering Researchers

J-Researchers

JOURNAL OF CIVIL ENGINEERING RESEARCHERS

Comprehensive Investigation of the Omega-Shaped Hybrid CFRP Sheet - Concrete Slab System: Experimental, Numerical and Analytical study

Amir Mohammad Bakhtiari,[a,*] Ali Harati[a]

[a] *Department of Civil Engineering, Arman Institution of Engineering and Technology, Tehran, Iran*

Journals-Researchers use only: Received date: 2023.06.21; revised date: 2023.08.05; accepted date: 2023.09.23

Abstract

Fiber Reinforced Polymer (FRP) composites have been broadly applied in substitution of steel members at rehabilitation interventions thanks to their lightweight, high strength, and high corrosion resistance. Producing novel FRP-concrete hybrid structures is the next step researchers are dealing with. In this context, the present study focuses on the numerical and analytical modeling of the experimentally obtained response of hybrid FRP-concrete slabs subjected to three points bending tests. The analyzed hybrid elements consisted of an omega shape Carbon Reinforced Polymer (CFRP) sheet on which a concrete layer was cast forming a unidirectional slab member. A Glass Fiber Reinforced Polymer (GFRP) fabric was bonded to the CFRP sheet and embedded into the concrete block to provide a connection between CFRP and concrete in one of the specimens. Simulation results showed agreement with the experimental response in terms of load-displacement curve, concrete plastic strain and failure mode. After validating the model, alternative designs (width, height, and thickness of CFRP sheet and concrete block on it) were numerically tested to study the influence of the geometry of the structural system on the load-bearing capacity. Lastly, analytical formulation assuming total compatibility and based on Euler-Bernoulli theory were implemented and contrasted with the experimental response. Overall results pointed out that the optimum design would be the one with increased height of both concrete and CFRP. For this improved configuration, the load-bearing capacity was increased by up to 44%. (DOI:**https//doi.org/10.52547/JCER.5.4.41**)

Keywords: Hybrid FRP-concrete; Carbon Fiber Reinforced Polymer (CFRP); Numerical model; Flexural behavior; Analytical model

1. Introduction

In bridges and high-rise buildings, steel-concrete composite structures are frequently used, especially composite floor systems consisting of a concrete deck poured on top of corrugated steel sheets [1], [2]. Considerations such as profile design, steel sheet width, concrete compressive strength, span, shear connectors and steel-concrete interface shear bond

* Corresponding author. Tel.: +989125148269; e-mail: bakhtiariamir96@gmail.com.

also affect the strength and performance of steel-concrete composite slabs [3], [4]. Over the last decades, extensive experiments have been carried out on the structural efficiency of one and two-span composite slabs with concrete and steel sheeting with or without embossing or mechanical connectors. In addition, researchers have performed a wide variety of finite element simulations of these composite slabs [5], [6]. Full scale tests of composite slabs were accurately modelled in the research by Veljkovic [7]. Numerical model results were compared with available experimental data of two types composite slabs and the corresponding m-k characterization by Eurocode-4. The outcomes confirmed the validity of the model and its simplicity with respect to other available models since a reduced number of variables were required to predict the structural behavior of the slabs in [8]. A general FEM (Finite Element Model) approach of composite sections was introduced in [9], in which the shear bond cooperation between the steel deck and the concrete was treated as a contact issue characterized by cohesion and friction. Comparison between experimental and FEM outcomes showed that the FEM analysis depended on the interface contact model. Model was capable of accurately predicting the performance and the load carrying capacity of composite slabs. Another procedure to implement 3D non-linear FEM models was introduced to simulate the longitudinal slip mechanics of composite slabs in "pull-out" tests [10].

It was also found, though, that these kinds of systems have problems with corrosion. It is well-known that the strength and stiffness of reinforced concrete and steel structures can be lost due to corrosion [11], Arc-spot welds (puddle welds) or screw pins (Hilti-screws) are currently used during construction to briefly fasten the metal deck sheets on top of the supporting members, promoting additional corrosion issues [12].

Because of durability it has been proposed to replace steel members by fiber composite ones. This substitution may allow easier and quicker building procedures that led to the workers' welfare and economic savings [13], [14]. These benefits would enable residential buildings to use the composite floor structure and make it more effective in manufacturing applications [15], [16]. Several pioneers have experimented with hybrid fiber-reinforced polymer (FRP)-concrete systems to address steel disadvantages [17].

However, the initial researches on FRP applications in building industry used fiber-reinforced polymer (FRP) profiles and laminates to strengthen concrete and masonry structures. FRP has become one of the key technologies for restoring and retrofitting existing structures as a result of the last decade's investigations. Deficiencies such as reinforcement erosion, concrete decay, and damage resulting from aging are commonly observed in Reinforced Concrete (RC) structures constructed in the last century [18], [19]. In this context, FRP strengthening elements were originally used in RC systems, resulting in greater corrosion resistance [20]. Smaller work crews, smaller machinery, and smaller supporting structures during construction are also needed for the FRP strengthening or hybrid FRP-concrete structures [21]. All these benefits resulted in improved FRP structures, such as applications with low stress, that perform better, last long, cost-effectively and with lower long-term maintenance costs in comparison to steel ones [22]. Since the mid-1990s, FRP deck implementations have gradually been introduced in the United States. Comprehensive research on stiffness and strength tests of different types of FRP decks with concrete top layer were undertaken [23].

On this basis, it is suggested the latest research on hybrid FRP profile-concrete structures and the existing composite steel sheet-concrete slabs to be combined to introduce new hybrid FRP sheet-concrete slabs. Modelling this novel type of structures is a must to discuss about their structural performance and to compare with the little existing experimental evidences. Two specimens were produced, tested and simulated to calibrated the numerical model aimed to accurately represent the experimentally obtained loading branch of two of these novel hybrid FRP-sheet – concrete slabs. Once validated, the numerical model was used for designing theoretical cases and it was applied to assess the specimens' optimum geometric configuration. This particular secondary numerical study included changes in height of concrete and CFRP, length and width of hybrid slab, and also changes in CFRP's dimensions, resulting in five additional theoretical cases.

On the overall, this research attempts to provide design guidelines for hybrid FRP-concrete slab

elements which can achieve the great benefits of FRP and hybrid steel-concrete slabs but overcoming steel sheet disadvantages.

Finally, an analytical calculation proposal on the basis of Euler-Bernoulli hypothesis is also investigated for simplicity and comparison with numerical model results

2. Experimental tests

Two carbon fiber reinforced polymer (CFRP) omega shape sheet – concrete hybrid slabs were tested. One of them had an only chemical connection on the CFRP-concrete interface by direct adhesion with no additional products. The other specimen included aggregate particles bonded to the inner face of the CFRP sheet. These particles were considered to increase frictional response and improve pre-sliding connection. Besides, this second specimen had a glass fiber fabric bonded to the top surfaces of the CFRP omega shape to improve the CFRP-concrete connection. Material properties, specimens' dimensions, experimental setup, and results of these tests used to fit the model are summarized herein.

2.1. Materials and specimens

Specimens' dimensions, CFRP and mesh configurations are shown in Figure 1. The average concrete properties were 21 MPa, 2.75 MPa, and 24 GPa for compressive strength, tensile strength, and modulus of elasticity respectively. These were obtained according to CEB-FIB [24]. Epoxy resin was used for laminating CFRP sheets, the properties of the resin were experimentally obtained with 8000 MPa, 95.5 MPa, and 23.0 MPa, respectively, for modulus of elasticity, compressive and tensile strength [25]. The average values of elastic modulus and ultimate tensile strength of CFRP sheets were 45550 MPa and 1120 MPa, respectively based on standard [26]. The thickness of the CFRP sheet was 2mm. Glass fiber mesh (alkali-resistant fiberglass) were applied as CFRP-concrete connectors. Mesh was bonded to the top surface of omega-shape CFRP using the same epoxy resin previously used for CFRP production. These meshes were used with dimensions of 2000mm × 400mm. Mechanical properties were ultimate tensile strength of 45kN/m and ultimate elongation of 0.018.

The same epoxy resin was used for laminating CFRP, bonding aggregates, and bonding glass fiber mesh. After casting CFRP laminates with the help of steel omega shape frame and edges' wooden frames, installing mesh on the crests with resin (in with mesh specimen) and concreting have been performed. Figure 1.b. shows specimen (with mesh) before concreting.

2.2. test setup

Three-point bending tests were conducted on simply supported specimens. The free span was 1800mm (L) and the load (F) was indirectly applied through an imposed downward displacement (Δ) at a rate of 1 mm/min until specimen failure. An oleo-hydraulic actuator of 50kN force range and 150mm displacement range equipped with a load cell and an LDVT was used for this purpose. A steel profile HEB120 was used as a loading tool for load distribution along slab width. Vertical displacement was also measured externally with two 100 mm range potentiometers with a linearity of 0.2 percent at the load application section. Two external LVDTs with a range of 20 mm and linearity of 0.2 percent were used to measure the relative longitudinal displacement between the CFRP sheet and the concrete block at both ends. Finally, at mid-span position on the external face of the CFRP sheet, two strain gauges of 350 ohms resistance connected with 4 wires were installed, Figure 2shows boundary and loading conditions of the experimental test setup.

2.3. Results of bending tests

The results of the experimented Omega Shape slabs in terms of load, deflection, relative yield displacement (dy), maximum relative displacement (du), general ductility ratio (μ) of the slab, dissipated energy and deformation at the maximum capacity and modes of failure, are reported in Table 1. The Force-displacement curve response for both considered experimental cases is shown in Figure 3.

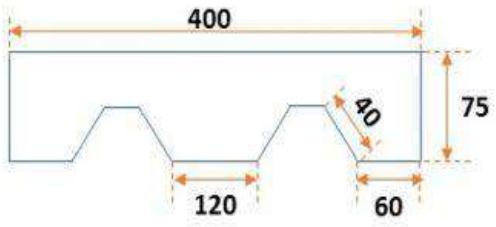

a. Concrete section

b. specimen (with mesh) before concreting

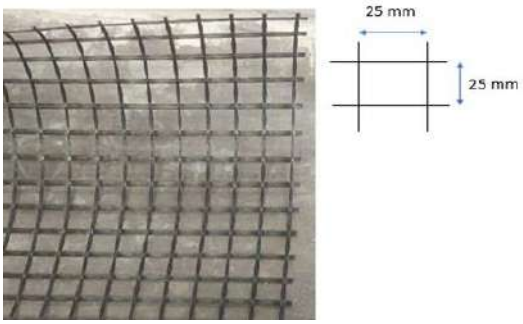

c. Glass fiber mesh

d. Carbon fiber

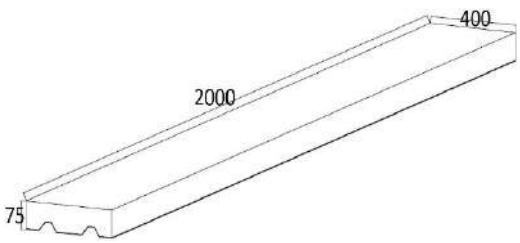

e. Whole model dimensions

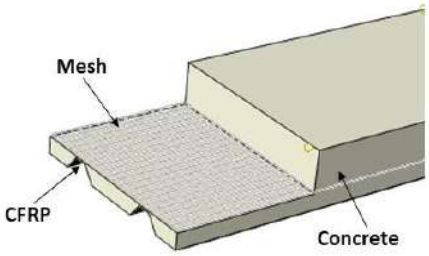

f. Schematic of main components

Figure 1. Experimental details and dimensions

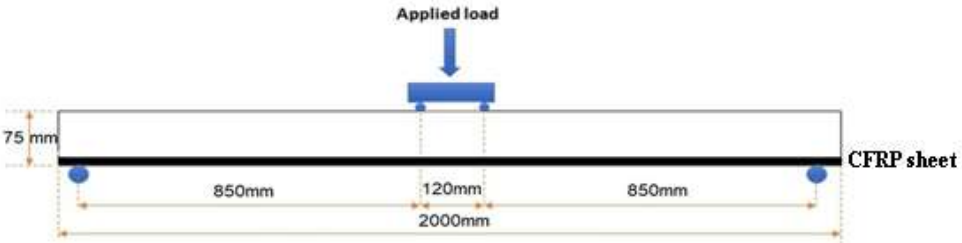

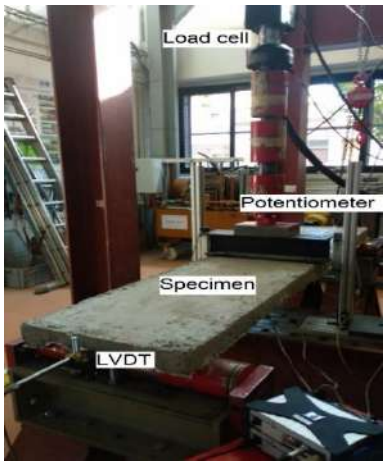

Figure 2. Boundary and loading conditions of the experimental test setup

Table 1.
Experimental results

Specimen	Maximum strength (kN)	Fu	Deformation at the maximum capacity (mm)	dy (mm)	du (mm)	dissipated energy (kN.mm)	$\mu = \frac{d_u}{d_y}$	Failure mode
With mesh	20.61	14.94	29.44	18.03	29.44	344.18	1.63	CFRP-concrete debonding
Without mesh	11.55	8.32	24.34	13.24	24.34	168.71	1.83	CFRP-concrete debonding

These are divided into two main parts; the first part corresponded with a linear-elastic response with a constant slope which ended with the first crack development and the second one showed a nonlinear slope in both specimens, also including the post cracking stage. Figure 4-a and Figure 4-b depict the failure mode of the experimented Concrete Omega Shape slab with and without mesh respectively. Both specimens failed by CFRP-concrete debonding, although the one with no mesh reached lower load-bearing capacity as shown in Figures 4-a and 4-b.

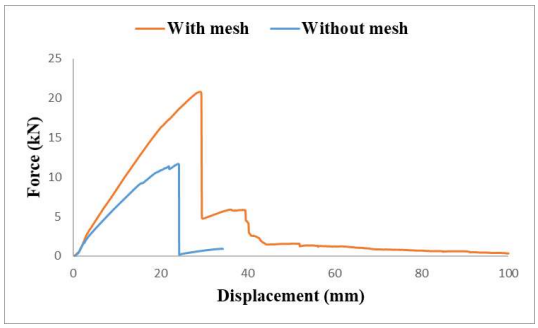

Figure 3. Force-Displacement curves obtained by experimental results

3. Finite element method (FEM)

ABAQUS [27] general-purpose finite element software was used to model experimental tests to provide a general procedure widely available for practitioners. Geometry, materials, mesh, boundary conditions, contacts, and calculation procedure definitions of the implemented model are described.

Geometry was defined according with definition of specimens (section 2.1). Concrete was represented by a single 3D part, CFRP omega-shape sheet was represented as 2D plate and the mesh was represented by 1D truss elements according to its geometric definition.

Concrete Damage Plasticity (CDP) was used in the composite slab simulation to define concrete behavior in FE modeling. The CDP model was developed based

on two concrete failure mechanisms: compressive crushing and tensile cracking [28], [29]. It combines isotropic damaged elasticity with isotropic tensile and compressive plasticity. Tensile cracking and compressive crushing of concrete are considered the two main failure mechanisms [30]. The following values for the Poisson's ratio (0.15) and dilation angle Ψ (30^0) were selected according to the literature [31–34] For nonlinear uniaxial behavior of concrete, the Kent and Park formulation was used [35]. According to this, compressive stress is calculated by equation (1):

$$\sigma_C = f'_{co}\left[2\left(\frac{\varepsilon_c}{\varepsilon'_c}\right) - \left(\frac{\varepsilon_c}{\varepsilon'_c}\right)^2\right] \quad (1)$$

(a)With mesh

(b)Without the mesh

Figure 4. Cracking pattern on the tension surface.

Where $\varepsilon_c$is a compressive strain, f'_{co} and ε'_c are the compressive strength of unconfined cylindrical concrete specimen and the related strain respectively. The value of ε'_c is considered to be 0.002.

The compression damage parameter (d_c), controls the unloading gradient of the stress-strain curve. In concrete and similar materials, such as masonry materials, the higher the plastic strain, the slope of the unloading curve will be reduced to a greater extent than the initial gradient (elasticity specimen). It is due to the damage caused by the loss induced in a brittle material. When damage starts, compressive stress is calculated based on the following equations (2) and (3) [36–38]:

$$\sigma_C = (1 - d_c)\, E_O\, (\varepsilon_C - \varepsilon_C{}^{\sim PL}) \quad (2)$$

$$\varepsilon_C{}^{\sim PL} = \left(\varepsilon_C{}^{\sim in} - \frac{1}{(1 - d_{c)}}\frac{\sigma_c}{E_0}\right) \quad (3)$$

Where $\varepsilon_C{}^{\sim PL}$ is an inelastic strain, ε_C is the compressive strain, E_O is elasticity modulus, d_c is compressive damage, $\varepsilon_C{}^{\sim in}$ is strain related to damage.

Finally, equation 4 is used to calculate the compressive damage value d_c [39]:

$$dc = 1 - \frac{\sigma_c}{f'_{co}} \quad (4)$$

Finally, to completely define the CDP material yield surface, dilation angle (Ψ), the ratio of the second stress invariant on the tensile meridian (K_c) and the viscosity parameter (μ) were defined. Ψ = 30, K_c = 0.667 and μ = 0.001 were recommended values by Abaqus [40]. Higher values of the dilation angle yield ductile response while lower values yield fragile response. Calculated damage parameter in compression (d_c) has remarkable influence on the bending response of concrete elements. Using greater viscosity parameter can considerably decrease the computational time, but results fitting is expected to be poorer. Thus, the choice of the viscosity parameter value in practicable calculations using the CDP material model should be constructed with great care and calibrated accordingly.

The concrete stress–strain compression relationship and the tensile post cracking behavior of concrete was defined according to CEB-FIB [24].

Two node linear 3-D truss elements (T3D2) were used to simulate the internal glass fiber mesh, 3D-solid elements (C3D8R) were used to discretize concrete volume and 3-node triangular general-purpose shell elements (S3R) were used for CFRP slab. Different mesh sizes depending on the thickness of each part (concrete, glass fiber mesh, and CFRP sheet) were used. The convergence of the numerical solutions was checked by using mesh sizes of 100, 75, 50, and 25 mm in the mesh and CFRP shell, resulting in selecting a 50mm mesh and CFRP shell size.

The contact between CFRP and concrete was assumed to be perfectly bonded (tie). Interaction

between glass fiber mesh and concrete was modeled as an embedded region and interactions between glass fiber mesh and CFRP were also are a tie. The slab model was simply supported at the corresponding span and the load was indirectly modeled as an imposed displacement of an area of 400mm x 120mm that was located on the top face in the middle of the slab. The reaction force associated with this imposed displacement was taken as the applied force. The procedure of analysis was done in implicit mode. Regarding quasi-static loading, the static general step was selected for analysis. For running seven models, calculation time was approximately 17 hours with Intel® core i7 CPU.

4. Model fitting

For the best fitting, the values corresponding to dilation angle, Kc, and viscosity parameter were taken as equal to 30, 1.16, and 0.667, respectively. These values met Abaqus recommendations for Concrete Damaged Plasticity and other researcher's data [41].

The results for the best fitting parameters are reported in Table 2 and shown in Figure 5. Good agreement can be seen between the experimental and numerical curves. In particular, maximum loads were predicted with an average relative error of 4.7% (19.58kN predicted vs. 20.61kN experimental for the cases with mesh and 11.05kN vs. 11.55kN for the cases without mesh). The numerical model tends to slightly underestimate experimental load-bearing capacity.

Regarding the stiffness, the model accurately predicts the force-displacement slope. Secant stiffness defined between 20% and 80% of the maximum load had an average relative error of 4.3% respect experimental results. Thus, the implemented model accurately predicts the loading branch as originally aimed. As long as the CFRP-concrete contact was supposed to be completely bonded, when this condition is lost the model convergence is no longer possible and there is no predicted data for the poet-critic response. Thus, FEM failure mode was CFRP-concrete disconnection, indicating that experimental failure mode was also correctly predicted.

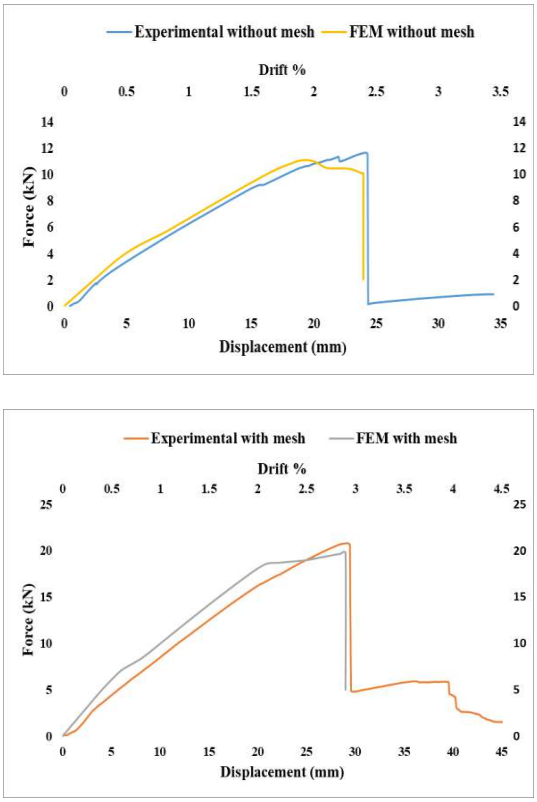

Figure 5. The experimental and numerical load-deflection curves of the specimen slab with and without mesh

5. Geometric parameters study

To evaluate the performance of the full hybrid omega shape CFRP sheet-concrete slab various geometries were simulated with the parameters fixed in the previous fitting process. The cases simulated with the previously validated model are summarized in Table 2 and Figure 6.

In Figure 7, force-displacement curves of cases A, B, C, D, and E are represented together with that representing experimental tested cases. Curve of case D was modified so to be comparable to the same width of the rest of the cases by multiplying force by the factor 400/480. In Table 2, the values of ultimate strength (F_p), Deformation at the maximum capacity (d_u), and the area beneath the force-displacement curve (dissipated energy-G_d) are introduced.

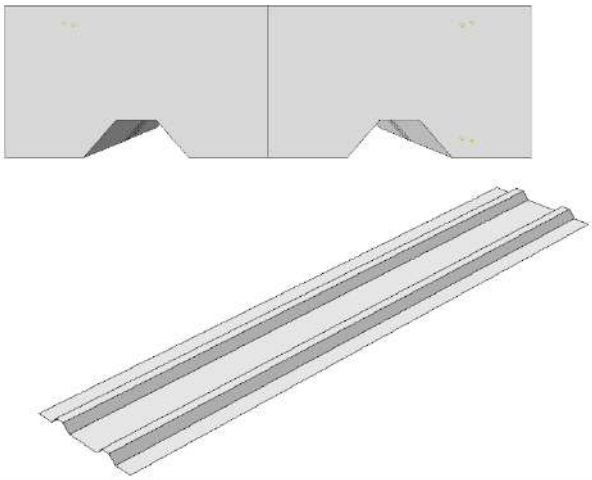

1) Case A. Increased concrete height

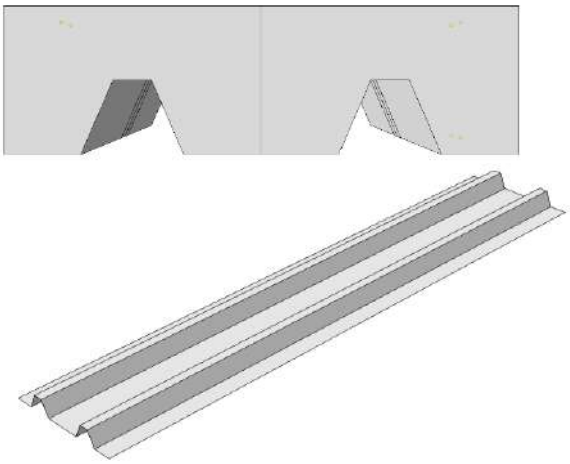

2) Case B. Increased concrete and CFRP height

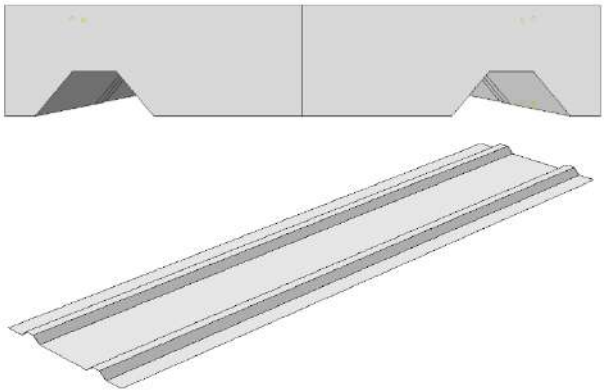

3) Case C. Increased distance between crests

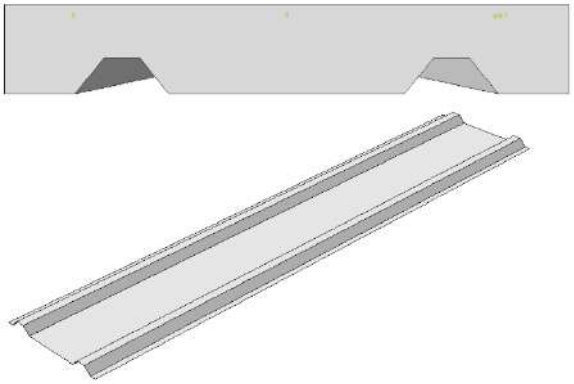

4) Case D. Increased concrete width and distance between crests

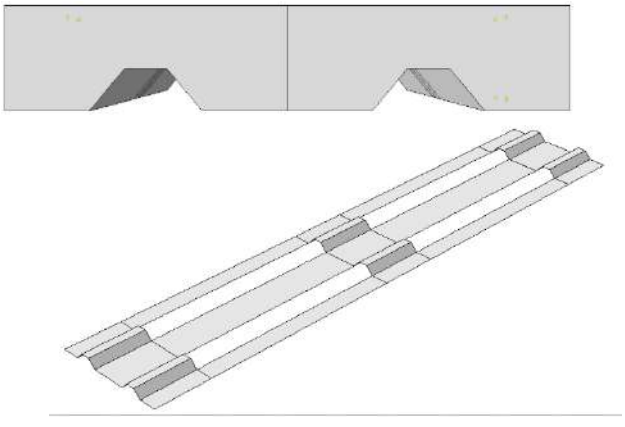

5)

Figure 6. Definition of hybrid omega shape CFRP sheet – concrete specimens for geometry parametric study.

Table 2.
Theoretical simulations

Case	Mesh	Concrete height (mm)	Concrete width (mm)	CFRP omega height (mm)	CFRP omega distance (mm)	CFRP continuity
With mesh	Yes	75	400	35	120	Continuous
Without mesh	No	75	400	35	120	Discontinuous
Case A	Yes	120	400	35	120	Continuous
Case B	Yes	120	400	60	120	Continuous
Case C	Yes	75	400	35	200	Continuous
Case D	Yes	75	480	35	200	Continuous
Case E	Yes	75	400	35	120	Discontinuous

Results showed that increasing the concrete cross-section significantly increased the load-bearing capacity. Cases A and B showed similar capacities, so increasing the height of the CFRP is no effect if the CFRP-concrete connection is assured. Case A had a greater concrete area so showed greater initial stiffness although the larger CFRP area of the B case brought higher maximum resistance. In the case of C, increasing the distance between Omega shapes reduces the CFRP amount in the center of the slab causing a reduction in the system's dissipated energy in comparison with the case With Mesh, although the maximum load-bearing capacity was maintained. Comparing case D with cases A and B showed that increasing the cross-section height is more effective than increasing the cross-section width against bending as it was expected. A comparison of case E with the experimental case with mesh revealed that reducing CFRP caused a decrease in the load-bearing capacity.

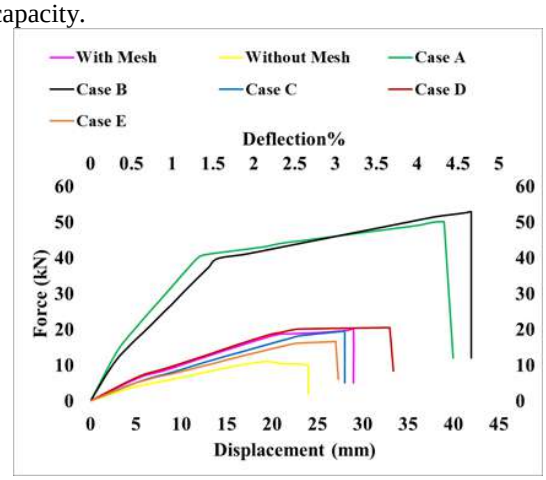

Deflection = (Δ*100)/(L/2) Δ: Vertical displacement in mid-span L: Length of the slab

Figure 7. Comparison of Force-Displacement curves for cases.

5.1. Analysis of the maximum plastic strain index

The ultimate plastic strain (PE) criterion is an appropriate parameter in estimating the damage in concrete. This is a suitable criterion for investigating the number of cracks and the tensile and compression failures along with their alignment. Concrete damage is related to the CFRP-concrete debonding process. However, enhancing capability depends on the integrity of the CFRP-concrete interface. The end of the CFRP plates is vulnerable to stress concentration, which can contribute to the emergence of micro-cracks at an early stage. Debonding failure happens initially at very small cracks and then expands to other parts of the structure. Debonding cracks in the internal interface of the framework are difficult to find in the engineering field. When cracks are linked to each other, the ability of the system would instantly collapse, which could ultimately lead to a huge loss of life and property [42]. Although these particular parameters are useful for evaluating the amount of damaged concrete, PE is more commonly used [41].

The model for the experimental case with mesh reached a maximum plastic strain value of about 1.23%, which indicated extensive tensile damage in concrete, and most of the cracks were formed at the center of the slab. Greatest cracks in this area were expected and obtained by the model as can be seen in Figure 8 and Table 3. If removing the mesh, the maximum principal plastic strain is increased to about 1.70% indicating a stress concentration and the corresponding damage increase.

Increasing the concrete height (case A) can significantly improve the bending capacity of the system and transfer the cracks out of the center of the slab region.

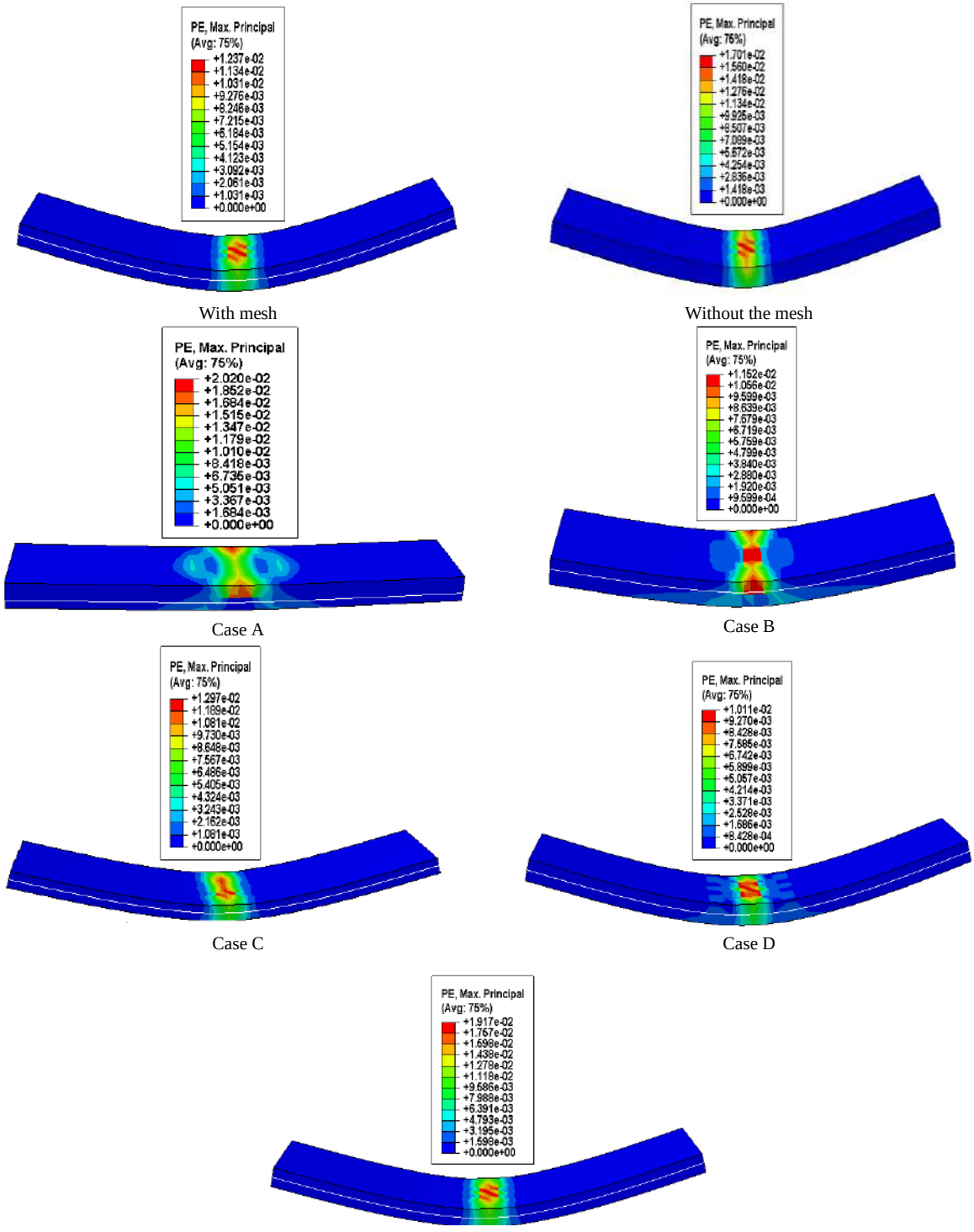

Figure 8. Maximum principal plastic strain in the base and the proposed cases

Table 3.
The maximum load-carrying capacity, the dissipated energy, and maximum principle plastic stain for all the cases

Cases	Maximum strength, F_n (kN)	Deformation at the maximum capacity, d_u (mm)	Dissipated energy, G_d (kN.mm)	maximum principle plastic strain (%)
With mesh	19.8	29	334	1.237
Without mesh	9.38	19	171	1.701
A	50.06	39	1525	2.02
B	52.94	42	1602	1.152
C	19.55	28	319	1.297
D	24.52	33	566	1.011
E	16.65	27	275	1.917

In this case, PE reached the greatest value among models: 2.02%. This fact indicates that this case was the one allowing more tensile damage development in concrete. In contrast, the case with increased height of both concrete and CFRP sheet (case B) showed that tensile damage in concrete was reduced (PE 1.15%) at increasing the height of the CFRP although higher loads were predicted to be resisted. When increasing the horizontal separation between omega shapes in CFRP (case C) there was less concrete at the longitudinal edges of the case and CFRP was concentrated there reducing the possible tensile damage in concrete to PE=1.01% but reaching similar load-bearing capacity to the experimental case with mesh. The increase of the total width of the case (case D) was related to a greater ratio of concrete in the tensile area so the PE index increased up to 1.30% because tensile stresses affect a greater area. However, the increase in load-bearing capacity is directly related to the increase in the case of size in this case. Finally, removing part of the bottom plates of the CFRP sheet decreased the overlapping between CFRP and concrete, causing more tensile stresses to be assumed by the concrete without increasing its section. This combination results in a higher PE, 1.92%, but the lower load-bearing capacity among all cases with mesh. A representative contour plot of the PE index is provided in Figure 8.

5.2. Analysis of secant stiffness

As a consequence of reversal and repeated actions of monotonic loading, the stiffness of a Concrete Omega Shape slab system assembly can deteriorate. Similarly, stiffness is also reduced along with load increase when plasticization effects took place. Secant stiffness related techniques use secant stiffness at the design reaction stage and the principle of equal viscous damping to describe the non-linear behavior of structural structures [43]. Figure 9 shows how the secant or effective stiffness, Keff, is defined as the strength ratio, V*B*, to the maximum displacement possible (Figure 9). For all modeled cases the secant stiffness is taken as the slope of the straight line which connects the load at every deformation point of study with the origin. To assess this stiffness degradation, the secant stiffness is calculated at different loading stages during the simulated monotonic load increase. Relationships are represented in Figure 10. All simulated cases were compared with the experimental case with mesh in the following plots.

Simulation of the experimental cases with and without mesh showed analogous qualitative stiffness response although the embedded mesh brought a constant stiffness increase of 400kN/m respect to the case with no mesh. Cases A, B, and D showed greater stiffness than the experimental case with mesh. All of them had greater concrete area than the comparison case, being more effective, the height increase (cases A and B) than the width increase (case D), as expected. Although CFRP had a higher modulus than concrete, its area and height increase did not compensate for the reduction of the concrete area from case A to case B. This difference is reduced as tensile damage in concrete progress being no appreciated for the highest loads. Increasing the separation between omega shapes of the CFRP sheet (case C compared with the experimental case with mesh) reduced the stiffness of

the system although differences tended to decrease as load increased and the tensile damage progress. Finally, removing a significant part of the bottom CFRP (case E) was associated with the lowest stiffness all simulated test long.

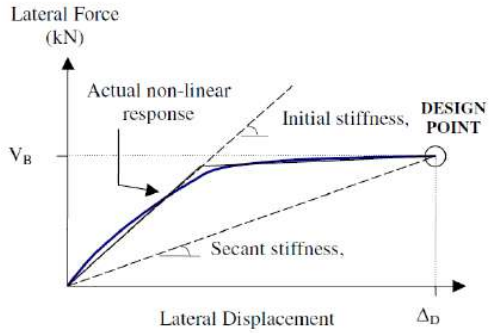

Figure 9. Usage of initial-stiffness and secant stiffness concepts related to the complete non-linear response of the structure and its equation [43]

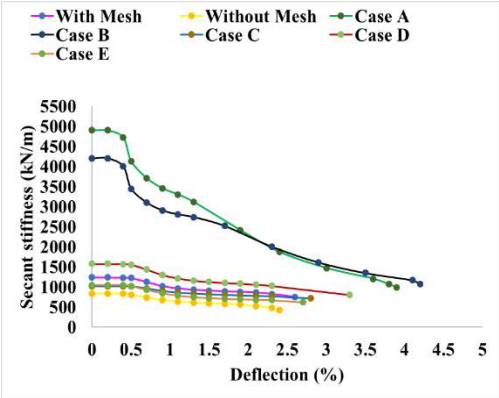

Figure 10. Secant stiffness evolution

6. Analytical methodology

Analytical post-processing of experimental data has been carried out to assess the interaction phenomenon or prove the total interaction of the tested connections. The calculations hypothesis is based on Euler-Bernoulli's assumptions of plane section and force and moment equilibrium in the calculation section. The linear-elastic response of FRP in tension and compression, the linear elastic response of mesh in tension, and the parabolic-constant response of concrete in compression were assumed. No compressive contribution of mesh neither tensile contribution of concrete was considered. Besides, total compatibility assumptions (strain continuity) were imposed in the calculation approach to assess the possibility of total interaction between concrete and FRP. First of all, a schematic representation of stress and strain distributions are included in Figure 11. For every measurement point along testing time up to failure point, the strain values at two different heights of the CFRP sheet at the center of length were used to determine the position of the neutral axis. From the position of the neutral axis, it was possible to obtain the strain distribution (linear and total compatibility hypothesis), so the corresponding stress distribution which led to the calculation of the corresponding bending moment effort obtained from the strain measurements, which was compared with the externally applied to bending moment.

Figure 12 shows a good balance between the experimental models' external moment with a calculated internal moment from proposed formulas. This evidence verifies that commonly known-by-practitioners formulations based on the Euler-Bernoulli hypothesis with total strain compatibility are applicable for the novel structural system herein analysed.

7. Conclusions

A comprehensive numerical study was carried out to investigate the performance of hybrid CFRP-concrete slabs characterized by the omega shape of the CFRP sheet. In particular, the case including flexible glass fiber mesh to connect CFRP sheet with concrete has been in-depth analyzed. After validating the model by comparison with two experimental specimens, five additional geometric definitions of hybrid CFRP-concrete slabs were simulated. Concrete Damaged Plasticity (CDP) was considered in all simulations carried out. From the pieces of evidence, the following conclusions can be drawn.

1. The proposed numerical model fitted full experimental force-displacement curves up to failure point with a slight underestimation of the maximum load-bearing capacity of less than 5%.

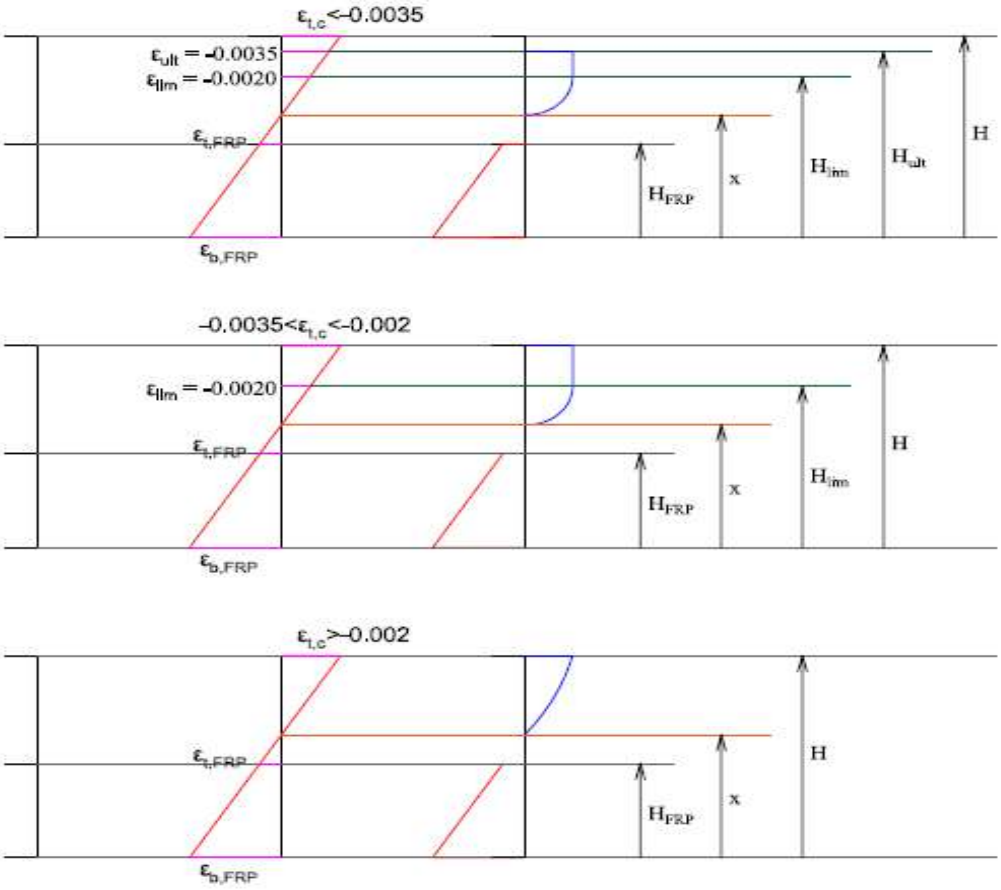

Figure 11. Strain and stress distribution for complete interaction hypothesis depending on the top concrete strain case.

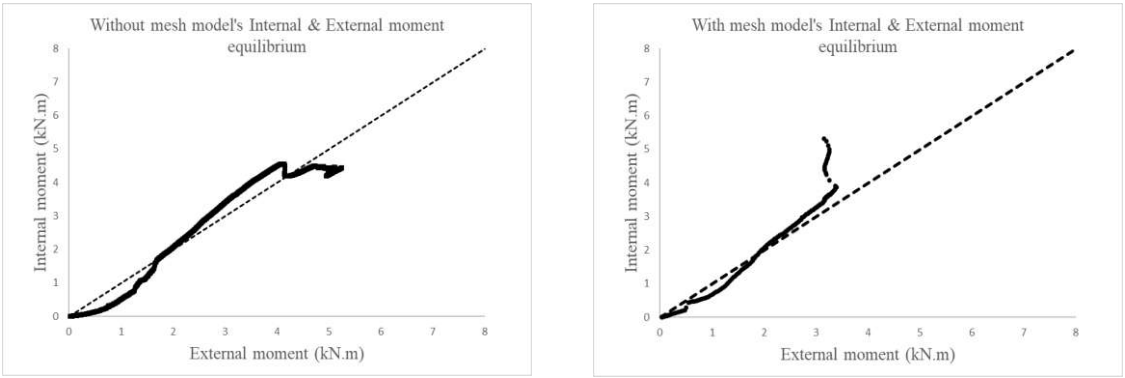

Figure 12. Experimental models' verification with proposed analytical formulas.

2. Concrete damage plasticity, dilation angle and viscosity are the most sensitive parameters to be adjusted in the numerical model.
3. Increasing the width of hybrid elements did not provide greater load-bearing capacity per unit width but a slightly stiffer response because of the higher proportion of concrete in the section. In the same reasoning line, increasing the separation between omega shape areas in the CFRP sheet was associated with no changes in the load-bearing capacity but lower initial stiffness because of the greater area of concrete in the central part of the analyzed element.
4. Increasing the height of the concrete over the CFRP omega shape sheet improved the bending capacity, reached greater concrete damage at the ultimate stage and showed the stiffest response at lower loads.
5. If the height of the CFRP omega shape sheet was simultaneously increased with the concrete height, less tensile concrete damage was predicted although final load-bearing capacity was slightly higher, and initial stiffness was lower than the case with only concrete height increase.
6. Removing part of the bottom CFRP plates was directly related to reducing the load-bearing capacity, increasing the tensile concrete damage, and lower stiffness because tensile stresses had to be supported mostly by concrete in some areas of this particular geometric definition case.
7. Analytical verifications illustrate a good balance between experimental results and calculated analytical results assuming total compatibility, so the common Euler-Bernoulli hypothesis applies to this novel CFRP sheet-concrete hybrid element typology.

References

[1] A. Mahboob, L. Gil, E. Bernat-Maso, and A. R. Eskenati, "Experimental and Numerical Study of Shear Interface Response of Hybrid Thin CFRP–Concrete Slabs," Materials, vol. 14, no. 18, p. 5184, Sep. 2021, doi: 10.3390/ma14185184.

[2] M. Abedi, O. Hassanshahi, J. A. O. Barros, A. Gomes Correia, and R. Fangueiro, "Three-dimensional braided composites as innovative smart structural reinforcements," Compos Struct, vol. 297, p. 115912, Oct. 2022, doi: 10.1016/j.compstruct.2022.115912.

[3] S. MOTAMEDPOOYA and E. ASNAASHARI, "Organizational project management maturity from the construction practitioners point of view," 2016.

[4] A. Mahboob, O. Hassanshahi, and A. S. Tabrizi, "Three-dimensional simulation of granular materials by discrete element method (DEM) by considering the fracture effect of particles," Journal of Civil Engineering Researchers, vol. 5, no. 2, pp. 14–28, 2023.

[5] A. Mahboob, O. Hassanshahi, A. Hakimi, and M. Safi, "Evaluating the Performance of Hollow Core Slabs (HCS)-Concrete and Simplifying Their Implementation," Recent Prog Mater, vol. 05, no. 02, pp. 1–15, Apr. 2023, doi: 10.21926/rpm.2302016.

[6] A. R. Eskenati, A. Mahboob, E. Bernat-Maso, and L. Gil, "Characterizing the Structural Behavior of FRP Profiles—FRCM Hybrid Superficial Elements: Experimental and Numerical Studies," Polymers (Basel), vol. 14, no. 6, p. 1076, Mar. 2022, doi: 10.3390/polym14061076.

[7] M. Veljkovic, "Behavior and resistance of composite slabs. Experiments and Finite Element Analysis," Lulea University of Technology, 1996.

[8] J. D. Ríos, H. Cifuentes, A. Martínez-De La Concha, and F. Medina-Reguera, "Numerical modelling of the shear-bond behaviour of composite slabs in four and six-point bending tests," Eng Struct, vol. 133, pp. 91–104, 2017, doi: 10.1016/j.engstruct.2016.12.025.

[9] S. Chen and X. Shi, "Shear bond mechanism of composite slabs - A universal FE approach," J Constr Steel Res, vol. 67, no. 10, pp. 1475–1484, 2011, doi: 10.1016/j.jcsr.2011.03.021.

[10] A. Mahboob, A. R. Eskenati, and S. Moradalizadeh, "Numerical Investigation and Cost Analysis of FRP-Concrete Unidirectional Hybrid Slabs," International Journal of Applied Mechanics and Engineering, vol. 26, no. 4, pp. 156–166, Dec. 2021, doi: 10.2478/ijame-2021-0056.

[11] S. Abbasi, A. Mahboob, H. Bakhtiari Zamani, M. R. Bilesan, E. Repo, and A. Hakimi, "The Tribological Behavior of Nanocrystalline TiO2 Coating Produced by Plasma Electrolytic Oxidation," J Nanomater, vol. 2022, pp. 1–13, Jan. 2022, doi: 10.1155/2022/5675038.

[12] M. Abedi et al., "A self-sensing and self-heating planar braided composite for smart civil infrastructures reinforcement," Constr Build Mater, vol. 387, p. 131617, Jul. 2023, doi: 10.1016/j.conbuildmat.2023.131617.

[13] A. Salles, M. Salati, and L. Bragança, "Analyzing the Feasibility of Integrating Urban Sustainability Assessment Indicators with City Information Modelling (CIM)," Applied System Innovation, vol. 6, no. 2, p. 45, Mar. 2023, doi: 10.3390/asi6020045.

[14] M. Salati, L. Bragança, and R. Mateus, "Sustainability Assessment on an Urban Scale: Context, Challenges, and

Most Relevant Indicators," Applied System Innovation, vol. 5, no. 2, p. 41, Apr. 2022, doi: 10.3390/asi5020041.
[15] M. Abedi et al., "A sustainable cementitious composite reinforced with natural fibers: An experimental and numerical study," Constr Build Mater, vol. 378, p. 131093, May 2023, doi: 10.1016/j.conbuildmat.2023.131093.
[16] C. L. Oh, K. K. Choong, T. Nishimura, J.-Y. Kim, and O. Hassanshahi, "Shape change analysis of tensegrity models," Latin American Journal of Solids and Structures, vol. 16, no. 7, 2019, doi: 10.1590/1679-78255407.
[17] A. R. Eskenati, A. Mahboob, E. Bernat-Maso, and L. Gil, "Experimental and Numerical Study of Adhesively and Bolted Connections of Pultruded GFRP I-Shape Profiles," Polymers (Basel), vol. 14, no. 5, p. 894, Feb. 2022, doi: 10.3390/polym14050894.
[18] A. Yousefi, N. M. Bunnori, M. Khavarian, O. Hassanshahi, and T. A. Majid, "Experimental investigation on effect of multi-walled carbon nanotubes concentration on flexural properties and microstructure of cement mortar composite," 2017, p. 020032. doi: 10.1063/1.5005663.
[19] M. Golabchi and E. Asnaashari, "Identification of Iran's road construction project risks in order to implement sustainable development (Pavement Technologies and Construction Activities)".
[20] W. Y. Peen, C. K. Keong, and O. Hassanshahi, "Behaviour of hollow circular section with multiple perforations under compression, flexure and torsion," Latin American Journal of Solids and Structures, vol. 16, no. 2, 2019, doi: 10.1590/1679-78255387.
[21] A. Mahboob, L. Gil, E. Bernat-Maso, and A. R. Eskenati, "Flexible Fiber Fabric for FRP–Concrete Connection of Thin Hybrid Slabs," Polymers (Basel), vol. 13, no. 17, p. 2862, Aug. 2021, doi: 10.3390/polym13172862.
[22] A. R. Eskenati, A. Mahboob, A. Alirezaie, R. Askari, and S. M. S. Kolbadi, "INVESTIGATING THE EFFECT OF LONGITUDINAL GALLERY ON DYNAMICAL RESPONSE OF GRAVITY CONCRETE DAMS USING FEM," Journal of Southwest Jiaotong University, vol. 56, no. 4, pp. 804–811, Aug. 2021, doi: 10.35741/issn.0258-2724.56.4.69.
[23] O. Hassanshahi, T. A. Majid, T. L. Lau, A. Yousefi, and R. M. K. Tahara, "Seismic performance of the typical RC beam–column joint subjected to repeated earthquakes," 2017, p. 120014. doi: 10.1063/1.5005755.
[24] CEB-FIP MODEL CODE 1990. 1993. doi: 10.1680/ceb-fipmc1990.35430.
[25] ASTMD3531, "Standard Test Method for Resin Flow of Carbon Fiber-Epoxy Prepreg," Annual book of ASTM standards, 2014.
[26] ASTM Committee D30.05, "ASTM D7565-10 Standard Test Method for Determining Tensile Properties of Fiber Reinforced Polymer Matrix Composites Used for Strengthening of Civil Structures," in Annual Book of ASTM Standards Volume 15.03, 2010. doi: 10.1520/D7565_D7565M-10.
[27] Hibbitt Karlsson & Sorensen inc., ABAQUS / Explicit User ' s Manual. Inso Corporation, 2000.
[28] J. Lubliner, J. Oliver, S. Oller, and E. Oñate, "A plastic-damage model for concrete," Int J Solids Struct, vol. 25, no. 3, pp. 299–326, Jan. 1989, doi: 10.1016/0020-7683(89)90050-4.
[29] J. Lee and G. L. Fenves, "Plastic-Damage Model for Cyclic Loading of Concrete Structures," J Eng Mech, vol. 124, no. 8, pp. 892–900, Aug. 1998, doi: 10.1061/(ASCE)0733-9399(1998)124:8(892).
[30] J. Lee and G. L. Fenves, "Plastic-Damage Model for Cyclic Loading of Concrete Structures," J Eng Mech, vol. 124, no. 8, pp. 892–900, Aug. 1998, doi: 10.1061/(ASCE)0733-9399(1998)124:8(892).
[31] Y. Sümer, M. A.-C. J. of Structural, and U. 2015, "Defining parameters for concrete damage plasticity model," Challenge Journal of Structural Mechanics, 2015, doi: 10.20528/cjsmec.2015.07.023.
[32] G. Zhao and A. Li, "Numerical study of a bonded steel and concrete composite beam," Comput Struct, vol. 86, no. 19–20, pp. 1830–1838, Oct. 2008, doi: 10.1016/j.compstruc.2008.04.002.
[33] M. H. Seleem, I. A. Sharaky, and H. E. M. Sallam, "Flexural behavior of steel beams strengthened by carbon fiber reinforced polymer plates - Three dimensional finite element simulation," Mater Des, vol. 31, no. 3, pp. 1317–1324, Mar. 2010, doi: 10.1016/j.matdes.2009.09.010.
[34] I. Vilanova, L. Torres, M. Baena, and M. Llorens, "Numerical simulation of bond-slip interface and tension stiffening in GFRP RC tensile elements," Compos Struct, vol. 153, pp. 504–513, 2016, doi: 10.1016/j.compstruct.2016.06.048.
[35] D. C. Kent and R. Park, "FLEXURAL MEMBERS WITH CONFINED CONCRETE," Journal of the Structural Division, Jul. 1971.
[36] R. Massarelli, J. E. Franquet, K. Shrestha, R. Tremblay, and C. A. Rogers, "Seismic testing and retrofit of steel deck roof diaphragms for building structures," Thin-Walled Structures, vol. 61, pp. 239–247, 2012, doi: 10.1016/j.tws.2012.05.013.
[37] X. Wang, C. Su, W. Deng, and Z. Wu, "Bond behavior between corrugated BFRP shell and concrete under monotonic and cyclic loads," Constr Build Mater, vol. 210, pp. 596–606, 2019, doi: 10.1016/j.conbuildmat.2019.03.072.
[38] Y. Ou, J. M. Gattas, D. Fernando, and J. L. Torero, "Experimental investigation of a timber-concrete floor panel system with a hybrid glass fibre reinforced polymer-timber corrugated core," Eng Struct, vol. 203, no. November 2019, 2020, doi: 10.1016/j.engstruct.2019.109832.
[39] B. W. Schafer, Z. Li, and C. D. Moen, "Computational modeling of cold-formed steel," Thin-Walled Structures, vol. 48, no. 10–11, pp. 752–762, 2010, doi: 10.1016/j.tws.2010.04.008.
[40] Hibbitt Karlsson & Sorensen inc., ABAQUS/Standard: User's Manual. Inso Corporation, 1998.
[41] H. Behnam, J. S. Kuang, and B. Samali, "Parametric finite element analysis of RC wide beam-column connections," Comput Struct, vol. 205, pp. 28–44, 2018, doi: 10.1016/j.compstruc.2018.04.004.
[42] Y. Liu, M. Zhang, X. Yin, Z. Huang, and L. Wang, "Debonding Performance of CFRP-Strengthened Nanomaterial Concrete Beam Using Wavelet Packet

Analysis," J Sens, vol. 2020, 2020, doi: 10.1155/2020/7526703.
[43] G. H. Powell, "Displacement-Based Seismic Design of Structures," Earthquake Spectra, 2008, doi: 10.1193/1.2932170.

Journal of Civil Engineering Researchers

J-Researchers

JOURNAL OF CIVIL ENGINEERING RESEARCHERS

The Effect of Polypropylene Fibers on the Behavior of Fiber Self-Compacting Concrete

Morteza Jamshidi [a,*]

[a]*Engineering faculty, Chalous Branch, Islamic Azad University, Chalous, 46615-397, Iran*

Journals-Researchers use only: Received date: 2023.07.21; revised date: 2023.08.23; accepted date: 2023.09.29

Abstract

Fiber self-compacting concrete (FSCC), is a concrete that has been combined with fiber in its mix design. Extensive benefits of self-compacting concrete (SCC) in full fill the mold and achieving full compaction without vibration, with good behavior after concrete cracking, raise the idea of self-compacting concrete production. The fundamental challenge in this area is the unsatisfactory performance of concrete with fibers; In other words, using fibers in concrete will reduce concrete fluidity. Therefore, determining the appropriate percentage of fibers in SCC can be a precursor to extending the use of FSCC. In this study, polypropylene fibers with 0.5, 1, 0.1, and 2% of concrete mix design have been added to the self-compacting concrete mix design. Its impact on the performance of concrete has been evaluated using time and diameter of slump-flow, L-Box, J-ring, and V-funnel flow time tests. Based on the criteria defined by EFNARC standard, it was indicated that the FSCC containing 0.5% polypropylene fibers has an acceptable performance. Additionally, the effect of polypropylene fiber on the mechanical properties of hardened concrete has been studied using compressive strength and tensile tests and shown that changes in FSCC compressive strength and tensile with 0.5% polypropylene fiber are negligible. (DOI:**https//doi.org/10.52547/JCER.5.4.56**)

Keywords: Fiber self-compacting concrete; Polypropylene; Compressive strength; Tensile strength.

1. 2. Introduction

For the last four decades, SCCs have been widely used to improve concrete casting. SCCs have the ability to fit and compress under their own weight with no or low energy requirements. Their adhesion is enough that during the transfer, grain detachment or bleeding does not occur. [1-3] This specification causes concreting in dense reinforcement structures (such as floor slabs, docks, and other structures) can be possible without vibration. On the other hand, due to the adequate fluidity of SCC, fast pumping, and in consequence, production of uniform and dense concrete surfaces would be possible. These advantages make extensive use of SCC in different areas of reinforced concrete structures implementation [4-8].

* Corresponding author. Tel.: +989111912549; e-mail: m.jamshidi@iauc.ac.ir.

Table 1.
Chemical and physical properties of cement

Chemical composition (%)								Physical properties
MgO	SiO2	Al2O3	Fe2O3	C3A	SO3	L.O.I	I.R	Specific surface
1.4	21.2	4.6	3.8	6	2.45	1	0.5	3100

Table 2.
Self-compacting concrete's mix design

	cement Kg/cm^2	Water Kg/cm^2	Micro silica	Sand Kg/cm^2	Gravel Kg/cm^2	super plasticizer Kg/cm^2	VMA Kg/cm^2
SCC	400	192	18	870	651	8	3.20

Table 3.
Polypropylene Physical properties

Length (cm)	width (cm)	Thickness (cm)	Ratio of length to diameter
2.06	0.18	0.05	20

Recent research showed that fibers can control crack propagation in concrete [9-12]. Therefore, impact resistance, fatigue, plastic shrinkage cracks reduction, remaining bending strength (after cracking), and energy absorption capacity of concrete be improved [13-15]. The effectiveness of fiber in concrete depends on the type and amount of fibers, shape, length, aspect ratio (ratio of length to the diameter of the fibers), tensile strength, and inhibitory mechanisms [12, 16]. FSCC simultaneously has both SCC and Fiber reinforced concrete (FRC) advantages together. But it should be noted that, if the fiber value exceeds the optimum required amount, fibers may cause a reduction in the performance of the concrete mix and as much as the amount of fiber gets more than the optimum value, the efficiency will be reduced. In this regard, the determination of the optimum amount of fibers used in SCC is the main objective of this research [10, 17-20]. Hence, the mechanical properties of FSCCs should be known to improve the behavior of the SCC while mixing with fibers [21]. In this study, the effect of polypropylene fibers addition on the performance of SCC has been evaluated using time and diameter of slump-flow, L-Box, J-ring, and V-funnel flow time tests. Also, mechanical properties, including tensile and compressive strength of FSCC mix designs were evaluated at the ages of 7, 28, and 90 days.

2. Materials and methods

In accordance with ASTM C105 standard, Portland cement type 2 has been used to prepare the specimens of this study, and its physical and chemical characteristics are presented in Table 1.

Natural sand and manufactured coarse aggregates have been used and limestone powder has been employed as a filler. Aggregates have been used in saturated surface-dry (SSD) conditions; the largest and smallest coarse are 0.12 and 0.475 centimeters respectively. Superplasticizers used in this study are based on high-performance poly-carboxylic with a specific gravity of 1.133 gr/cm. The viscosity modifying additives (VMA) has been used to maintain the integrity of the concrete, and also for the prevention of aggregate detachment and concrete bleeding. VMA specific gravity is 13 gr/cm. Table 2 presents the SCC mix design, used in this study. As shown in Table 2, polypropylene fiber with values of 0.5, 1, 1.5, and 2% of mix design has been added to provide FSCC with the physical characteristics presented in Table 3.

For making concrete, Initially, the dry materials are mixed for 1 minute and then half of the water (which is obtained in the mix design) is added to the mixture

gradually along with the superplasticizer and mixed for another three minutes. After stopping the operation for 1 minute, the other half of the water along with VMA is added and mixed for 2 minutes.

For cylindrical specimens, a standard metal mold with dimensions of 35× 10 cm is used. After the materials were mixed, tests have been conducted on fresh concrete. Then concrete is poured into the lubricated mold where all molds are filled without any vibration or shock in one step. After 24 hours all the specimens have been transformed and kept in water. In this research 24 specimens were prepared with 0.5, 1, 1.5, and 2% polypropylene fibers and 6 control specimens.

Table 4.

FSCC Performance Testing Results

specimens	Slump Flow Time (*sec*)	Slump Flow Diameter (*cm*)	J-Ring (*cm*)	L-Box (H_2/H_1)	V-Funnel Time *(Sec)*
A	2.20	76.00	2.50	0.81	4.40
B	2.50	73.00	3.00	0.79	6.80
C	2.70	69.00	3.00	0.73	11.40
D	3.10	65.00	4.00	0.69	16.50
E	3.80	61.00	5.00	0.61	18.80

3. Results and discussion

After the materials were mixed in the mixer, a performance test has been conducted. The flow speed of SCC depends on its viscosity. SCCs must meet the following four features:

1. The ability to fill the mold with its own weight
2. Segregation resistance of the aggregate
3. The ability to pass through the rebar without segregation of aggregates
4. The smooth surface

The capability of specimens to achieve SCC characteristics has been evaluated using time and diameter of slump-flow, L-Box, J-ring and V-funnel flow time tests where the results show in Table 1. (A) is the control specimen and specimens B, C, D and E have 0, 0.5, 1, 1.5 and 2% of propylene respectively.

The slump flow time test (T50) is a criterion to determine the viscosity of SCC. In Figure 2, the alteration chart of (50T) slump flow time, due to the use of propylene fibers in concrete mix design is provided. As can be seen, with increasing fiber content, the slump flow time increases which show that the concrete fluidity has fallen. Although increasing the use of polypropylene fibers decreases the fluidity, according to the specification for SCC (EFNARC) standards all specimens have appropriate slump time as self-compacting concrete (Based on the specification for the SCC EFNARC standard, the flow time of self-compacting concrete should be between 2 and 0 seconds).

a) L-Box

b) J-ring

c) V-funnel

Figure 1. SCC test instruments

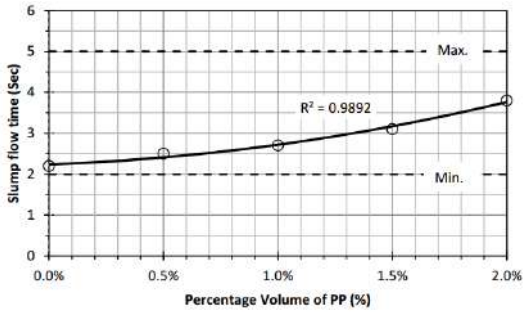

Figure 2. Slump flow time test results (50T)

The results of the diameter of slump flow test is shown in Figure 3. This test is a common method for determining the flow properties of concrete, in the horizontal plane with no obstructions. It is equal to the average of diameter of the concrete after removing the Abram cone. As can be seen by increasing the percentage of polypropylene fibers, slump flow diameter decreases. For example, using 2% of polypropylene fibers in concrete mix designs, thereby reducing the diameter of the slump from 76 to 61 cm. Thus, according to the specification for SCC (EFNARC) standard, when polypropylene fibers amount is more than 1.5%, the concrete cannot be considered as SCC (Based on the specification for the SCC EFNARC standard, the diameter of the slump flow should be between 65 to 80 cm).

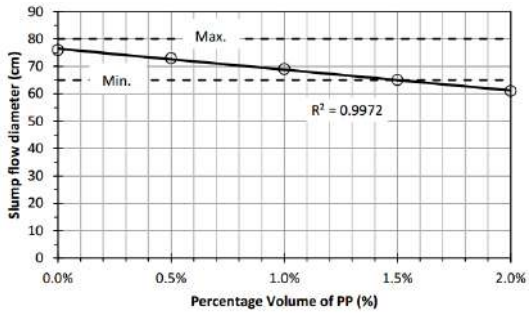

Figure 3. Diameter of slump flow test results

The results of the J-ring test are provided in Figure 4. This test is to identify the SCC's capability to pass through the rebar. As can be seen, by increasing the percentage of propylene fibers, the results of this experiment increased which is indicate that the fluidity of SCC decreases. But according to the specification for SCC (EFNARC) standard all specimens satisfy the J-ring test to be considered as SCC. (Based on the specification for the SCC EFNARC standard, the J-ring results should be between 1 to 5 cm).

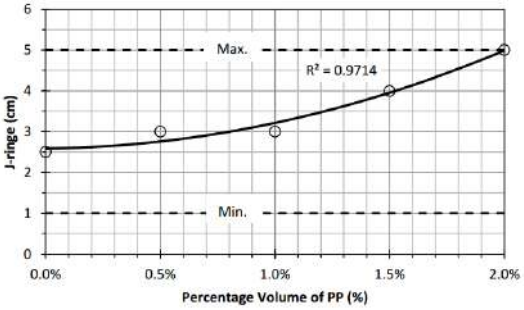

Figure 4. J-ring test results

The results of the L-Box test, show the passing ability of concrete through reinforcement in enclosed spaces (Figure 5). As can be seen, by increasing the percentage of propylene fibers, the passing ability decrease drastically. Based on the specification for EFNARC standard the least value obtained from the L Box test should not be less than 2.5. Hence, only the specimen without fiber and also the specimen with 0.5% polypropylene (Specimen B) with the ratio of H2/H1 which is respectively equal to 0.82 and 0.8, satisfy the specification of SCC. For the rest of the specimens prepared with a higher amount of polypropylene fiber, the ratio of H2/H1 decreases. It shows that concrete cannot fill a significant section of the end part of the horizontal L-Box. This test shows that specimens C, D, and E do not satisfy the specification of SCC.

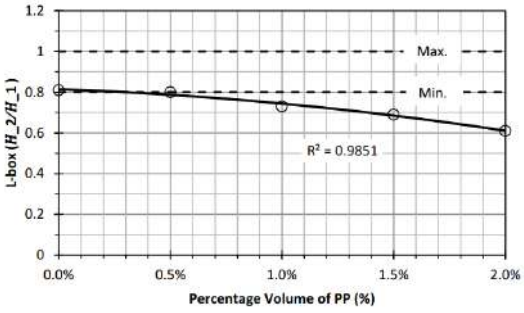

Figure 5. L-Box test results

The V-funnel flow time tests, evaluate the ability of self-compacting concrete to fill the mold. The diagram of V-funnel flow time test results is presented in Figure 6. As can be seen, for the specimen without

fiber, the flow time is 4.4 seconds which is less than the minimum value defined by the EFNARC standard. With the addition of fiber, flow time increases. For example, the specimens with 0.5% and 1% of fiber, with a time of 6.8 and 11.4 seconds, satisfy the specification of SCC (According to the specification for the SCC EFNARC standard, the V-funnel flow time tests results should be between 6 to 12 cm). Flow time is considerably increased by the addition of more fibers (1.5 and 2%) so that it goes beyond the limits defined (Figure 6).

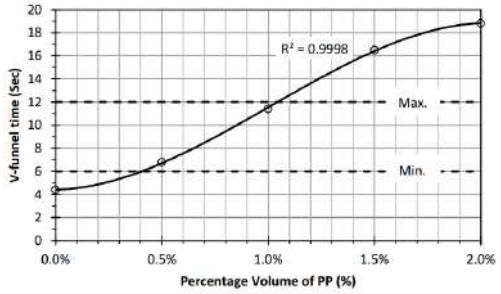

Figure 6. V-funnel flow time tests results

According to Table 4 and figures 2 to 6, the addition of fibers to the concrete leads to reduce the concrete performance (This trend has also been observed for the use of steel fibers in concrete). However, according to Table 5 (where acceptance of each of the specimens is defined based on the limits on the EFNARC standard) specimen (B) can be known as SCC. Concrete performance decreased by increasing the amount of fiber. The first concrete inefficiency is revealed through the L-box test for specimen (C) with 1% fiber. By increasing the percentage of polypropylene fiber to 1.5% the weakness would be more evident as far as specimen D would not satisfy the specification of SCC for V-funnel flow time tests.

3.1. Mechanical properties of FSCC

3.1.1. FSCCs Compressive strength

The compressive strength values of specimens at the age of 7, 28, and 90 days are presented in Table 6.

Table 5.
acceptability of specimens based on the limits of the EFNARC standard

specimens	**Slump Flow Time (*sec*)**	**Slump Flow Diameter (*cm*)**	**J-Ring (*cm*)**	**L-Box (H_2/H_1)**	**V-Funnel Time *(Sec)***
A	✓	✓	✓	✓	✓
B	✓	✓	✓	✓	✓
C	✓	✓	✓	×	✓
D	✓	✓	✓	×	×
E	✓	×	✓	×	×

Table 6.
Compressive strength of FSCC

specimens	compressive strength Kg/cm^2		
	7 dayes	28 days	90 days
A	288	389	469
B	261	372	452
C	245	343	438
D	234	331	407
E	221	315	401

In a research study, used polypropylene fibers (1.5 and 0.3%) to improve the physical and mechanical characteristics of concrete in their studies. The result showed that fibers, cause a slight increase in the compressive strength of concrete (about 5%). While Kakoei et al [22] Shown that using higher amounts of fibers (1.5, 2 kg/m3) noticeably increased compressive strength of the concrete. As noted, in the most studies, using of fibers increases the compressive strength of the concrete, however, in this study, the adding fiber to the SCC leads to the reduction of compressive strength of concrete. This decrease in resistance can be attributed to a decrease in concrete performance (due to the use of fiber), by increasing the proportion of fibers, condensing capacity of the SCC will reduce.

Based on the results of section 3.1., specimen (B), with 0.5% fiber, respected all limitations in the standard. As can be seen in figure 7, the use of 0.5% polypropylene fiber in the SCC mix design, reduces the compressive strength of concrete to 4.4% at the age of 28 days. This difference was reduced to 3.6% after 90 days. This difference can be neglected in return for the benefits of polypropylene fibers. On the other hand, for specimen (C) with 1% polypropylene fibers, strength reduction after 28 and 90 days is 12 and 6.5% respectively.

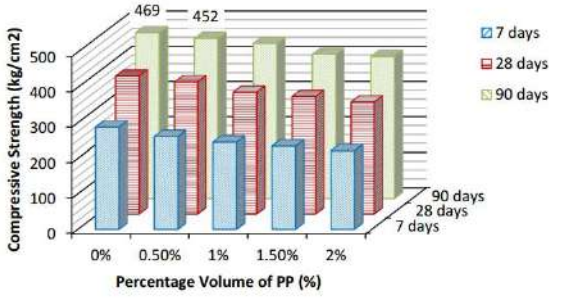

Figure 7. FSCC's compressive strength in different ages

3.1.2. FSCC's tensile strength

Tensile strength at the ages of 7, 28, and 90 days has been shown in Table 7 and figure 8. As can be seen, by increasing the percentage of fiber, the tensile strength increases. That this reflects the positive impact of propylene fibers in enhancing the tensile strength and ductility of concrete.

Table 5.
Tensile strength of FSCC

specimens	Tensile strength Kg/cm^2		
	7 days	28 days	90 days
A	21.1	32.6	33.7
B	21.9	33.2	34.8
C	23.3	36.5	37.3
D	24	38.8	39.1
E	26.9	44.2	45.4

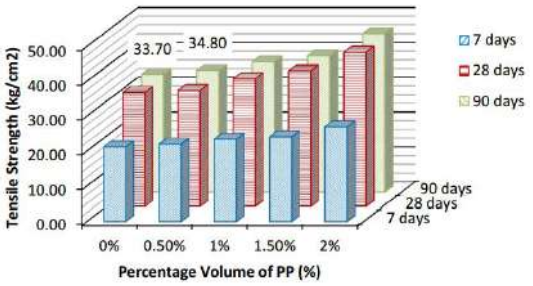

Figure 7. FSCC's Tensile strength in different ages

Investigation on FSCCs shows that by applying 3% polypropylene fiber, the specimen's rupture resistance will be increased to 13.6%. While in this research, after 28 days, the rupture resistance will be increased to 1.8 and 1.2% by adding 0.5 and 1% of fiber respectively. As can be seen, after 90 days, the compressive strength of the specimen (C) is almost equal to the specimen without fiber (by 6.5% reduction) and also by a 12% increase in rupture resistance, which has been able to satisfy the specifications required for SCC. On the other hand, by the experiments carried out on fresh concrete in accordance with the same mix design, specimen (C) can be also considered SCC. In other words, the proposed mix design in accordance with specimen (C), simultaneously has the advantages of both fiber concrete and self-compacting concrete.

4. Conclusion

The present research has shown that adding fiber caused a reduction in the compressive strength of concrete while the tensile strength and ductility of the concrete increased. Although adding 0.5% polypropylene fiber in the SCC mix design, reduces

the compressive strength by 3.6%, this value is negligible in return for its several advantages. The results also showed that specimen (C) with 1% polypropylene fiber can satisfy both FSCC and SCC specifications and its compressive strength is almost equal to the specimen without fiber; but its rupture resistance increased up to 12%. The results of the L-BOX test for the specimen (C) revealed that increasing the fiber percentage reduces self-compacting concrete performance.

References

[1] Mardani-Aghabaglou A., Tuyan M., Yılmaz G., Arıöz Ö., Ramyar K.: Effect of different types of superplasticizer on fresh, rheological and strength properties of self-consolidating concrete. Construction and Building Materials, 47, 1020-1025 (2013). DOI: https://doi.org/10.1016/j.conbuildmat.2013.05.105

[2] Saikia N., de Brito J.: Use of plastic waste as aggregate in cement mortar and concrete preparation: A review. Construction and Building Materials, 34, 385-401 (2012).

[3] Sahmaran M., Yaman I. O.: Hybrid fiber reinforced self-compacting concrete with a high-volume coarse fly ash. Construction and Building Materials, 21, 150-156 (2007). DOI: https://doi.org/10.1016/j.conbuildmat.2005.06.032

[4] Mohamad N., Zulaika M., Samad A., Goh W., Hadipramana J., Wirdawati A.: Fresh State and Mechanical Properties of Self Compacting Concrete Incorporating High Volume Fly Ash. in MATEC Web of Conferences. EDP Sciences (2016).

[5] Jen G., Trono W., Ostertag C. P.: Self-consolidating hybrid fiber reinforced concrete: Development, properties and composite behavior. Construction and Building Materials, 104, 63-71 (2016).

[6] Cazacu N., Bradu A., Florea N.: Self Compacting Concrete in Building Industry. Buletinul Institutului Politehnic din lasi. Sectia Constructii, Arhitectura, 62, 85 (2016).

[7] Cazacu N., Bradu A., Florea N.: Self Compacting Concrete Structures: A Techno-Economic Analysis. in Advanced Engineering Forum. Trans Tech Publ (2017).

[8] Kristiawan S., Murti G.: Porosity of Self-Compacting Concrete (SCC) incorporating high volume fly ash. in IOP Conference Series: Materials Science and Engineering. IOP Publishing (2017).

[9] Coppola B., Di Maio L., Courard L., Scarfato P., Incarnato L.: Development and use of foamed recycled fibers to control shrinkage cracking of cementitious mortars. in Proceedings of the 4rd Workshop" The New Boundaries of Structural Concrete". (2016).

[10] Al-Rousan R. Z., Alhassan M. A., Al-Salman H.: Impact resistance of polypropylene fiber reinforced concrete two-way slabs. Structural Engineering and Mechanics, 62, 373-380 (2017).

[11] Moradi M., Valipour H., Foster S.: Fatigue behaviour of transversely restrained precast steel fibre reinforced concrete slabs in a deconstructable composite deck. Construction and Building Materials, 132, 516-528 (2017).

[12] Marar K., Eren Ö., Roughani H.: The influence of amount and aspect ratio of fibers on shear behaviour of steel fiber reinforced concrete. KSCE Journal of Civil Engineering, 1-7 (2016).

[13] Yu R., Spiesz P., Brouwers H.: Energy absorption capacity of a sustainable Ultra-High Performance Fibre Reinforced Concrete (UHPFRC) in quasi-static mode and under high velocity projectile impact. Cement and Concrete Composites, 68, 109-122 (2016).

[14] Wang S., Le H. T. N., Poh L. H., Quek S. T., Zhang M.-H.: Effect of high strain rate on compressive behavior of strain-hardening cement composite in comparison to that of ordinary fiber-reinforced concrete. Construction and Building Materials, 136, 31-43 (2017).

[15] Kim S.-W., Park W.-S., Jang Y.-I., Yun H.-D.: Tensile Performance of Fiber-Reinforced Cement Composites with Hybrid Fibers. (2016).

[16] Yoo D.-Y., Kim S., Park G.-J., Park J.-J., Kim S.-W.: Effects of fiber shape, aspect ratio, and volume fraction on flexural behavior of ultra-high-performance fiber-reinforced cement composites. Composite Structures, 174, 375-388 (2017).

[17] Kamal M. M., Safan M. A., Etman Z. A., Kasem B. M.: Mechanical properties of self-compacted fiber concrete mixes. HBRC Journal, 10, 25-34 (2014).

[18] Sathishkumar R., Ranjith S.: EFFECT OF COIR FIBER AND POLYVINYL ALCOHOL FIBER ON DURABILITY PROPERTIES OF ENGINEERED CEMENTITIOUS COMPOSITES. (2017).

[19] Meng W., Valipour M., Khayat K. H.: Optimization and performance of cost-effective ultra-high performance concrete. Materials and Structures, 50, 29 (2017).

[20] Gopi P. N., Sateesh A.: Experimental investigation of Cement Concrete with partially replacing the Fine Aggregate with Local available Soil and Adding coir and human hair Fibers. (2016).

[21] Akcay B., Tasdemir M. A.: Mechanical behaviour and fibre dispersion of hybrid steel fibre reinforced self-compacting concrete. Construction and Building Materials, 28, 287-293 (2012)

[22] Kakoei, S., Akil, H. M., Jamshidi, M., & Rouhi, J. The effects of polypropylene fibers on the properties of reinforced concrete structures. Construction and Building Materials, 27(1), 73-77 (2012).

Author Guidelines EditEdit Author Guidelines

GENERAL GUIDELINES FOR AUTHORS

Journal of civil engineering researches invites unsolicited contributions of several forms: articles, reviews and discussion articles, translations, and fora. Contributions should fall within the broad scope of the journal, as outlined in the statement of scope and focus. Contributors should present their material in a form that is accessible to a general anthropological readership. We especially invite contributions that engage with debates from previously published articles in the journal.

Submissions are double-blind peer-reviewed in accordance with our policy. Submissions will be immediately acknowledged but due to the review process, acceptance may take up to three months. Submissions should be submitted via our website submission form (see links above for registration and login). Once you login, make sure your user profile has "author" selected, then click "new submission" and follow the instructions carefully to submit your article. If problems arise, first check the FAQ and Troubleshooting guide posted below. If you are still experiencing difficulty, articles can be submitted to the editors as email attachments.

Each article should be accompanied by a title page that includes: all authors' names, institutional affiliations, address, telephone numbers and e-mail address. Papers should be no longer than 10,000 words (inclusive of abstract 100-150 words, footnotes, bibliography and notes on contributors), unless permission for a longer submission has been granted in advance by the Editors. Each article must include a 100 words "note on contributor(s)" together will full institutional address details, including email address. We request that you submit this material (title page and notes on the contributors) as "supplementary files" rather than in the article itself, which will need to be blinded for peer-review.

We are unable to pay for permissions to publish pieces whose copyright is not held by the author. Authors should secure rights before submitting translations, illustrations or long quotes. The views expressed in all articles are those of the authors and not necessarily those of the journal or its editors. After acceptance, authors and Special Issue guest editors whose institutions have an Open Access library fund must commit to apply to assist in article production costs. Proof of application will be requested. Though publication is not usually contingent on the availability of funding, the Journal is generally under no obligation to publish a work if funding which can be destined to support open access is not made available.

Word template and guidelines

Our tailored Word template and guidelines will help you format and structure your article, with useful general advice and Word tips.

(La)TeX template and guidelines

We welcome submissions of (La)TeX files. If you have used any .bib files when creating your article, please include these with your submission so that we can generate the reference list and citations in the journal-specific style

Artwork guidelines

Illustrations, pictures and graphs, should be supplied with the highest quality and in an electronic format that helps us to publish your article in the best way possible. Please follow the guidelines below to enable us to prepare your artwork for the printed issue as well as the online version.

Format: TIFF, JPEG: Common format for pictures (containing no text or graphs).

EPS: Preferred format for graphs and line art (retains quality when enlarging/zooming in).

Placement: Figures/charts and tables created in MS Word should be included in the main text rather than at the end of the document.

Figures and other files created outside Word (i.e. Excel, PowerPoint, JPG, TIFF, EPS, and PDF) should be submitted separately. Please add a placeholder note in the running text (i.e. "[insert Figure 1.]")

Resolution: Rasterized based files (i.e. with .tiff or .jpeg extension) require a resolution of at least 300 dpi (dots per inch). Line art should be supplied with a minimum resolution of 800 dpi.

Colour: Please note that images supplied in colour will be published in colour online and black and white in print (unless otherwise arranged). Therefore, it is important that you supply images that are comprehensible in black and white as well (i.e. by using colour with a distinctive pattern or dotted lines). The captions should reflect this by not using words indicating colour.

Dimension: Check that the artworks supplied match or exceed the dimensions of the journal. Images cannot be scaled up after origination

Fonts: The lettering used in the artwork should not vary too much in size and type (usually sans serif font as a default).

Authors services:

For reformatting your manuscript to fit the requirement of the Journal of Civil Engineering Researchers and/or English language editing please send an email to the following address:

researchers.services@gmail.com

Noted: There is a fixed charge for these mentioned services that is a function of the manuscript length. The amount of this charge will be notified through a reply email.

FAQ AND TROUBLESHOOTING FOR AUTHORS

I cannot log in to the system. How do I acquire a new user name and password?

If you cannot remember your username, please write an email to (journals.researchers@gmail.com), who will locate your username and notify you. If you know your username, but cannot remember your password, please click the "Login" link on the left-hand menu at homepage. Below the fields for entering your username and password, you will notice a link that asks "Forgot your password?"; click that link and then enter your email adddress to reset your password. You will be sent an automated message with a temporary password and instructions for how to create a new password. TIP: If you do not receive the automated email in your inbox, please check your SPAM or Junk Mail folder. For any other issues, please contact our Managing Editor,Kamyar Bagherinejad (admin@journals-researchers.com).

How do I locate the online submission form and fill it out?

First you need to register or login (see above). Once you are logged in, make sure the "roles" section of your profile has "Author" selected. Once you assign yourself the role of "Author," save your profile and then click the "New Submission" link on your user home page.

Once you arrive at the submission form page, please read the instructions carefully filling out all necessary information. Unless specified otherwise by the editors, the journal section to be selected for your submission should be "Artlcles." Proceed to the remaining sections, checking all boxes of the submission preparation checklist, and checking the box in the copyright notice section (thus agreeing to journals-researchers's copyright terms). Once the first page is completed, click "Save and Continue." The next page allows you to upload your submission. Use the form to choose your file from your computer. Make sure you click "Upload." The page will refresh and you may then click "Save and Continue." You will then proceed to a page for entering the metadata for your article. Please fill out all required fields and any further information you can provide. Click "Save and Continue." The next page allows you to upload supplementary files (images, audiovisual materials, etc.). These are not required, but if you wish to provide supplementary materials, please upload them here (do no forget to click "Upload." Then click "Save and Continue." This brings you to the final page of the submission form. Please click "Finish Submission" in order to close the

submission process. You wil then be notified by email that your article has been successfully submitted. TIP: If you do not receive the automated email in your inbox, please check your SPAM or Junk Mail folder. For any other issues, please contact our Managing Editor, Kamyar Bagherinejad (admin@journals-researchers.com).

Why am I not receiving any email notifications from HAU?

Unfortunately, some automated messages from Open Journal Systems arrive in users' Spam (or Junk Mail) folders. First, check those folders to see if the message was filtered into there. You may also change the settings of your email by editing your preferences to accept all mail from [jcer] and related journals-researchers.com email accounts.

I am trying to upload a revised article following an initial round of peer-review, but I cannot locate where to upload the article. Where do I submit a revised article?

Follow the login process outlined above and when you successfully login you will see on your user home page a link next to "Author" for "active" articles in our system (usually it is only one article, but if you have mulitple submissions currently in our system, the number could be higher. Click the "Active" link and you will be led to a page that lists your authored articles currently in our system. Click the link under the column labeled "Status" and this will take you to a page showing the current review status of your article. At the very bottom of the screen, you will see an upload form under the heading "Editor decision." Here you may upload your revised article. An automated email will be sent to the editors and you may also notify them directly via email. You may then logout.

I successfully submitted an article; how long will it take for the editors to respond to me with a decision.

For all articles that are recommended for peer-review, the editors of JCER strive to notify authors of a decision within 4-6 weeks. You may contact JCER's Managing Editor, Kamyar Bagherinejad (admin@journals-researchers.com). if you have any questions relating to the review process and its duration.

For all other inquiries, please contact: Kamyar Bagherinejad (Managing Editor)

Privacy Statement

The names and email addresses entered in this journal site will be used exclusively for the stated purposes of this journal and will not be made available for any other purpose or to any other party.

Articles

Section default policy

Make a new submission to the Articles section.

Copyright Notice EditEdit Copyright Notice

Journal of Civil Engineering Researchers follows the regulations of the International Committee on Publication Ethics (COPE) and the ethical principles of publishing articles in this journal are set based on the rules of this committee, and in case of problems, it will be treated according to these rules.

Privacy Statement EditEdit Privacy Statement

The names and email addresses entered in this journal site will be used exclusively for the stated purposes of this journal and will not be made available for any other purpose or to any other party.

Scholars Pavilion

Scholars Pavilion or **Scholars Chartagi** is a monument donated by the Islamic Republic of Iran to the United Nations Office at Vienna. The monument architecture is claimed by the Islamic Republic News Agency of Iran to be a combination of Islamic and Achaemenid architecture, although the latter clearly predominates in the decorative features, with Persian columns and other features from Persepolis and other remains from the Achaemenid dynasty. The Chahartaq pavilion form runs through the architecture of Persia from pre-Islamic times to the present.

Statues of four famous Persian medieval scholars, Omar Khayyam, Al-Biruni, Muhammad ibn Zakariya al-Razi and Ibn-Sina are inside the pavilion. This monument donated in June 2009 in occasion of Iran's peaceful developments in science.

J-Researchers